Geotechnical Properties and Foundation Requirements for the Satellite and Lunar Laser Ranger at the Matjiesfontein Space Geodesy Observatory

by
Susan Bothma

Thesis presented in fulfilment of the requirements for the degree of Master of Engineering in the Faculty of Civil Engineering at Stellenbosch University

Supervisor: Mr Leon Croukamp

December 2015

DECLARATION

By submitting this thesis electronically, I declare that the entirety of the work contained therein is my own, original work, that I am the sole author thereof (unless to the extent explicitly otherwise stated), that reproduction and publication thereof by Stellenbosch University will not infringe any third party rights and that I have not previously in its entirety or in part submitted it for obtaining any qualification.

December 2015

ABSTRACT

The basic idea of Satellite and Lunar Laser Ranging (S/LLR) is to improve our understanding of gravity. The earth-moon system is a good workspace to test the theories of gravity. By measuring the distance between the earth and the moon, the precise orbital shape of the path can be determined with millimetre precision. This enables scientists to test general relativity (GR), which is the predicted deviation from the Newtonian gravity and is supposed to exactly predict the correct orbital path of the moon. With the measurements obtained from S/LLR experiments, scientists can compare the values to those predicted by GR and this will help them to understand and prove the GR theorem.

The intention of this thesis is to identify, analyse and evaluate the required aspects for the emplacement of an S/LLR at the Matjiesfontein Space Geodesy Observatory (MSGO). The 7 ton S/LLR needs a very stable foundation to ensure accurate measurements as well as pointing to the exact location on the satellite/lunar surface. The aspects evaluated is the bearing capacity of the rock mass, settlement of the foundation, slope stability, excavatability of materials, the wind loads on the shed as well as the management of risks. The following data is needed to complete the evaluation:

- Field survey and tests:
  - Geometric data capturing;
  - Joint survey;
  - DCP tests (Dynamic Cone Penetrometer); and
  - Core Drilling.
- Laboratory tests:
  - UCS tests (Unconfined Compression Strength);
  - Point load tests; and
  - Petrographic analyses.

It was calculated that the applied bearing pressure is much smaller than the bearing capacity of the rock and thus a safe assumption can be made that the rock mass is more than sufficient to withstand the load of the structure.

From the result of the settlement calculation it is clear that settlement would not be a factor influencing the operation of the S/LLR. It is recommended that the level of the foundation should be calibrated after the hardening of the concrete and before the instrument is placed.

Slope stability analyses were done for potential circular failure, wedge failure, planar failure and toppling. All of the slope stability analyses have shown that the areas are safe against slope instability

and no extra precautions need to be taken to keep the area safe. It is however important to do new analyses if any cuts or excavations are made to build a road or building.

Bedrock can be found within 500 mm to 600 mm below ground level. The assessment of the excavatability of materials yielded that the method of ripping should be used to excavate the material on site. This indicates that the topsoil can be removed without the need for blasting to reach deep intact rock.

Thin sections were prepared from the core samples and petrographic analyses were done to determine the origin, composition, distribution and structure of the rocks. It is important to establish which clay minerals are present to determine if the rock mass could be expansive and have a resultant destabilising effect on the foundation. The petrographic studies have shown that clay minerals such as kaolinite and chlorite are present in the samples. It can thus be concluded that, as these are non-expansive minerals, it can be assumed to be a non-expansive rock mass.

The conclusion that can be drawn from this study is that the design of the foundations of the S/LLR at MSGO will be the same as at HartRAO. This conclusion can be made as none of the factors that were evaluated have shown a potential destabilising effect on the S/LLR.

ACKNOWLEDGEMENTS

I would like to thank the following people:

- Mr Leon Croukamp, for his guidance as my supervisor;
- Dr Marius de Wet, for his support and guidance throughout the project;
- Dr Stoffel Fourie, for his support and enabling me to visit the CERGA observatory in France;
- Dr Ludwig Combrink, enabling me to visit HartRAO in Gauteng, South Africa;
- Dr Peter Day, for his guidance and input towards my thesis;
- Ms Danél van Tonder, for her assistance with the petrographic analyses;
- Mr Jurgens Schoeman, for assisting with surveying and his knowledge of geological concepts;
- Mr Jaco Pentz and Mr Lenmar Malan, for assisting with the surveying;
- The laboratory assistants (geotechnical lab and structural lab), for their kind support; and
- My parents and sister, for their support and understanding during the course of the project.

TABLE OF CONTENTS

LIST OF FIGURES

LIST OF TABLES

CHAPTER 1: INTRODUCTION

1.1. BACKGROUND

Matjiesfontein is situated ±250 km Northeast from Cape Town via the N1 on the way to Laingsburg in the Great Karoo, Western Cape. **Figure 1** shows where Matjiesfontein is situated in the Western Cape. The town dates back to 1884, when James Logan bought the farm. He then turned it into a luxurious spa that was known far and wide (Anonymous, 2010).

FIGURE 1: MAP OF THE WESTERN CAPE (ANONYMOUS, 2015)

Although it was a very small town, Matjiesfontein lacked nothing. It had the longest private phone line, its main street was lit by London street lamps, and it was the first village in South Africa to replace gas with electricity. Matjiesfontein's history also includes the first cricket match played between South Africa and England, Olive Schreiner's residency, controversial war crime hearings and accommodated the Cape Command headquarters during the Anglo-Boer War.

1.2. MOTIVATION FOR RESEARCH

The donation of a 1 m Cassegrain telescope by France to HartRAO (Hartebeesthoek Radio Astronomy Observatory) created the opportunity to develop the Matjiesfontein Space Geodesy Observatory (MSGO). Instruments such as a Satellite and Lunar Laser Ranger (S/LLR), gravimeter, seismograph and a Global Navigation Satellite Systems (GNSS) receiver will be part of this observatory. In addition to the mentioned instruments, the site could be considered for the installation of one or two 34 m dishes as part of the NASA Deep Space Tracking Network. These dishes may be suitable for International Celestial Reference Framework VLBI (Very Long Baseline Interferometry) experiments. The possible future installation of a DORIS (Doppler Orbitography and Radiopositioning Integrated by Satellite) system will further enhance satellite tracking and orbit calculations.

As the S/LLR is one of the main instruments on site, it is of utmost importance to ensure that the instrument is stable and safe. This thesis will investigate all aspects needed to endorse the emplacement.

1.3. RESEARCH PURPOSE AND OBJECTIVES

The objective of this study is to ensure safe and stable emplacement of the S/LLR at the MSGO. To do this, the geotechnical properties of the site need to be determined and various aspects need to be taken into consideration. This includes aspects such as bearing capacity, settlement, slope stability, excavatability of materials and wind loading. Another objective is to identify possible risks that may occur before, during or after construction, and to define an action to mitigate these risks.

1.4. LIMITATIONS OF RESEARCH

The research was limited to the effect of static loads on the ground such as the weight of the foundation and the weight of the telescope. The vibrations and movement of the telescope was not taken into consideration. The study is furthermore limited to only those aspects deemed critical to determine the stability of the foundation, and not all aspects and risks were taken into consideration.

1.5. THE MSGO SITE

The site, where all the instruments will be placed, is situated ± 5 km to the south of Matjiesfontein. This site was proposed for the MSGO as an outstation for HartRAO. The location is ideal, because it is situated in a small depression that shields it from radio frequency interference emitted by cell phones and microwave sources (Combrinck, *et al,.* 2007). This site is also favourable due to the many cloudless days and clear skies which allow the S/LLR to increase its data collection efficiency. **Figure 2** shows the site layout of the MSGO.

FIGURE 2: SITE LAYOUT OF THE MATJIESFONTEIN SPACE GEODESY OBSERVATORY

1.5.1. BIOPHYSICAL ATTRIBUTES

The topography of this site is generally flat, with a ridge to the northern border of the site and a steep slope (the Witteberg Mountains) to the South. The soil is usually shallow on top of weathered or hard rock. Following a geotechnical investigation of eight test pits, the general regolith profile of this area could be described as:

- 0.2 m: Dry, light brown, loose, intact, boulders and gravel in a sandy matrix. Hill wash.
- 0.5 m: Slightly moist, dark reddish-orange, dense, intact, boulders and gravel with limited sandy matrix. Hill wash.
- 0.6-1 m: Refusal on highly to moderate weathered thinly bedded shale or mudstone. Bedding planes sub-vertical (Combrinck, *et al.,* 2007).

The vegetation present in this area is Matjiesfontein Shale Renosterveld and Koedoesberge-Moordenaars Succulent Karoo. None of the vegetation or species found in this area is classified as threatened and critically endangered, and no vulnerable, threatened or critically endangered species were found in this area (Ecosense, 2015). This area, however, falls in a Critical Biodiversity Area, but has not been formalized into a bioregional plan. A number of drainage channels run through this area,

but no wetlands are present. There is an access road to the site which is in a poor condition and eroded in some areas. Three non-operational boreholes are present on site with a water pipeline towards one, but it is not connected.

1.5.2. GEOLOGY

The MSGO site lies within the Greater Karoo and is close to the contact point between the Cape and Karoo Supergroups. This area has gone through many geological stages starting with the breakup of Pangea and turning into a shallow inland sea, later to be covered by large glaciers and then becoming a sea again. After millions of years it finally became as dry and open as it is today. The layers in this area have twisted and folded over long periods of time as a direct result of formation of the Cape Fold Belt. Formations found in this area include the Waaipoort, Floriskraal and Kweekvlei Formations from the Witteberg Group in the Cape Supergroup and the Dwyka Formation and Group in the Karoo Supergroup.

1.5.3. WEATHER CONDITIONS

Weather conditions play a major part in activating slope movement (Tarbuck, *et al.*, 1996), thus it is important to investigate weather patterns thoroughly. There are no available weather data for Matjiesfontein, but Sutherland is assumed to have similar conditions, so it is considered suitable to use the same data for Matjiesfontein.

The Karoo region has a semi-arid climate with the mean annual precipitation (MAP) less than 250 mm (Combrinck, *et al.,* 2007). **Figure 3** shows climate data obtained of Sutherland.

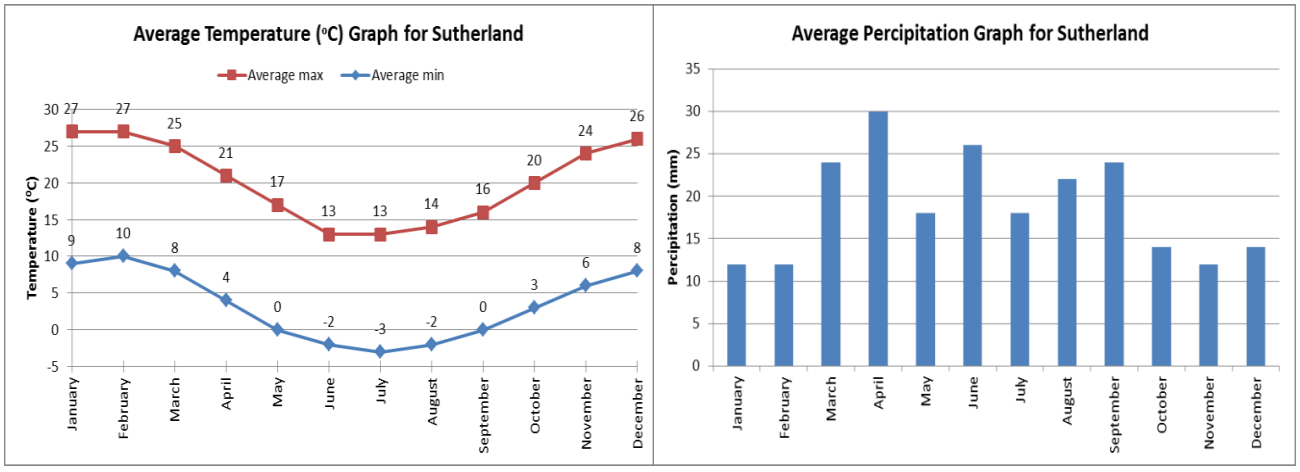

FIGURE 3: CLIMATE CHART OF SUTHERLAND (ANONYMOUS, 2014)

1.5.4. SEISMIC ACTIVITY

South Africa is not generally known for large seismic events, but due to the fact that an activity can cause slopes failure processes to activate, it needs to be investigated. A hazard map of South Africa, **Figure 4,** was created by Kijko *et al.,* (2003). Matjiesfontein lies in an orange region with a peak ground acceleration (PGA) of 0.16 g. This value is used in calculations when slope stability is investigated.

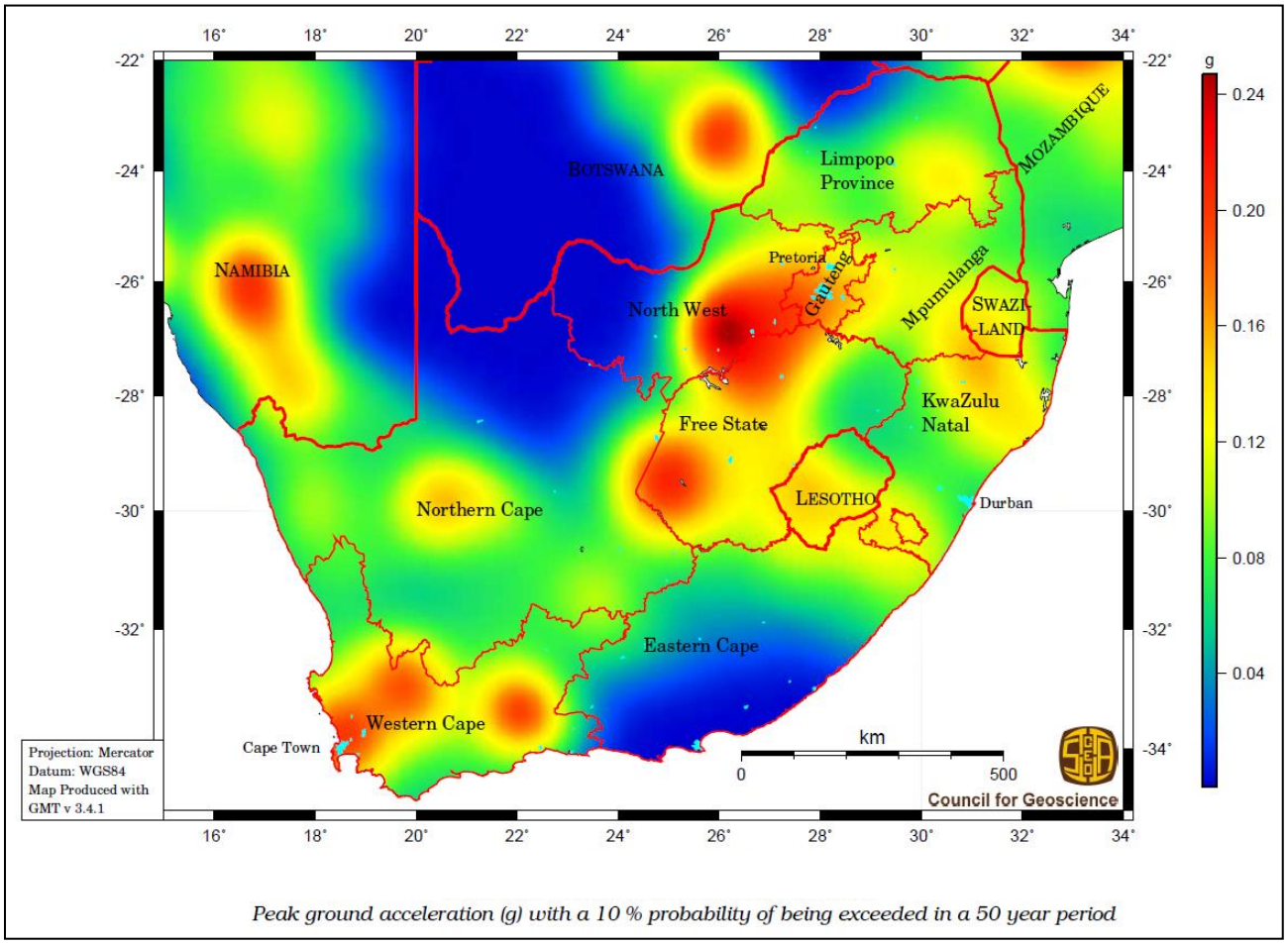

FIGURE 4: SEISMIC HAZARD MAP OF SOUTH AFRICA (KIJKO *ET AL.*, 2003)

1.6. REPORT LAYOUT AND STRUCTURE

This thesis consists of five chapters, which include an introduction, a literature review, data collection, analysis of data and evaluation of site, and risk management, followed by conclusions and recommendations. Each chapter will be described in short.

The literature review, in Chapter 2, starts with LLR and gives a brief history thereof, how it works and other stations in the world. The geology of the site is described with attention paid to the Cape Supergroup as well as the Karoo Supergroup. The swelling potential of a rock mass is discussed in addition. Previous studies done at the MSGO are included and followed by the discussion of slope

stability. The next section discusses different types of foundations and the chapter ends off with the description of the S/LLR at HartRAO.

The data collection chapter, Chapter 3, deals with all activities associated with collection of data on the site, including fieldwork and testing. Field work consists of geometric data capturing, a joint survey, dynamic cone penetrometer tests as well as core drilling. The laboratory tests conducted were the unconfined compression test, the point load test and petrographic analyses.

The analysis of the data obtained as well as the evaluation thereof is in the fourth chapter. The aspects evaluated are the bearing capacity of the rock mass, settlement of the foundation, slope stability, excavatability of materials, the wind loads on the shed as well as the management of risks.

In the final chapter, Chapter 5, conclusions are drawn and appropriate recommendations are made. In the appendices, the extended calculations can be found as mentioned in the text.

CHAPTER 2: LITERATURE REVIEW

This chapter will discuss the literature that was studied in order to understand the problem as stated in ***Section 1.3***. It includes the history of LLR, the geology of the site, previous studies done and different types of foundations which are used in practice.

2.1. LUNAR LASER RANGING

In order to understand the concept of LLR, a brief history and breakdown of the main elements of LLR need to be discussed. In conjunction herewith, other LLR stations in the world are discussed with particular attention paid to the S/LLR at HartRAO.

2.1.1. HISTORY OF S/LLR

According to Alley (1972), in the 1950's a small group of scientists, from Princeton University under Robert H. Dicke, gave substance to the concept of what would become the technique of optical laser ranging. The group wanted to investigate the fundamentals of gravity and suggested that a powerful, pulsed search light should be aimed at a reflector on a satellite. This would enable them to analyse the orbital characteristics of the satellite.

Parallel to this process the concept of receiving laser light rebounds from the lunar surface proceeded. The rough topography of the moon caused light to disperse and thus impossible to determine the distance as precise as the satellite measurements, which then lead to the need, development and placement of retroreflector arrays. The first retroreflector array was placed on the moon on 22 July 1969 (Dickey, 1994) during the Apollo 11 mission by Neil Armstrong and Buzz Aldrin. The first lunar laser ranging observation of Apollo 11 was done shortly thereafter. This event made the concept of lunar laser ranging (LLR) a reality. During the Apollo 14 and Apollo 15 missions additional retroreflectors were placed on the moon and unmanned Soviet rovers (Lunokhod 1 and Lunokhod 2) carrying a French-built reflector was placed on the surface as well (Murphy, 2013). No return signals were detected from Lunokhod 1 after 1971, but in April 2010 a team from University of California rediscovered it with the use of lunar images from NASA.

2.1.2. HOW DOES THE S/LLR WORK?

The basic idea of LLR is to improve our understanding of gravity and the earth-moon system is a good workspace to test the theories. By measuring the distance between the earth and the moon, the precise orbital shape of the path can be determined with millimetre precision. This enables scientists to test general relativity (GR), which is the predicted deviation from the Newtonian gravity and supposed to

exactly predict the correct path of the moon (Murphy, 2013). With the measurements obtained from the LLR experiment, scientists can compare the values to those predicted by GR and this will help them understand and prove the GR theorem.

SLR and LLR are very valuable techniques which can contribute to a wide variety of fields such as geodynamics, geodesy, astronomy, lunar science, relativity and gravitational physics (Veillet *et al.*, 1993). To use the technique of laser ranging, various elements need to work together. First a laser pulse needs to be created and sent through the transmitter to the exact location on the lunar surface or satellite, secondly a reflector must reflect the pulse back to earth and lastly a receiver must be able to detect these pulses, measure the time of flight and calculate the distance. **Figure 5** shows a simple illustration of these elements.

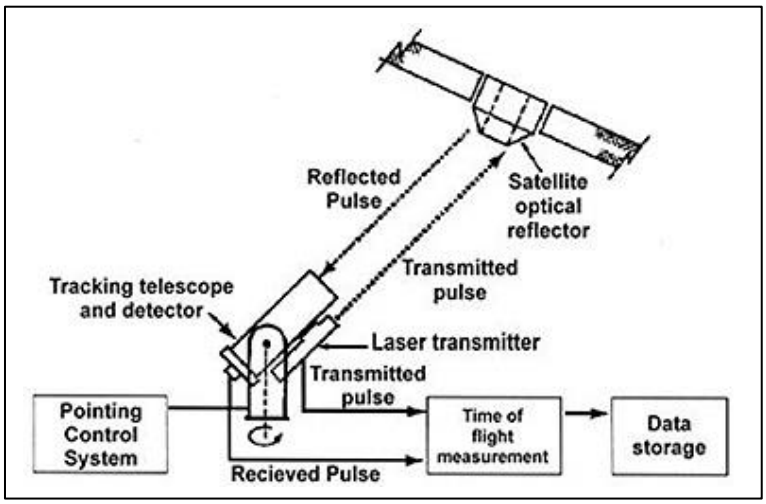

FIGURE 5: A SCHEMATIC DIAGRAM OF A TYPICAL S/LLR SYSTEM (SHORT, 2005)

SLR operation is very similar to LLR, with only a few differences which include the speed of the telescope itself and different types of pulses. As a satellite is much lower or closer to Earth than the moon, the telescope have to move much faster to track a satellite, but needs less energy per pulse to reach it.

2.1.2.1. The Laser Pulse

The pulse that is transmitted needs to be created on a laser table similar to that in **Figure 6**. The pulse is created by an excited atom that duplicates a passing photon into a photon of the same energy. This cloning process where a photon passes through a bulk material of excited atoms creates an exponential growth in the light intensity. This process takes place until the light intensity is high enough to be released by the laser system. The process is called the process of Stimulated Emission (Botha, 2015).

Once the pulse leaves the laser system, it is reflected by mirrors through the coudé path, to the point where it can be transmitted to either the reflector on the lunar surface or the satellite. Stations that do both SLR and LLR usually have a mirror that can turn to allow different types of laser pulses from different laser tables to be transmitted. This is very useful as it makes it possible to do various measurements with one telescope.

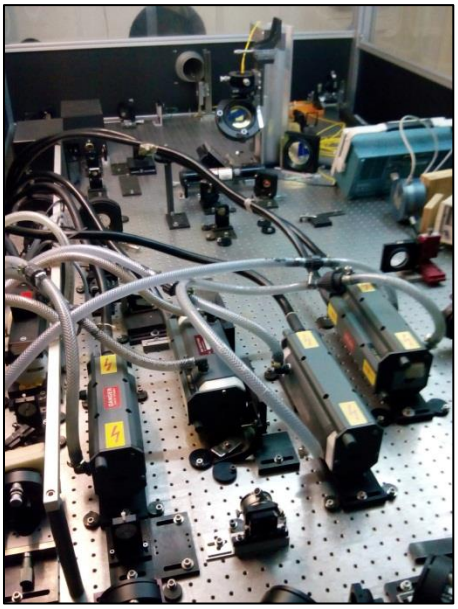

FIGURE 6: LASER TABLE

2.1.2.2. The Retroreflectors

A retroreflector is an array of corner cube reflectors, such as used in surveying, which reflects the light directly back to its source independently of the angle of the beam. This is unlike a reflective surface such as a mirror where the light is reflected back at the same angle as it arrived, as seen in **Figure 7**. A flat mirror will only reflect the beam directly back to its source if the beam strikes the surface at exactly 90 degrees. **Figure 8** shows an example of the Apollo 14 reflector on the moon that is used in LLR.

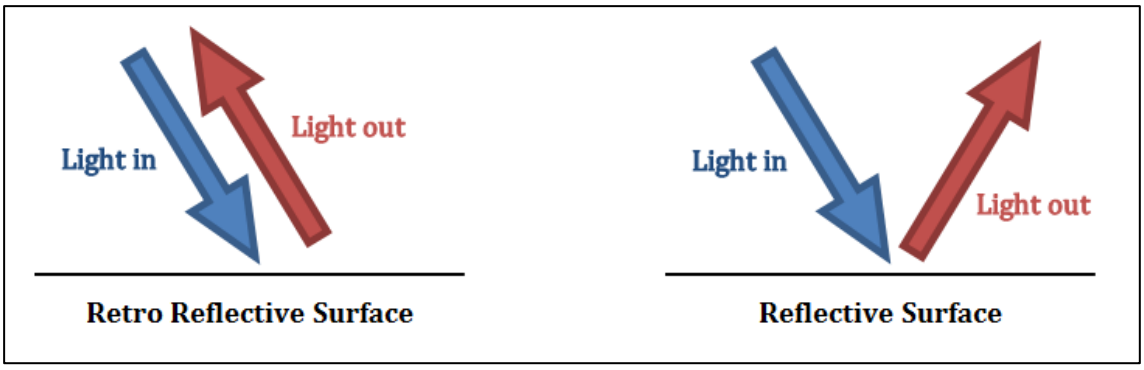

FIGURE 7: DIFFERENCE BETWEEN RETROREFLECTOR AND A REFLECTIVE SURFACE

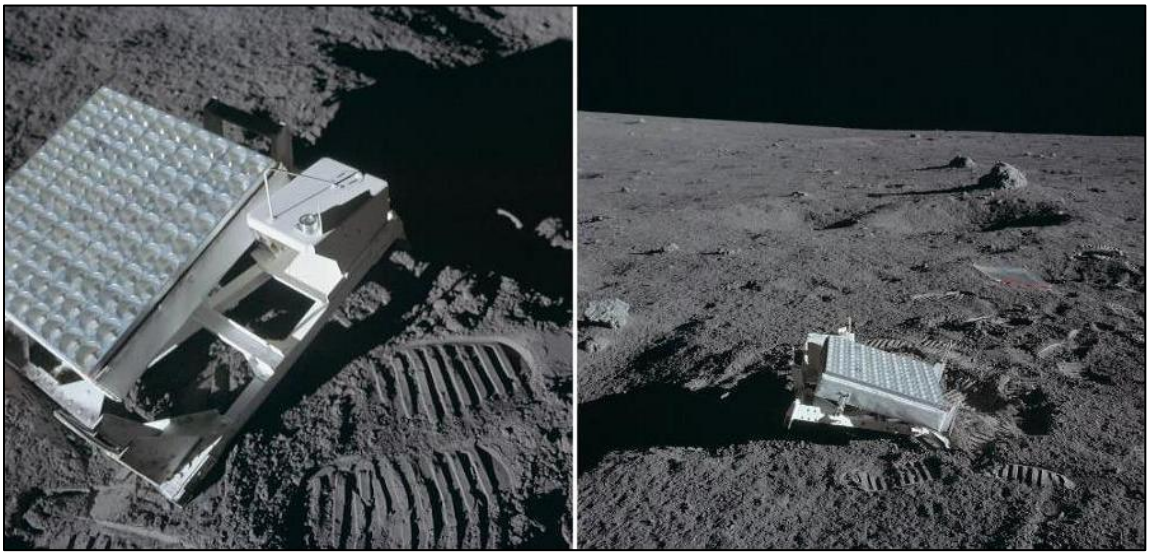

FIGURE 8: THE APOLLO 14 RETROREFLECTOR ON THE MOON (JONES & GLOVER, 2013)

2.1.2.3. The Receiver

The distance between the earth and the moon is measured by the time it takes for the light pulse to travel to the moon and back. This can be anywhere from 2.34 to 2.71 seconds, depending on the distance to the moon at that time, and can be measured to an accuracy of a few picoseconds (Murphy, 2013).

In a period of a few hours, when the moon is at its highest, measurements are taken from all the visible reflectors. By doing this over a few months or even years, the shape of the moon's orbit will be defined to such precision that assumptions can be made about the working of gravity.

However, to make such highly accurate measurements, as much laser light as possible is needed on the reflector. The light pulses sent out must be as parallel and non-diverging as possible (Murphy, 2013). This is why a laser is suitable, both for the short pulses of light it can give, and that a laser's light is highly directional. Due to the turbulent atmosphere of the Earth, the beam can be distorted up to 1.8 km at the surface of the moon, which is very large considering that the reflector array is only 1 m^2 and means that most of the light will not reach its intended target. The width of the beam is about 15 km across when it reaches the earth, which results in only 3 to 4 photon returns per minute (Murphy, 2013).

The light detector is the instrument that receives the photons in order to calculate the time. The detector must also be orientated to the same location as the laser. The detector is programmed to accept only the photons that were sent out by its system. This is possible because each photon is 'time stamped' as it leaves the laser, the exact wavelength is known and the detector is only open for 100 nanoseconds when the photons are expected to return. They also incorporate an interferential filter

that only transmits light with that specific wavelength (Chapront & Francou, 1973). Laser ranging cannot be done when it is full moon, as there would be too much background light and the detection of the photons would be impossible.

The returning light from SLR and LLR differs. SLR returns a pulse of light which can be measured by a Photo-Multiplier Tube (PMT). LLR returns only a single photon and a single-photon detection device is used (typically an Avalanche Photo Detector (APD)).

A big uncertainty comes with the duration of a specific photon as it is impossible to know whether the returning photon was at the beginning or at the end of the pulse that was emitted. The pulse can be shortened with modern technology but this decreases the number of photons, and energy, which are available to reach the moon (Veillet *et al.*, 1993). A photon at the beginning of a pulse can differ as much as 30 millimetres from the photon that is emitted last. A number of measurements are made over a period of a few minutes and a statistical analysis can be made if 900 – 2500 photons are detected, to improve the accuracy of 30 – 50 mm for one photon to 1 mm (Murphy, 2013).

There are a few elements to consider during the calculations. For accurate measurements the position of the telescope relative to the centre of the earth should be known. This is, however, not a fixed distance as the continental plate drifts and the tides from the moon and sun make the earth's crust expands whereas weather systems can also push the local crust down (Murphy, 2013). The gravitational fields of other planets and celestial bodies can also have an effect (Combrinck, 2015). All of these influences must be taken into consideration to determine the exact centre-to-centre distance between the earth and the moon.

2.1.3. Other S/LLR Stations in the World

After the reflectors were placed by Apollo 11, the first LLR observation was made by Lick Observatory in California, for the purpose of quick acquisition and confirmation (Anonymous, 1993). Along with this, LLR began at the McDonald Observatory and for 15 years the McDonald Observatory was the only station that regularly ranged to the moon. Successful LLR was conducted in the early days by the following observatories:

- Air Force Cambridge Research Laboratories Lunar Ranging Observatory in Arizona;
- Pic du Midi Observatory in France; and
- Tokyo Astronomical Observatory.

Other stations that also accomplished lunar laser ranging in the past 40 years are Haleakala Observatory on Maui Hawaii, the former Soviet Union, Australia and Germany. Currently there are only a few operational LLR stations around the world, where most of the stations are shared SLR and LLR

stations (Dickey, 1994). The only stations to yield regular observations are the McDonald station in the USA and the CERGA station in France.

McDonald Observatory is located near the community of Fort Davis in Jeff Davis County, Texas. The observatory is situated in the Davis Mountains (west of Texas). There are two facilities in the observatory, one on top of Mount Locke and the other on top of Mount Fowlkes.

McDonald Observatory was first approached by LURE (Lunar Ranging Experiment) when the 2.7 m reflecting telescope became operational. This telescope was mostly funded by NASA for a major planetary observation program. The operational telescope created the possibility for long-term LLR activities at this site. McDonald Observatory became the leading LLR station in the world in the 1970's and early 1980's (Silverberg, 1974)

The first LLR station in France was at Pic du Midi Observatory in the Pyrenees. A few echoes were obtained from different reflectors, but it was difficult to sustain the operation as the site was isolated and the team in charge of the experiment was situated in Paris. The team gained the necessary experience and efforts were made for a dedicated LLR station (Veillet *et al.*, 1993). The decision was made to create a new observatory, CERGA (Centre d'Etudes et de Recherche en Géodynamique et Astronomie), situated near Grasse, France. The observatory aimed to collect data (measurements in astronomy) on the same site with several techniques, which includes astrolabes, a Schmidt telescope and a SLR.

2.1.4. THE S/LLR AT HARTRAO

As discussed in *Section 2.1.2.*, there is a difference in the pulse of SLR and LLR. The SLR at HartRAO has a high rate of firing and low power with a frequency of 1 kilohertz, energy of 0.5 millijoule and a pulse length of 20 picoseconds. The LLR has more power and thus more photons per pulse and a higher peak pulse power with a frequency of 20 hertz, energy of 130 millijoule and a pulse length of 80 picoseconds (Combrink, 2015).

The foundation of the S/LLR at HartRAO was designed by *Endecon Ubuntu (Pty) Ltd Engineering Consultants.* **Appendix A** contains the as built drawing for the shed structure and foundation of the S/LLR at HartRAO. As seen in **Figure 9**, the foundation consists of the base on which the S/LLR is founded and 3 tracks for the runoff shed. **Appendix B** shows photos taken during the construction of the S/LLR at HartroRAO.

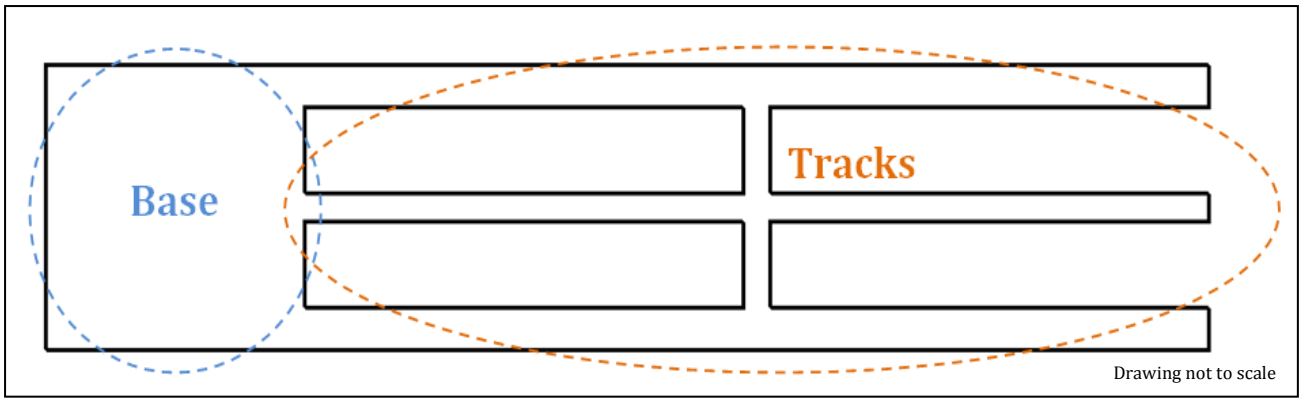

FIGURE 9: SIMPLIFIED DRAWING OF THE FOUNDATION OF THE S/LLR AT HARTRAO

The S/LLR is protected by a runoff shed which opens during operation and closes afterwards. It takes approximately 2 minutes and 30 seconds for the shed to open or close. This process is activated manually. The shed runs on three IPE 180-beam tracks, as seen in **Figure 10**. The strip footings are 25 MPa reinforced concrete and 350 mm deep. The shed is constructed with steel segments, which can be disassembled, resulting in easier transportation.

FIGURE 10: RUNOFF SHED WITH TRACKS

The base consists of a square ground floor which is underlain by two diagonal beams and a deep base at each corner. **Figure 11** shows a detailed drawing of the base and tracks, which is an extract from **Appendix A**. All elements in the base are constructed from 30 MPa reinforced concrete. The ground floor is 350 mm deep, the beams 600 mm deep and the corner bases 1200 mm deep.

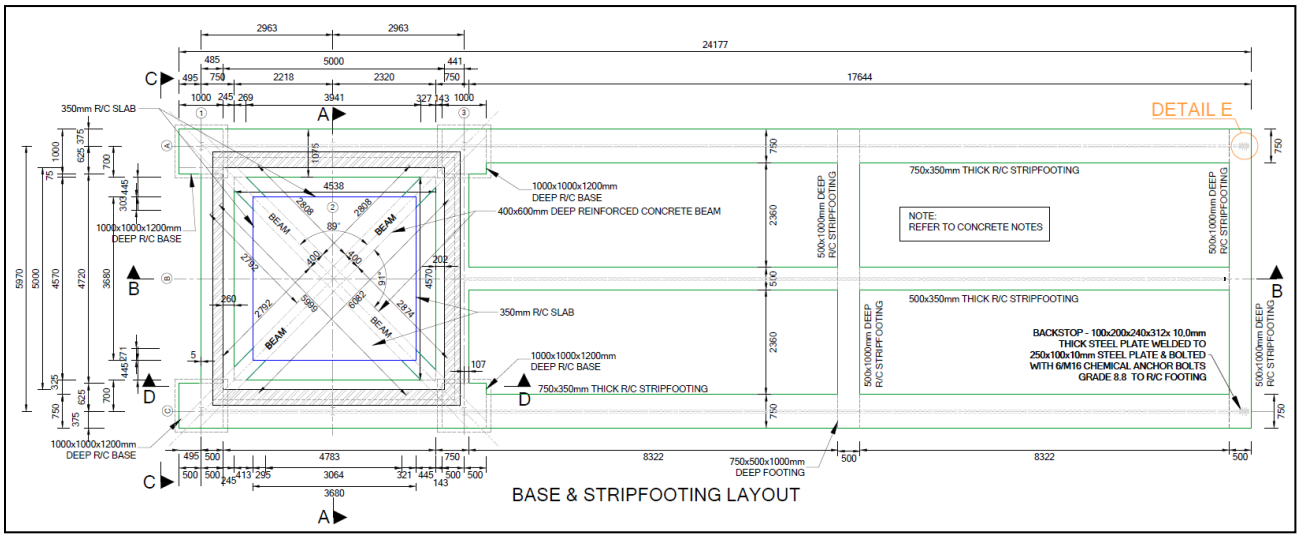

FIGURE 11: DETAILED DRAWING OF THE BASE AND TRACKS

Before ranging can take place, the S/LLR's position needs to be calibrated and this is done with the use of 5 levelling beacons. A beacon is a 0.7 m diameter, 2 m high, concrete pillar, with a corner cube reflector on top. They are placed all around the S/LLR and are founded on bedrock to ensure stability.

The control room is situated next to the S/LLR, built in a temperature regulated container. The room houses the laser table as well as the computers to control operation. The container is placed on the ground, but the laser table's foundation is independent. The legs of the table are drilled through the floor of the container and stand on two I-beams, which are placed on the piers founded on bedrock. **Figure 12** shows the layout of the S/LLR covered by the shed as well as the control room.

FIGURE 12: S/LLR SITE LAYOUT

2.2. GEOLOGY

This section will describe the geology of the Cape- and Karoo- Supergroup with more attention paid to the local geology. Formations found in the study area include the Waaipoort-, Floriskraal- and Kweekvlei- Formations from the Witteberg Group in the Cape Supergroup and the Dwyka Formation and Group in the Karoo Supergroup. **Table 1** indicates each formation as well as where each formation could be found on site. These formations will be discussed in more detail in this section.

TABLE 1: GEOLOGY OF MSGO WITH FORMATIONS ORDERED FROM YOUNGEST (TOP) TO OLDEST

Super-Group	Sub-Group	Formation	Properties	Age	Influence on MSGO site
Karoo	Dwyka	Dwyka	Glacier Diamictite Tillite small to large clasts within a fine-grained clay rich matrix	Carboniferous to Permian Period	Access road from town southwards to contact with Witteberg Group.
Cape	Witteberg	Waaipoort	Shale. Fine-grained shale rock and very porous	Carboniferous Period	Access road further South from contact with Dwyka and S/LLR site.
Cape	Witteberg	Floriskraal	Sandstone. Fine to medium grained rock, more robust	Carboniferous Period	At the S/LLR site.
Cape	Witteberg	Kweekvlei	Shale. Very fine-grained and thinly laminated layers	Carboniferous Period	Small outcrops in the most southern side of the site.

2.2.1. THE CAPE SUPERGROUP

The Cape Supergroup can be found all along the southern and south-western coast in the Western Cape (Brink, 1981) as seen in **Figure 13**. This Group was deposited between 500 – 330 million years ago, also known as the Early Ordovician to the Early Carboniferous period (Johnson *et al.*, 2006). The group can be seen from the north, Niewoudtville towards Ceres and west to Port Alfred. The western part of this group is known for its rugged mountains similar to the Cederberg where harder quartzitic sandstone can be found on the mountain tops and a softer mudrock in the valleys. The southern part constitutes the Cape Fold Belt, which includes mountains such as the Swartberg, Langkloof and Outeniqua with rocks that are severely folded and faulted (Brink, 1981).

The Cape Supergroup consists of three groups namely, the Table Mountain, Bokkeveld and Witteberg Groups. The oldest Group, the Table Mountain Group, is a sandstone sheet subdivided into several formations (Johnson *et al.*, 2006). The Table Mountain Group is conformably overlain by the Bokkeveld Group that comprise of fine-grained sandstone and mudrock. The youngest of the three Groups, the Witteberg Group, consists mostly of sandstones, but also contains finer sediments such as shales, siltstone and mudstone.

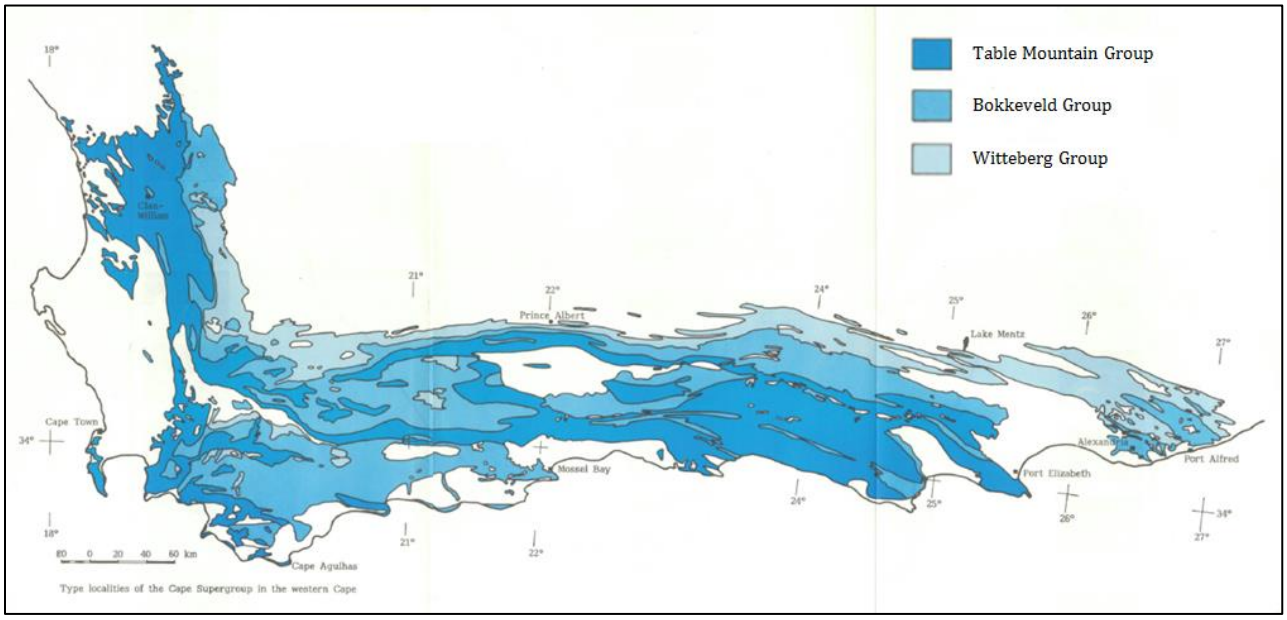

FIGURE 13: LOCATION OF THE CAPE SUPERGROUP ROCKS (BRINK, 1981)

The Cape Supergroup consists of three groups namely, the Table Mountain, Bokkeveld and Witteberg Groups. The oldest Group, the Table Mountain Group, is a sandstone sheet subdivided into several formations (Johnson *et al.*, 2006). The Table Mountain Group is conformably overlain by the Bokkeveld Group that comprise of fine-grained sandstone and mudrock. The youngest of the three Groups, the Witteberg Group, consists mostly of sandstones, but also contains finer sediments such as shales, siltstone and mudstone.

Within the Witteberg Group there are three formations applicable to the study area with Waaipoort Formation as the uppermost and youngest, Floriskraal Formation and the Kweekvlei Formation. They were deposited in the Palaeozoic Era around 370 – 330 million years ago at the time the area was covered by the Agulhas Sea. Primitive fish-, brachiopods- and bivalves- fossils can still be found today (Norman & Whitfield, 2006).

The slopes generally have little soil and vegetation but ample quartzitic debris. According to Brink (1981) the rocks would provide sufficient strength for the founding of structures because of the hardness of the quartzites and quartzitic sandstones. The joint patterns are usually well developed, and should be taken into account.

The aggregate in the Cape Supergroup is prone to alkali reactions (Brink, 1981). It is important to test the reactivity before using it with cement. Some tests done have shown that the quartzites can possibly be reactive. Another problem, according to Brink (1981), can be encountered with rotary drilling. It becomes difficult to recover a good core in interbedded shale layers and often double or triple tube core

barrels are needed to ensure good recovery. The quartzites are quite difficult to drill through and thus the drill rates are slow and time consuming.

2.2.2. THE KAROO SUPERGROUP

The Karoo Supergroup, the biggest basin in Southern Africa, as seen in **Figure 14**, was deposited between 290 – 190 million years ago, also known as the late Carboniferous to the early Jurassic period (Johnson *et al.*, 2006). Radiometric dating showed that some parts of the basin continued to form up until the separation of Africa and South America roughly 120 million years ago. This Supergroup comprises of various rocks with a thickness of nearly 8 kilometres, including mudrock and sandstone, tillite at the bottom, basalt as the top and coal about halfway up (Brink, 1983). The majority of the strata are horizontal, but parts of the basin alongside the Cape Fold Belt have been folded under pressure.

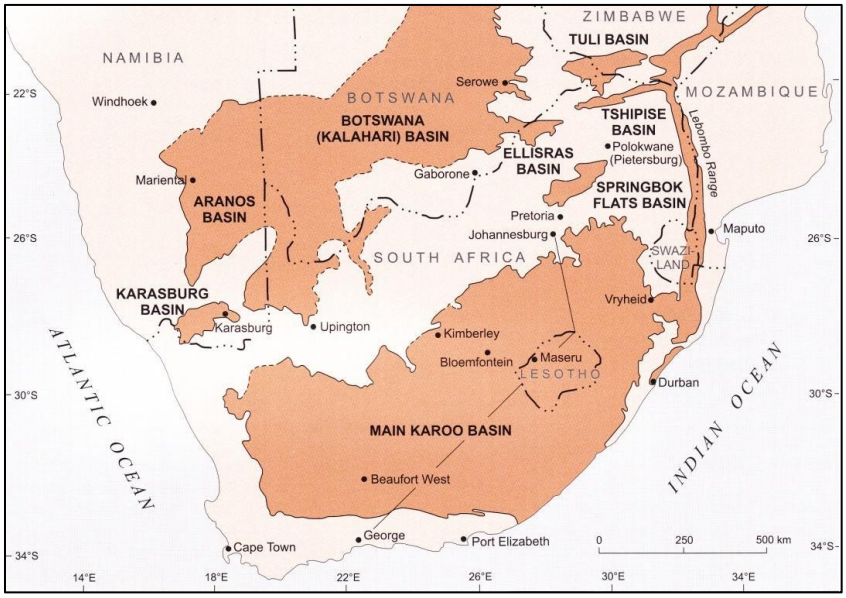

FIGURE 14: LOCATION AND DISTRIBUTION OF THE KAROO BASIN IN SOUTH AFRICA (JOHNSON *ET AL.*, 2006)

The basin consists of the Dwyka group, the Ecca Group, the Beaufort Group, the Drakensberg Group and the Lebombo Group. These rocks include mudrock, sandstone, tillite, basalt, coal and dolerite intrusions (Brink, 1983).

The oldest in the Karoo Supergroup and the youngest in the study area, the Dwyka Formation overlies the Cape Supergroup unconformably in the South with various lithology types that have been recognized (Johnson *et al.*, 2006). The Dwyka Group is a diamicitite tillite formation, consisting of small to large clasts within a fine-grained, clay rich matrix and in some areas, no clasts at all.

Sediment was fed by ice streams into the south-western part of the Karoo Basin. It was redistributed by sediment gravity flows and turbidity currents. Together these deposits formed large subaqueous fans that were controlled by the ice sheet dynamics (Visser *et al.*, 2004).

2.2.3. SWELLING POTENTIAL OF A ROCK MASS

It is important to quantify the potential for swelling of a rock mass as it may have an adverse effect on the stability of tunnels, slopes and foundations (Pettersen, 2014). To be able to determine the swelling potential of a rock mass, a study of the clay minerals is needed. Most clay minerals have a basic structural unit of a silicon-oxygen tetrahedron and an aluminium-hydroxyl octahedron (Craig, 2004). These units combine to form different sheet structures as seen in **Figure 15**. Tetrahedral units combine by the sharing of oxygen ions to form a silica sheet and the octahedral units combine by shared hydroxyl ions to form a gibbsite sheet. The layers are formed by the bonding of a silica sheet with either one or two gibbsite sheets. Stacks of these layers, with different bonding between them, make up the clay minerals particles (Craig, 2004).

Clays, rich in montmorillonite (or smectite), may expand when it comes into contact with water, which means that it has a swelling potential. The degree of expansion depends on the minerals present in the clay. Clay minerals such as montmorillonite, vermiculite, illite or kaolinite can be expected and their sensitivity to water varies. Montmorillonite is a highly expansive clay mineral, where vermiculite is moderately expansive and illite or kaolinite non-expansive.

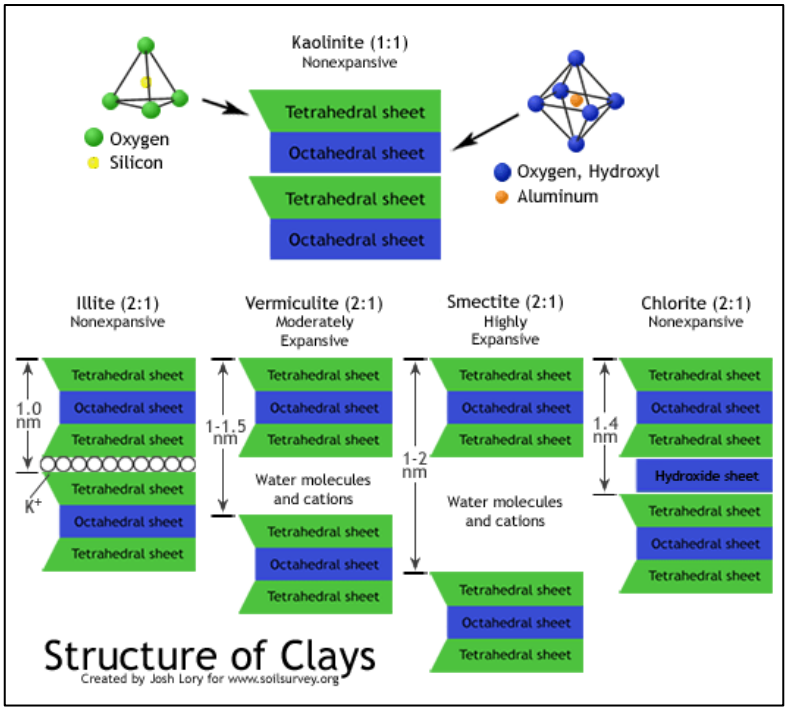

FIGURE 15: STRUCTURE OF CLAYS (LORY, [S.A.])

Two factors are needed to set this expansion into action, namely the internal factor, which is the ability of the clay minerals to expand (chemical composition) and the external factor, the presence of water (Pettersen, 2014). Exposed rock masses can be de- and resaturated which in turn result in swelling and shrinkage and even fracturing (Zhang *et al*., 2010). Clay minerals present in the intact rock will not result in expansion of the rock mass, but clay minerals present in the fractures and cracks may result in expansion.

The chemical composition of clay minerals can be determined by the study of thin sections, also known as petrographic analyses. This is the description and classification of rocks, but this optical identification can be difficult when it is finely grained (Zhang *et al.*, 2010). The better identification method will be by means of x-ray examination.

There are two types of x-ray examination, X-Ray Diffraction (XRD) and X-Ray Fluorescence (XRF). XRD can determine the presence and amounts of minerals species in a sample, as well as identify phases. XRF will give details of the chemical composition of a sample but will not indicate what phases are present in the sample. **Table 2** shows the clay minerals and their corresponding elements and chemical compounds.

TABLE 2: COMPOSITION OF THE CLAY MINERALS SHOWING BOTH ELEMENTS AND CHEMICAL COMPOUNDS (PETTERSEN, 2014)

Montmorillonite: $Na_{0.2}Ca_{0.1}Al_2Si_4O_{10}(OH)_2(H_2O)_{10}$				**Vermiculite:** $Mg_{1.8}Fe^{2+}_{0.9}Al_{4.3}SiO_{10}(OH)_2{\bullet}4(H_2O)$			
Element	**[%]**	**Chemical compound**	**[%]**	**Element**	**[%]**	**Chemical compound**	**[%]**
Sodium (Na)	0.84	Na_2O	1.13	Magnesium (Mg)	8.68	MgO	14.39
Calcium (Ca)	0.73	CaO	1.02	Aluminium (Al)	23.01	Al_2O_3	43.48
Aluminium (Al)	9.83	Al_2O_3	18.57	Iron (Fe)	9.97	FeO	12.82
Silicon (Si)	20.46	SiO_2	43.77	Silicon (Si)	5.57	SiO_2	11.92
Hydrogen (H)	4.04	H_2O	36.09	Hydrogen (H)	2	H_2O	17.87
Oxygen (O)	64.11			Oxygen (O)	50.77		
Illite: $K_{0.6}(H_3O)_{0.4}Al_{1.3}Mg_{0.3}Fe^{2+}_{0.1}Si_{3.5}O_{10}(OH)_2{\bullet}(H_2O)$				**Kaolinite:** $Al_2Si_2O_5(OH)_4$			
Element	**[%]**	**Chemical compound**	**[%]**	**Element**	**[%]**	**Chemical compound**	**[%]**
Potassium (K)	6.03	K_2O	7.26	Aluminium (Al)	20.9	Al_2O_3	39.5
Magnesium (Mg)	1.87	MgO	3.11	Silicon (Si)	21.76	SiO_2	46.55
Aluminium (Al)	9.01	Al_2O_3	17.02	Hydrogen (H)	1.56	H_2O	13.96
Iron (Fe)	1.43	FeO	1.85	Oxygen (O)	55.78		
Silicon (Si)	25.25	SiO_2	54.01				
Hydrogen (H)	1.35	H_2O	12.03				
Oxygen (O)	55.06						

2.3. PREVIOUS STUDIES DONE AT MSGO

There have been various studies done at Matjiesfontein. These studies include slope stability analyses, preliminary designs for the low level water crossings, investigations and solutions for the eroded surface of the access road, services to the site as well as rock mechanics for construction purposes. The relevant topics discussed include foundation requirements for a LLR at MSGO, slope stability analyses, a geotechnical site investigation and an EIA for the MSGO.

2.3.1. RESEARCH INTO THE FOUNDATION REQUIREMENTS FOR A LLR AT MATJIESFONTEIN.

This preliminary study focuses on the foundation requirements for the emplacement of the LLR. The foundation will be responsible for the stable platform from where the LLR will operate (Croukamp *et al.,* 2011). The foundations should be built in such a way that it would cushion even minute movement of the ground. It was suggested that the foundation of the LLR should be isolated from the foundations of the auxiliary buildings as vibrations of footsteps is enough to induce detectable ground movement.

The positions of the LLR need to be calibrated locally before any observations can be done. This will be done by means of at least 4 beacons within about 300 m from the instrument. Each beacon will consist of a circular column with a corner cube reflector on top. These beacons will be embedded into the bedrock to minimize vertical and horizontal movement. Croukamp *et al.,* (2011) found that the total pressure which the foundation and the 7 ton LLR will exert on the rock mass is small compared to the bearing capacity of the rock mass.

Since this study was conducted, the proposed site for the S/LLR has changed, resulting in new research being required.

2.3.2. PALAEO-LANDSLIDES

Waters (2011) investigated palaeo-landslides at the MSGO. There was a need to determine whether the site was safe for development as reactivation of the landslides can have a destabilizing effect on the instruments on site.

The project included the surveying and mapping of two palaeo-landslides. The origin of the landslides had to be determined to evaluate the possibility of reactivation of the slides, or new slides forming in the region. The investigation included a joint survey, a slip-circle analysis, the potential for re-activation of the landslides due to development and the possibility of rock toppling.

Various methods that were used in the assessment showed that slope-failure will not occur under the investigated circumstances. All calculated safety factors were acceptable. Waters (2011), however,

suggested that the study could be improved by further testing and determining at what depth the bedrock layer lies. He concluded that the development could continue as the slopes proved to be stable.

2.3.3. SLOPE STABILITY FOR EMPLACEMENT OF LUNAR LASER RANGER (LLR)

Visser (2012) investigated the slope stability of the area where the LLR was originally intended to be placed. The study was done to determine whether the proposed site was suitable for this emplacement. A new position for the S/LLR has since been identified, but data collected during the Visser study is still valid.

Visser (2012) had done a GPS survey and created a 3D model. Various ways were identified in which the slope was able to fail. On the southern side of the slope, planar failure and circular failure may occur and on the northern side planar and wedge failure. It was concluded that the southern side of the slope was stable, as the safety factors obtained were greater than 1.5. However, on the northern side of the slope it was not stable or safe to cut more than 1 m, should an access road be constructed. Visser (2012) concluded that, if no cuts are to be made on the northern side of the slope, the emplacement of the LLR may continue.

2.3.4. GEOTECHNICAL SITE INVESTIGATION

A geotechnical site investigation was done at Matjiesfontein (Combrinck, *et al.,* 2007), when it was proposed for the new space geodetic observatory. The suitability of the location needed to be verified in order to start with the project.

During the site investigation the following geophysical methods were used:

- Magnetic Method;
- Electromagnetic Method; and
- Seismic Refraction Method.

Geotechnical investigation methods used included a walk-over site survey, digging of test pits and description of the soil profile according to the MCCSSO system. After the investigation was completed, the initial results showed that the site would be suitable for this project, but that further investigation should be done around the foundations of each building. It was also recommended that the palaeo slope failure, on the southern portion of the MSGO site and the northern slope of the Witteberg Mountains, should not be disturbed.

2.3.5. EIA FOR PROPOSED MSGO

Ecosense Consulting Environmentalists cc was approached to do the screening report for the proposed MSGO project. A basic assessment in terms of the National Environmental Management Act Environmental Impact Assessment regulations would be required, because of the river crossings and clearance of vegetation for access roads to the site. It was recommended by Ecosense (2010) that:

1. Alternative location for the emplacement of the instruments must be investigated.
2. An alternative to permanent river crossing structures (temporary structures) should be investigated.
3. Current crossings should be repaired in such a way that it would avoid damming during flash floods.
4. The EIA studies done for the road built by the municipality must be consulted for an operational management plan.

2.4. SLOPE STABILITY

Failures are caused by the geometry of the slope and the type of materials combined with gravity, but is frequently affected by water and water content of the materials. A general term used for all types of failure is *slope movement*. Slope movement can be divided into five different types namely falls, topples, slides, spreads and flows (Mathewson, 1981). **Table 3** shows the classifications of the processes and **Figure 16** illustrates them.

TABLE 3: CLASSIFICATION OF SLOPE PROCESSES (MATHEWSON, 1981)

TYPE OF MOVEMENT	TYPE OF MATERIAL		
	Rock	Soil	
		Coarse Grain	Fine Grain
Fall	Rock Fall	Debris Fall	Earth Fall
Topple	Rock Topple	Debris Topple	Earth Topple
Rotational Slide	Rock Slump	Debris Slump	Earth Slump
Translational	Rock Block Slide	Debris Block Slide	Earth Block Slide
Slide	Rock Slide	Debris Slide	Earth Slide
Spread	Rock Spread	Debris Spread	Earth Spread
Flow	Rock Flow	Debris Flow	Earth Flow
Complex	Combination of Any of the Above		

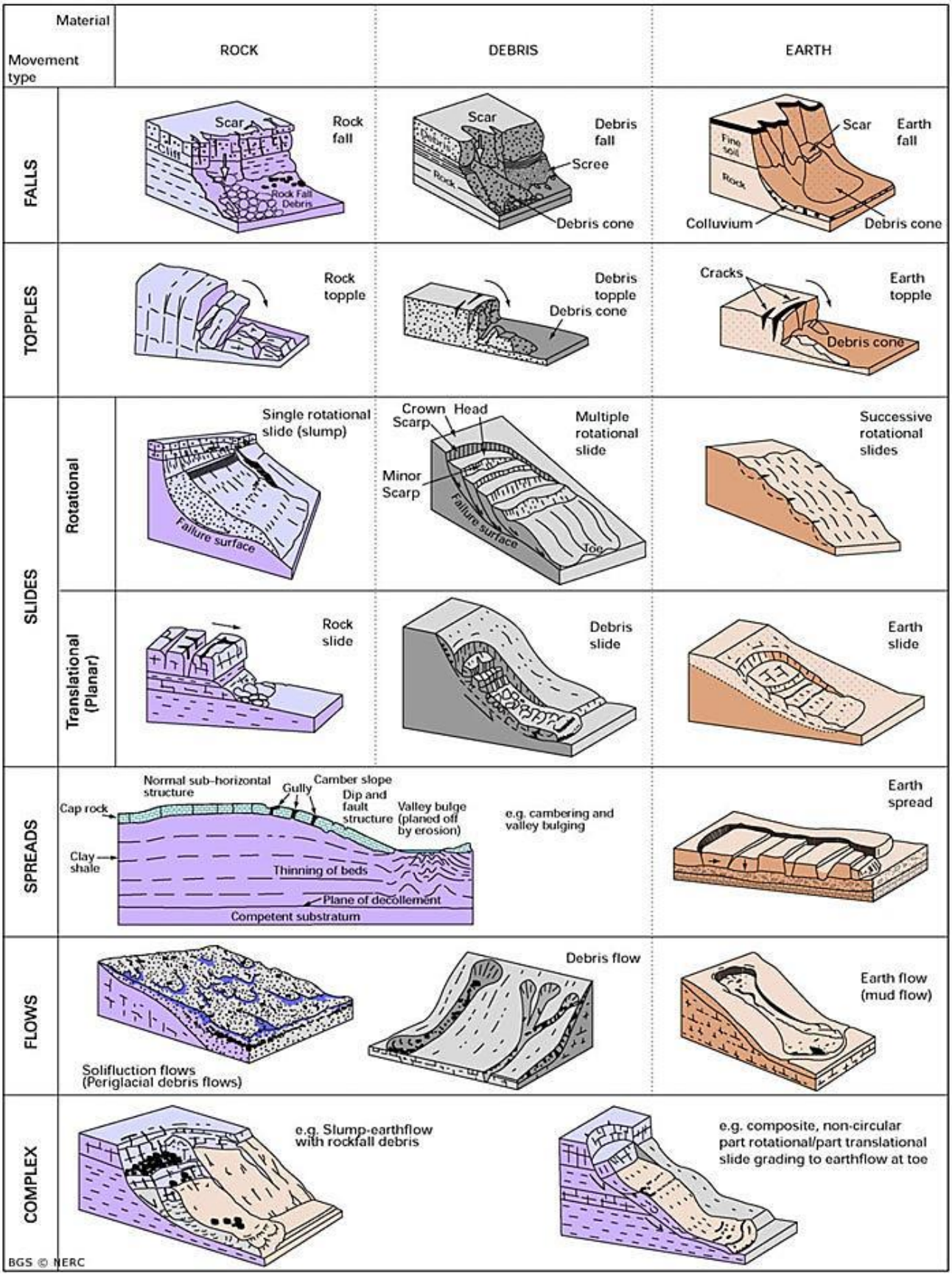

FIGURE 16: CLASSIFICATION OF SLOPE PROCESSES (*ANONYMOUS, 2013*)

Mass wasting can be seen on both submarine and terrestrial slopes, and has been detected on Earth, Mars, Venus, and Jupiter's moon, Io. Factors that change the potential of mass wasting includes any change in slope angle, the weakening of material due to weathering, fluctuation in water content, changes in vegetation cover, and overloading (Tarbuck, 1996).

There are many ways of analysing the safety factors relevant to the stability of the slope. Each type of failure needs to be analysed in a different way to determine its respective factor of safety (FOS). The first step in analysing a slope is to predict the form of failure that can possibly take place. A few key factors also need to be taken into consideration before the analysis starts (Hunt, 2005).

These key factors are:

- History of slope failure in the region and the factors that caused it;
- The slope geometry;
- Indications of instability at the surface (e.g. creep or tension cracks); and
- Weather conditions (rainfall and temperatures).

A mathematical solution can only be formulated if the shape of the failure path can be defined in some way, thus failures such as avalanches and flows cannot be solved mathematically. The four types of failure that were investigated, as shown in **Figure 17**, are **(a)** circular slip, **(b)** planar failure, **(c)** wedge slip and **(d)** toppling. These four types were investigated because they are the main failure types that were expected to potentially occur at the site.

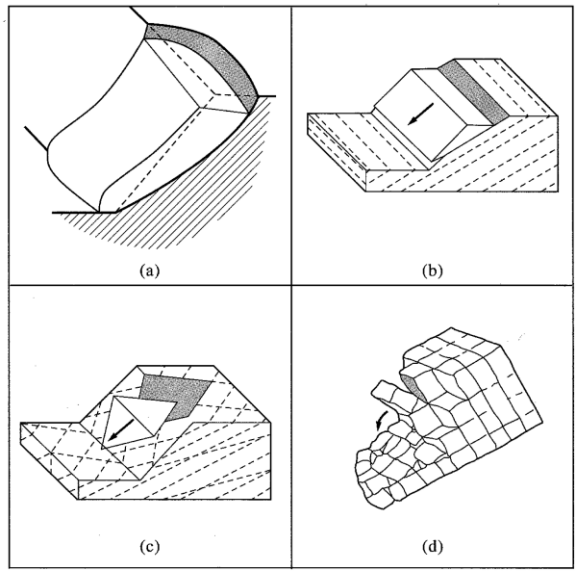

FIGURE 17: FOUR BASIC TYPES OF FAILURE (A) CIRCULAR SLIP, (B) PLANAR FAILURE, (C) WEDGE SLIP AND (D) TOPPLING (HOEK & BRAY, 1981)

2.4.1. CIRCULAR SLIP

Circular slip, or curvilinear slip, is a term used to describe any failure where the slip surface is circular. The type of material determines the shape of the slip circle. If it is isotropic material the surface tends to be circular in section. If it is anisotropic material, the slip surface tends to be elongated in a direction parallel to the structural feature, as illustrated in **Figure 18**.

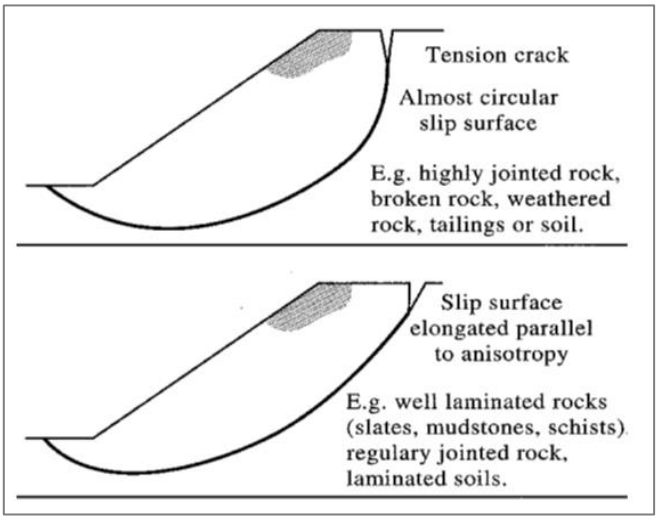

FIGURE 18: SHAPE OF CIRCULAR SLIPS (GOOGLE IMAGES)

The most common way of solving the circular slip problem is by means of the method of slices. By using **Figure 19 (a)** the analysis of the stability with this 2D method can be explained (Craig, 2004). The arc *ABC* is the potential failure surface with centre *O* and radius *r*. The soil above this surface is divided into vertical slices with a width of *b*. The width for each slice does not have to be the same and the base of each slice is assumed to be a straight line (Das, 2002). The forces acting on each slice are obtained by considering the mechanical equilibrium for the slices. **Figure 19 (b)** shows an example of an n^{th} slice. The moment about *O* of each slice is calculated separately and added to determine the destabilising moment. The FOS is determined by the ratio of the stabilising moments to the destabilising moments about point *O*.

As seen in **Figure 19 (b),** there are many unknown parameters, but only three equilibrium equations, resulting in a statically indeterminate calculation. The three equilibrium equations are as follows:

$$\sum F_y = 0 \;\; ; \;\; \sum F_x = 0 \;\; and \;\; \sum M = 0$$

To solve this problem, assumptions need to be made to reduce the number of unknowns. Bishop, Fellenius and Morgenstern etc. all made their own assumptions to simplify the problem. Bishop's assumptions will be discussed as it is the most widely used solution for circular slip. A negative aspect

of Bishop's method is that all equilibrium equations' conditions are not taken into account (De Wet, 2013). Only the moment equilibrium condition is satisfied.

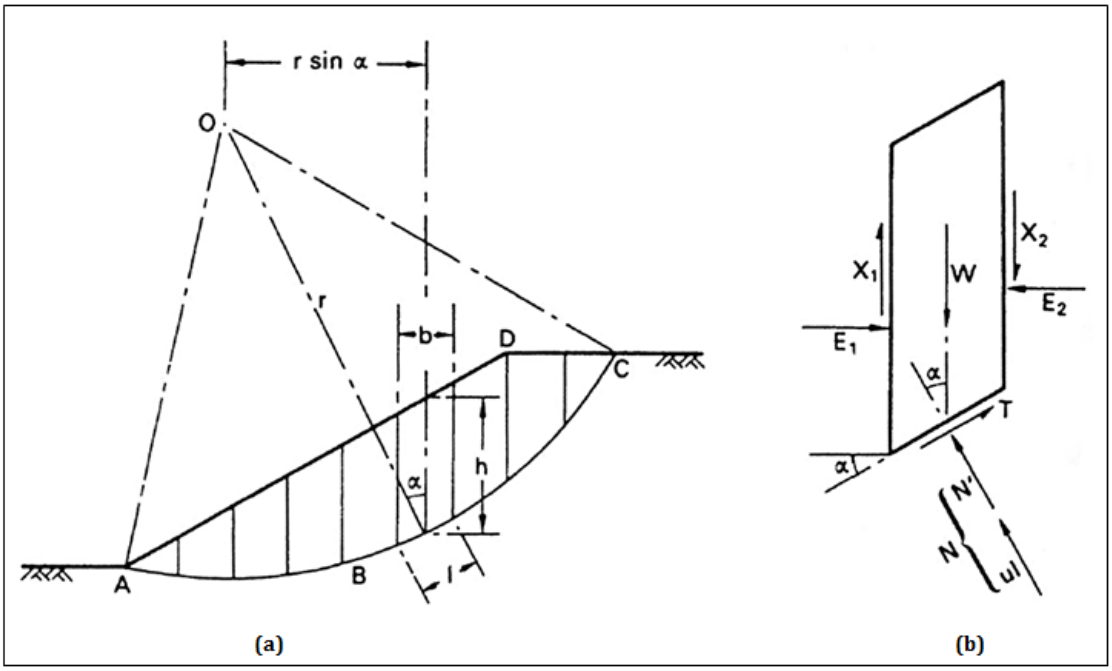

FIGURE 19: STABILITY ANALYSIS WITH THE METHOD OF SLICES (CRAIG, 2004)

Bishop assumed that the resultant forces acting on the sides of each slice are horizontal. Thus:

$$X_1 - X_2 = 0$$

To maintain equilibrium, the shear force on the base of the slices is:

$$T = \frac{1}{F}(c'l + N'tan\emptyset') \tag{1}$$

By resolving the forces in the vertical direction:

$$N' = \frac{\left[W - \left(\frac{c'l}{F}\right) sin \propto -ulcos \propto\right]}{\left[cos \propto + \frac{tan\emptyset' sin\propto}{F}\right]} \tag{2}$$

By manipulating the following equation from the method of slices:

$$F = \frac{c'\, L_a + tan\emptyset' \sum n'}{\sum W \sin \propto} \tag{3}$$

For convenience, substituting $l = bsec \propto$, the equation Bishop use to determine the FOS is as follows:

$$F = \frac{1}{\sum W \sin \propto} \sum \left[\{c'b + (W - ub) tan\emptyset'\} \frac{sec \propto}{1 + \left(\frac{tan \propto tan\emptyset'}{F}\right)} \right] \quad (4)$$

As the FOS appears on both sides of the equation, a process of approximation (Craig, 2004) must be used to solve *F*. Due to the fact that this iteration needs to be done for a large number of trial surfaces, solution by computer software is ideal. With software, more complex slope geometry can be solved.

2.4.2. PLANAR FAILURE

A planar slide is a mass that slides downward on top of another inclined plane. This failure surface is usually a structural discontinuity, such as bedding planes, faults, and joints or the interface between bedrock and an overlying layer of weathered rock (Hunt, 2005). Planar failure is rare compared to other types of failures, because of the geometric conditions needed to make it kinematically feasible. **Figure 20** illustrates the feasibility.

There are a few things that need to be considered to determine the feasibility of such a failure, namely:

- The dip of the slope must exceed the dip of the potential slip plane;
- The potential slip plane must daylight on the slope plane;
- The dip of the potential slip plane must be such that the strength of the plane is reached; and
- The slip plane must strike within 20° to the slope plane.

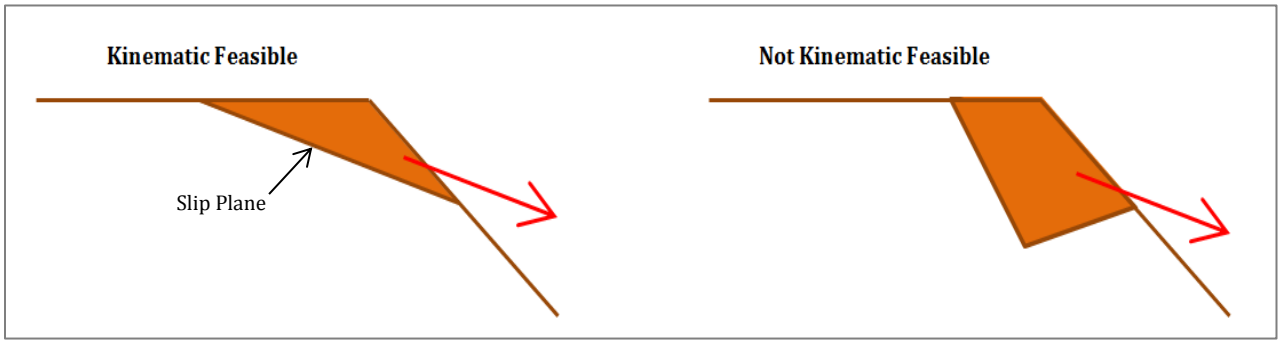

FIGURE 20: KINEMATIC ANALYSIS OF PLANE SLIDING

In order to analyse planar failure, a few assumptions have to be made. These assumptions include:

- The sliding mass translates as a rigid body;
- The sliding mass does not undergo any rigid body rotation;
- All forces acting on the body pass through its centroid; and
- Distribution of stress along the sliding plane is constant.

If all the above assumptions are combined, the analysis of planar failure is very close to the calculations done for a block sliding down an inclined plane as indicated in **Figure 21**.

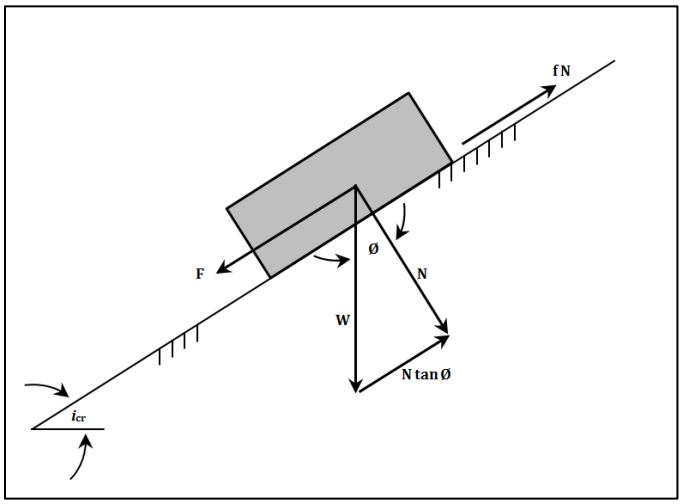

FIGURE 21: BLOCK SLIDING DOWN AN INCLINED PLANE (HUNT, 2005)

The factor of safety (FOS) for planar failure can be defined as follows:

$$FS = \frac{Total\ Resisting\ Force}{Total\ Driving\ \ Force}$$

The resisting force comprises of the shear strength of the failure plane and other external forces to stabilize the plane. The driving force consists of the component down slope due to gravity, external (upper slope) forces and other forces generated by seismic activity or water pressures.

By assuming that this is a single planar failure with no water pressures present, the driving force, F (weight component) can be defined as:

$$F_{Driving} = W \sin i \tag{5}$$

The resisting force, T is:

$$\begin{aligned} T &= N \tan Ø \\ &= (W \cos i) \tan Ø \end{aligned} \tag{6}$$

Thus the FOS is:

$$FS = \frac{(W \cos i) \tan Ø}{W \sin i} \tag{7}$$

Where $i_{cr} = Ø$

2.4.3. WEDGE FAILURE

Wedge failure can be seen as a special case of planar failure. It can be considered as sliding along two planes simultaneously. There are 3 things to consider while determining the feasibility of such a failure:

- The dip of the slope must exceed the dip of the line of intersection of the two wedge-forming discontinuity planes;
- The same line of intersection must daylight on the slope plane; and
- The dip of the line of intersection must be such that the strength of two planes is reached.

To understand wedge failure, some geometrical terms need to be defined. The dip is the inclination of a discontinuity plane to the horizontal. The dip direction is the direction measured clockwise from north, of the horizontal trace of the line of dip. The strike can be defined as the trace of the intersection of an obliquely inclined plane with a horizontal reference plane. It is always at a right angle to the dip direction (Hoek & Bray, 1981). **Figure 22** illustrates the difference between the strike, the dip direction and the angle of dip.

According to Hoek & Bray (1981) the following assumptions are made when analysing wedge failures:

- The wedge keeps contact with both discontinuities during the slide;
- The wedge is not influenced by moments;
- The shear strength is defined by a linear relationship; and
- The sliding of the wedge is kinematically possible.

With wedge failure, the data needs to be presented by means of a stereonet, as seen in **Figure 23 (a)**. Equal area projection is used to represent spherical shapes of the earth on a flat surface. By adapting this technique, it can be used to plot the traces of planes of discontinuity as in **Figure 23 (b)**.

2.4.4. TOPPLING

Toppling, as seen in **Figure 16** and **Figure 17 (d)**, is another main type of failure. There are two types of toppling that can occur, namely direct and flexural toppling. Direct toppling occurs when the centre of gravity lies outside the outline of the block and topples over, due to a big overturning moment. Flexural toppling occurs when a layered rock mass outcrop at a rock slope and the principle stresses are parallel to the slope. This triggers a slip between the layers causing intact rock to fracture and overturn.

The stability of toppling can be analysed by numerical and physical models. These analyses can be time consuming and the facilities required to do such analysis may not be readily available (Duncan, 1980).

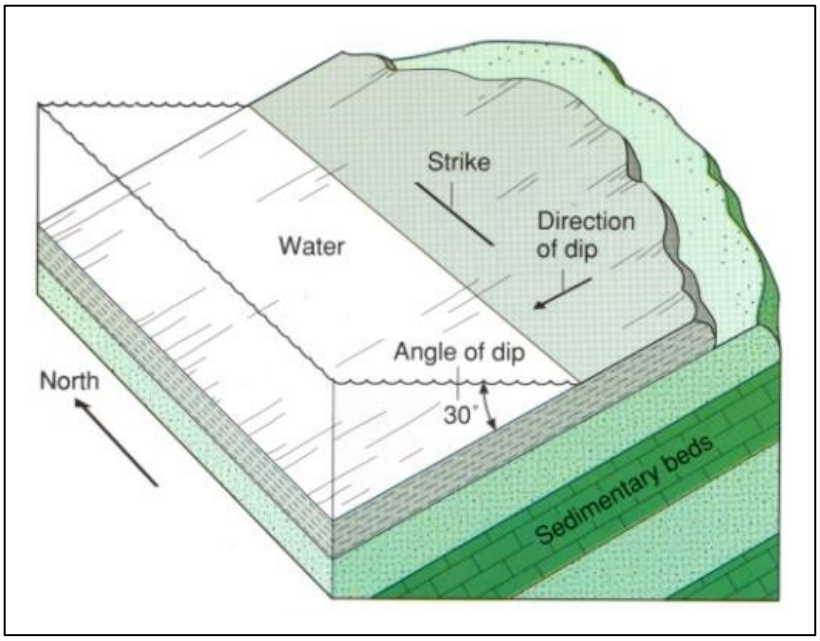

FIGURE 22: DEFINITION OF GEOMETRICAL TERMS (GOOGLE IMAGE)

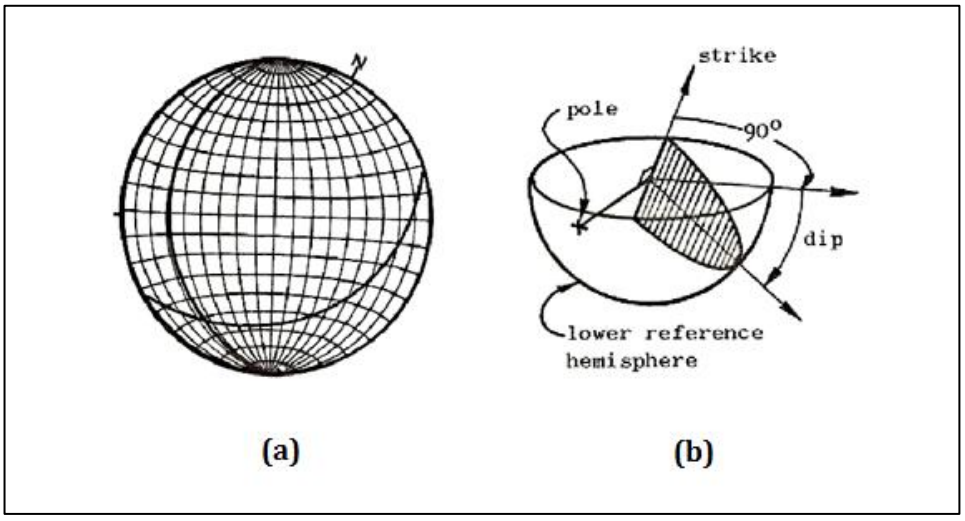

FIGURE 23: GRAPHICAL PRESENTATION OF WEDGE FAILURE (HOEK & BRAY, 1981)

2.5. FOUNDATION TYPES

The purpose of foundations is to transfer the load of the structure to the surrounding ground (Day, 2014). Different types of foundations are used for different conditions on site. There are two main types of foundations, namely shallow foundations and deep foundations. Shallow foundations include spread footings and raft footings, where-as deep foundations include piles and spread footings. **Figure 24** shows the different types of foundations.

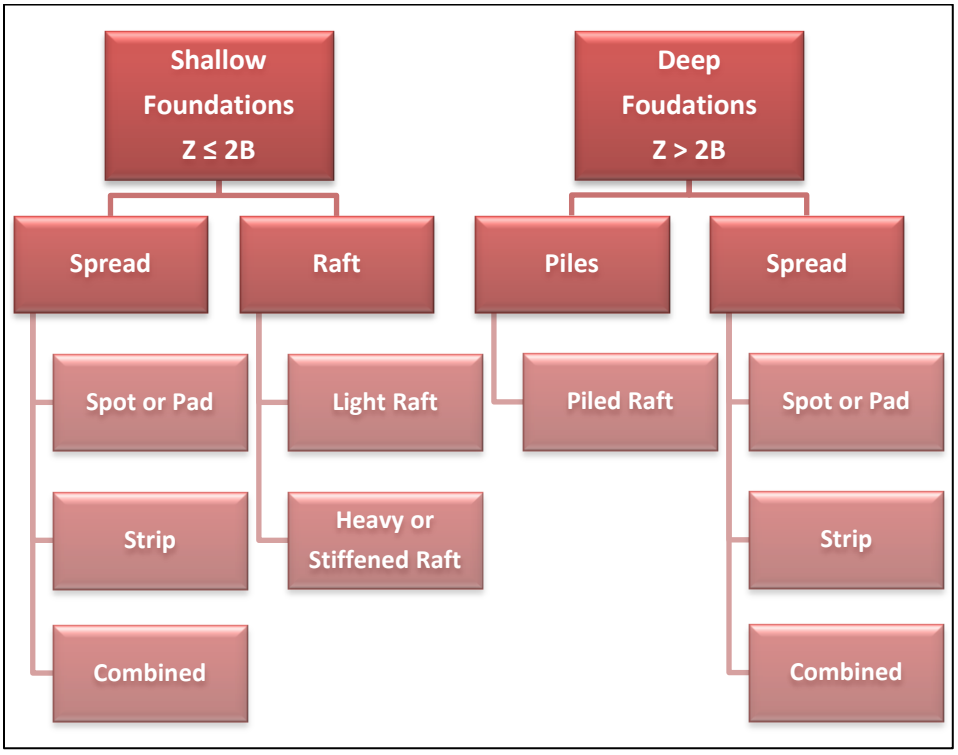

FIGURE 24: DIFFERENT TYPES OF FOUNDATIONS (DAY, 2014)

2.5.1 SHALLOW FOUNDATIONS: SPREAD FOOTINGS

Spread footings consist of spot or pad footings, strip footings or a combination of the two. These are typical isolated footings that are easy to construct and design, are reinforced and concentrically loaded. Spot or pad footings are square, rectangular or circular and are used below a column or a point load (Day, 2014). Even though they are easy to construct and design, they settle and rotate independently from the other footings, which may cause damage to the structure. Strip footings have a length over width ratio of more than 5 and are typically used below walls or other line loads. However, have a poor capacity to resist transverse moments. Combined footings are suitable for paired and eccentric loads, but have a limited lateral load and moment capacity.

2.5.2. SHALLOW FOUNDATIONS: RAFT FOOTINGS

Raft foundations can be divided into two categories: light raft foundations and heavy or stiffened raft foundations. Both types of rafts can be used as a combined floor slab and foundation. Light raft foundations or "slab-on-grade" foundations are normally used together with a soil raft to form a foundation (Day, 2014). This is suitable for light line loads, typically found in smaller houses. It is easy to construct but it has a low resistance to bending and is thus not suitable for unstable grounds. Stiffened rafts have a high bending stiffness and therefore can be used on heaving clays or to span dolomite sinkholes. It is suitable for light and heavy structures, but costs more than strip footings, especially for large structures.

2.5.3. DEEP FOUNDATIONS: PILES

Piles are commonly used where the bedrock is very deep and where high axial stiffness and low settlement are required. They are often used in groups, but there are many different types for different conditions. There are three classifications of the construction of piles:

- Displacement or replacement;
- Driven or excavated; and
- Cast *in situ.*

Displacement piles are put in place without removing the soil, for e.g. hammering a precast pile or screwing a pile into the ground. Replacement piles are constructed by replacing the soil with a stronger material such as concrete or steel (Day, 2014).

Piled raft foundations are a combination of shallow and deep footings. The piles are placed only to increase the vertical stiffness of the ground; the piles stop short of the rocks. The raft provides the stiffness and the piles reduce the settlement, but do not carry the full load and are typically used for high-rise buildings and large tanks.

CHAPTER 3: DATA COLLECTION

Before evaluation can take place data needs to be collected and tests need to be done to determine the characteristics of the materials on site. This section deals with all the activities associated with collection of data on the site, including fieldwork and laboratory testing.

3.1. FIELD SURVEY AND TESTS

In this section, the methods of the field tests that were done will be discussed, which included geometric data capturing, a joint survey, Dynamic Cone Penetrometer (DCP) tests and core drilling.

3.1.1. GEOMETRIC DATA CAPTURING

A survey of the area adjacent to the S/LLR's location was done and a three dimensional (3D) model was then created with coordinates accurate to 5 cm. The data was captured with a Trimble R4 GPS system which consists of a GPS atop of a 2 m pole. The pole enables the device to maintain a constant height above ground-level and the 2 m of height above ground-level is automatically corrected in the calculations done by the GPS. The data points were taken on a grid of roughly every 5 m. Points were taken closer to one another in areas where a sudden change in height occurred, to ensure the 3D model would represent the area appropriately. Measurements were taken in post processing mode, which will ensure that bad weather or cloud coverage will not affect the data. Once the survey was completed, *Trimble Business Center* software was used to process the data. After processing the data, it was exported to an Excel file, which can be opened or used by various software packages such as *Surfer* and *Arc Scene*. This model was used to determine the slope stability, as well as to be an addition to the 3D model of the whole MSGO site.

3.1.2. JOINT SURVEY

A joint survey was done to determine the dip and strike of the rocky outcrops, by means of the application *Rocklogger*. This is a rock logging application by RockGecko, developed for geologists with Android devices and it uses the device's orientation, compass and GPS sensors to measure the dip & strike, or dip & dip direction of rock outcrops. The BreitHaupt Kassel Compass was used to calibrate and test whether the application gave accurate values.

The data from the joint survey was processed with *Stereonet8*. The stereonet obtained from this software can be seen in **Figure 25**. The three main dip directions, as seen in **Table 4,** was identified form the Rose diagram in the centre of **Figure 25**.

TABLE 4: MAIN DIP DIRECTIONS

	Dip	Strike
Direction 1	17	66
Direction 2	10	195
Direction 3	9	155

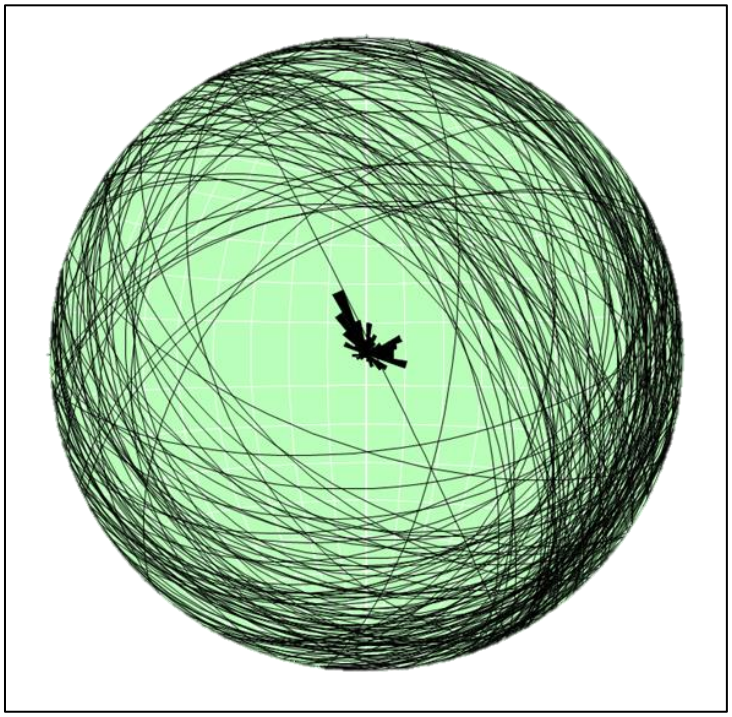

FIGURE 25: STEREONET FROM SOFTWARE

3.1.3. DYNAMIC CONE PENETROMETER TEST

The dynamic cone penetrometer (DCP) test is done to determine the stiffness and strength of the soil. From these values one can determine the different layers and give an indication of excavatability. The DCP has four parts, namely an 8 kg hammer, the upper rod, a ruler, a bottom rod and a 60° angle cone. The hammer falls a distance of 575 mm and the cone, at the end or tip of the bottom rod, penetrates the soil. **Figure 26** shows an illustration of the components of the DCP. The penetration depth after 5 blows (hammer falls) is captured and this continues until a maximum depth of 900 mm is reached, or if solid rock is reached. It can be considered solid rock if after 15 blows the cone does not penetrate any further.

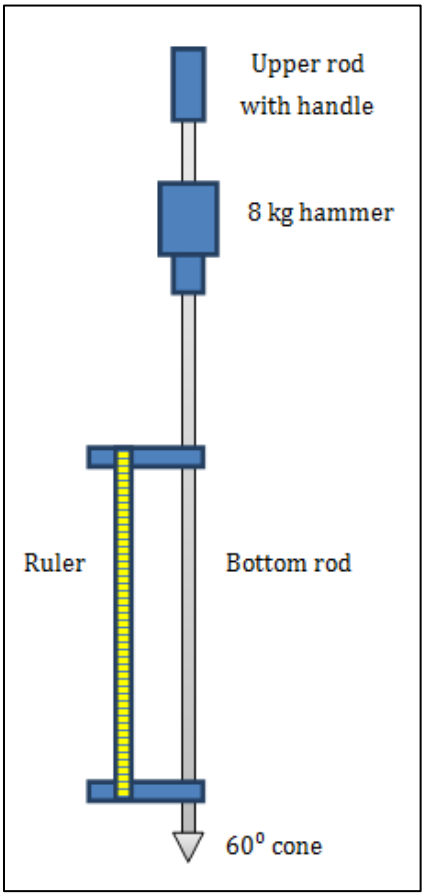

FIGURE 26: COMPONENTS OF THE DCP

The DCP test was done to determine the approximate depth to bedrock. Six DCP tests were done in the surroundings of the S/LLR's location. The data collected from the DCP tests can be seen in **Table 5**. It was important to keep the upper rod as straight as possible as penetration should be at a right angle to the ground level.

TABLE 5: DATA FROM DCP TESTS

Blows	Penetration Depth in [mm]					
	Test 1	Test 2	Test 3	Test 4	Test 5	Test 6
0	55	20	30	40	50	60
5	140	60	40	35	55	55
10	165	105	95	110	135	125
15	180	130	115	145	170	140
20	195	145	125	160	205	145
25	200	160	135	175	220	155
30	205	175	145	185	235	160
35	215	185	155	195	240	170
40	220	200	160	200	245	180
45	225	210	165	210	250	190
50	230	220	170	215	255	205
55	240	230	170	230	255	210
60	240	230	170	240	255	225
65	245	240		245		240
70		245		250		250
75		245		255		260
80		250		260		270
85		260		265		295
90		260		275		315
95				280		330
100				290		340
105				305		350
110				315		360
115				330		365
120				345		375
125				360		385
130				375		390
135				385		400
140				395		415
145				400		430
150				405		430
155				410		440
160				415		450
165						455
170						460
175						465
180						470

3.1.4. CORE DRILLING

Shallow core drilling was done to determine how deep the rock is weathered, to do the unconfined compression strength (UCS) test and point load test to determine the strength. Petrographic studies were also done to determine the mineralogy. The topsoil was removed before drilling, to allow the drill to go deeper into the rock. The depth of soil removed was determined by the DCP test as discussed in ***Section 3.1.3***.

The three borehole locations were chosen in such a way that it would give a representation of the whole area where the foundation would be. It was important to ensure, after each barrel of core was removed from the borehole, that it was placed in the correct order into the core box. **Figure 27** shows **(a)** the core drilling machine, **(b)** a sample of core from borehole 1 and **(c)** the core samples in the core box. Borehole 1 starts at the top right corner, borehole 2 in the middle and borehole 3 on the left. Once the drilling was completed the core needed to be logged, as seen in **Table 6,** and this procedure was done according to the Core Logging Committee of the South African Section of the Association of Engineering Geologists (1976).

FIGURE 27: (A) CORE DRILLING MACHINE, (B) CORE SAMPLE AND (C) CORE SAMPLES IN CORE BOX

TABLE 6: CORE LOGGING SHEET

SCHEME SITE	Matjiesfontein Space Geodesy Site													BH				SHEET OF		LOGGED BY	Susan Bothma	DATE LOGGED	11-Jun-2015
																		Core photographed, date			18-Jun-2015		
GRAIN SIZE		1	Fine	2	Medium	3	Coarse	ROCK FABRIC TYPE		1	Massive	2	Bedded	3	Folliated	4	Cleaved	5	Schistose	6	Gneissose	7	Laminated
RECOVERY							ROCK FABRIC			JOINTS													
DEPTH (m)	MATER. RECOV	CORE RECOV.		R.Q.D. (0.10m)			Grain size	Fabric type	Fabric spacing (mm)	Fabric inclin.	No of sets	Inclin.(S)	Spacing (mm)	Roughness	Fill type	Fill thickness (mm)	Fracture frequency	GENERAL DESCRIPTION Weathering, Joint spacing, Colour, Fabric, Strength, Rock name, Interpretive remarks					
0.45																							
0.78	60%	100%		0%			1	3	5	45°	>50	45°	10	Very Rough	Filled	1	>20	Highly weathered, Closely jointed, Greyish Banded White & Red, Fine grained, Medium hard rock, Phyllite, Loose fragments.					
												-30°	20	Very Rough	Filled	1	>20						
1.08	100%	100%		100%			1	3	50	45°	4	45°	>50	Rough	Filled	1	3	Slightly weathered, Medium jointed, Greyish Banded White & Red, Fine grained, Medium hard rock, Solid piece of core.					
												-45°	>50	Rough	Filled	1	2						
1.45	100%	100%		(290/370) = 78%			1	3	>10	45°	>5	45°	>50	Rough	Filled	1	4	Slightly weathered, Medium jointed, Greyish Banded White & Red, Fine grained, Medium hard rock, Loose fragments.					
												-45°	>50	Rough	Filled	1	3						
0.57																							
0.72	60%	0%		0%			1	3	>10	45°	>50	45°	-	Very Rough	Filled	1	>20	Highly weathered, Closely jointed, Blackish Banded White, Fine grained, Soft rock, Phyllite, Loose fragments.					
												-80°	-	Very Rough	Filled	1	>20						
1.32	90%	40%		(200/600) = 33%			1	3	>2	90°	3	90°	-	Rough	Filled	1	1	Slightly weathered, Medium jointed, Greyish Banded White, Fine grained, Medium hard rock, 1 core and big fragments.					
												-45°	50	Rough	Filled	1	2						
												70°	-	Rough	Filled	1	1						
1.97	90%	95%		(330+190/ 650) = 80%			1	3	2-5	80°	2	0°	100	Rough	Filled	1	3	Slightly weathered, Medium jointed, Greyish Banded White, Fine grained, Medium hard rock, Solid piece of core.					
												80°	-	Rough	Filled	1	1						
0.5																							
1	90%	50%		(200/500) = 40%			1	3	>5	45°	2	45°	>50	Rough	Filled	1	10	Slightly weathered, Closely jointed, Brownish Streaked White & Red, Fine grained, Soft rock, Phyllite, 1 core and loose fragments.					
												80°	-	Very Rough	Filled	>1	2						
1.48	80%	10%		(100/480) = 21%			1	3	>5	45°	>2	45°	>30	Rough	Filled	1	>20	Medium weathered, Closely jointed, Brownish Streaked White & Red, Fine grained, Soft rock, Phyllite, weathered with fragments of 5 - 8 cm.					
												60°	50	Rough	Filled	1	1						

3.2. LABORATORY TESTS

Three tests were done in the laboratory; these tests include the unconfined compression strength test (UCS), the point load test, as well as petrographic analyses.

3.2.1. UNCONFINED COMPRESSION TEST

The unconfined compression strength test (UCS) was done in accordance with the American Society of Testing and Materials (ASTM) code number D2938-02 [6] (2002) requirements. Samples from the core drilling were chosen and handled as described below.

Preparation of the sample

The samples selected from the core needs to represent an average of the rock type and need to be prepared as follows:

1. The specimen should be cut at right angles to the longitudinal axis.
2. The diameter and length should be determined to the nearest 0.1 mm and the weight to the nearest 0.01 kg.
3. The length-to-diameter ratio should be between 2.0 and 2.5, with a diameter not less than 47 mm.

Test procedure

The specimens prepared as above should be tested as follows:

1. Wipe clean the upper and lower face of the bearing faces and the specimen.
2. Place the specimen on the lower bearing face and align properly. A small axial load of 100 N may be applied if needed.
3. Apply the load continuously and without shock in such a way that failure will be reached within 2 to 15 minutes. The applied rate of the force should be the same for all the samples.
4. Record the maximum load that the specimen can bear.

Calculations

1. **Cross-sectional area** of the specimen, A, in [m^2]:

$$A = \frac{\pi D^2}{4} \tag{8}$$

Where: D = average specimen diameter in [m].

2. **Volume** of the specimen, V, in [m^3]:

$$V = A \times L \tag{9}$$

Where: L = average specimen length in [m] and

A = cross-sectional area of the specimen in [m^2].

3. **Density** of the specimen, ρ, in [kg/m^3]:

$$\rho = \frac{M}{V} \tag{10}$$

Where: M = average specimen mass in [kg] and

V = volume of the specimen in [m^2].

4. **Compressive strength** of the specimen, σ, in (Pa):

$$\sigma = \frac{P}{A} \tag{11}$$

Where: P = maximum load in [N] and

A = cross-sectional area of the specimen in [m^2].

Only samples from boreholes one and two met the minimum requirements, and no sample from borehole three could be tested. **Figure 28 (a)** shows a sample in the UCS test machine and **(b)** the sample after failure. The data obtained from the UCS test can be seen in **Table 7**. **Appendix C** shows figures of all of the samples after testing.

TABLE 7: UCS TEST DATA

Sample	Diameter	Area	Length	Volume	Mass	Density	Maximum Load	Compressive Strength
	D	A	L	V	M	ρ	P	σ
	[m]	[m^2]	[m]	[m^3]	[kg]	[kg/m^3]	[kN]	[MPa]
1C	0.093	0.01	0.154	0.001046	2.64	2523.64	55.9	8.23
2C	0.093	0.01	0.129	0.000876	2.245	2561.95	112.5	16.56
2D	0.093	0.01	0.099	0.000672	1.656	2462.46	66.2	9.75
2E	0.093	0.01	0.161	0.001094	2.829	2586.73	70.8	10.42

FIGURE 28: (A) SAMPLE IN UCS TESTING MACHINE AND (B) SAMPLE AFTER FAILURE

3.2.2. POINT LOAD TEST

The point load test was done in accordance with the ISRM suggested method for determining point load strength (Ulusay and Hudson, 2006). Samples for this test were obtained from the core drilling.

Preparation of the sample

The point load test can be done on various sample types, either from a core, cut blocks, or irregular lumps. **Figure 29** illustrates **(a)** the diametral, **(b)** axial test, **(c)** the block test and **(d)** the irregular lump test. The sample type explained in this section is the block test.

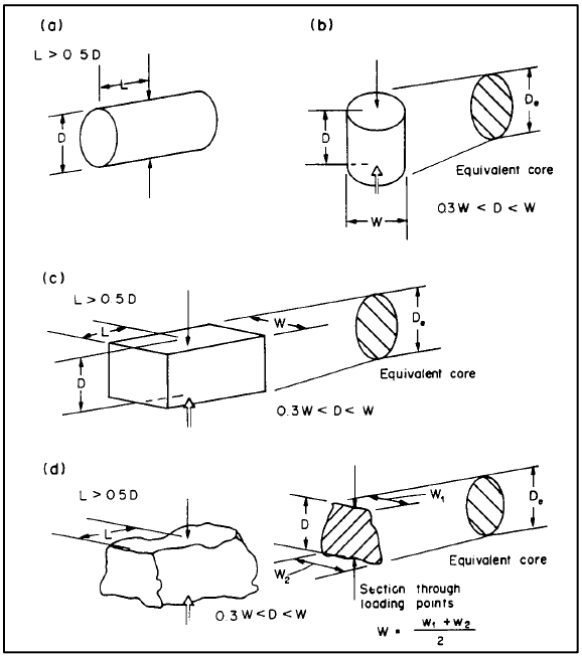

FIGURE 29: SPECIMEN SHAPE REQUIREMENTS FOR (A) THE DIAMETRAL TEST, (B) THE AXIAL TEST, (C) THE BLOCK TEST, AND (D) THE IRREGULAR LUMP TEST (ULUSAY AND HUDSON, 2006)

The samples selected needs to represent an average of the rock type and need to be prepared in the following manner:

1. Lumps of size 50 ± 35 mm and the shape in **Figure 29 (c)** are suitable for this test.
2. The depth (D) over width (W) ratio should be between 0.3 and 1.
3. The length (L) should be at least half of the width (W).
4. The sample may be trimmed into smaller specimens by saw cutting.

Test procedure

The specimens prepared as above, should be tested as follows:

1. The specimen is placed between the two platens and a small load should be applied to keep the specimen in place.

2. Apply the load continuously and in such a way that failure will be reached within 10 to 60 seconds.
3. The test should be rejected if failure passes through only one loading point.
4. The failure load (P) should be recorded.

Calculations

1. **Cross-sectional area** of the specimen, A, in [m²]:

$$A = W \times D \tag{12}$$

Where: W = width of specimen in [m] and

D = depth of specimen in [m].

2. **Equivalent core diameter** for rock lump, ${D_e}^2$, in [m]:

$${D_e}^2 = \frac{4A}{\pi} \tag{13}$$

Where: A = cross-sectional area of the specimen in [m²].

3. **Size Correlation Factor**, F:

$$F = \left(\frac{D_e}{0.050}\right)^{0.45} \tag{14}$$

Where: D_e = equivalent core diameter for rock lump in [m].

4. **Corrected Point Load Strength Index,** Is_{50}, in (Pa):

$$Is_{50} = \frac{P}{{D_e}^2} \times F \tag{15}$$

Where: P = failure Load in [N];

${D_e}^2$ = equivalent core diameter for rock lump in [m] and

F = size correlation Factor.

Samples from all boreholes met the standards and could be used for the test. As the diameter of the core samples were 100 mm and the point load test machine could only test samples of a maximum of 75 mm, the samples were cut into blocks. Thus the block test was performed. **Figure 30 (a)** shows the point load test machine, **(b)** the sample in the point load machine and **(c), (d)** and **(e)** show the samples after failure. The test on sample 2G (**Figure 30 (e)**) should be rejected as the failure passed through only one loading point. **Appendix D** shows figures of all of the samples tested. The data obtained from the point load test can be seen in **Table 8**.

TABLE 8: POINT LOAD TEST DATA

Sample	Width	Depth	Area	Equivalent core diameter		Size Correlation Factor	Failure Load	Point load index
	W	D	A	${D_e}^2$	D_e	F	P	Is_{50}
	[m]	[m]	[m^2]	[m^2]	[m]		[N]	[MPa]
1D	0.07980	0.06125	0.00489	0.00622	0.07889	1.22777	3969	0.78303
1E	0.05921	0.07034	0.00416	0.00530	0.07282	1.18434	3402	0.75981
~~**2G**~~	~~0.07450~~	~~0.06027~~	~~0.00449~~	~~0.00572~~	~~0.07561~~	~~1.20455~~	~~5670~~	~~1.19465~~
2F	0.06141	0.05889	0.00362	0.00460	0.06786	1.14731	4536	1.13022
3C	0.06190	0.05453	0.00338	0.00430	0.06556	1.12964	1701	0.44711
3D	0.05767	0.05714	0.00330	0.00420	0.06477	1.12355	1701	0.45551
3E	0.05970	0.07641	0.00456	0.00581	0.07621	1.20885	2835	0.59005
3F	0.05828	0.05764	0.00336	0.00428	0.06540	1.12843	1701	0.44877

FIGURE 30: (A) POINT LOAD TEST MACHINE, (B) SAMPLE IN POINT LOAD TEST MACHINE AND (C), (D) AND (E) SHOWS SAMPLES AFTER FAILURE

3.2.3. PETROGRAPHIC ANALYSIS

Literature suggests that there are significant similarities between the Waaipoort and underlying Floriskraal Formation mudrock facies. Samples were investigated petrographically to verify the stratigtraphic position thereof.

Samples investigated showed very little variations and can be described as rhythmites, comprising alternating coarser and finer grained material with different compositions and colours associated with each layer (**Figure 31**). The petrographic study showed that the degree of sorting vary from poorly to moderately sorted. Grains are typically sub-angular to sub-rounded, and this probably implies a short transport distance of sediments from the source location. Mineral composition in sediments varies considerably as a function of particle size. The quartz content of the studied rocks varies according to grain size distribution from 10 to 70% approximately. Quartz is the dominant detrital grain constituent and the highest quartz content is found in Sample No. 3A. Quartz grains typically present uniform to undulose extinction under stage rotation, and commonly exhibit quartz overgrowths at the margins (**Figure 32**). Undulose extinction is a result of strain or grain fracturing which can either be inherited from the sediment source or resulting from mechanical compaction.

Other major detrital components are feldspar. Feldspathic alterations are very difficult to examine under a petrographic microscope due to the fine-grained nature of the rocks. Also due to the very fine grained nature of the rocks, it was not possible to distinguish known heavy minerals (zircon, rutile, tourmaline, and apatite), usually found in varying proportions in this unit.

The matrix generally ranges from 5 to 80%, in some layers, and is dominated by detrital clay. Mica (predominantly biotite) is a typical constituent and in some cases exhibit alteration to clay-rich mica or clay minerals such as kaolinite and chlorite. Micas do not possess a predominant preferred orientation, although some grains are aligned. These minerals occur as both subangular grains and aggregates. Opaque minerals (Iron oxide) form a significant portion of the matrix. In **Appendix E,** the description of each sample as well as photos can be seen.

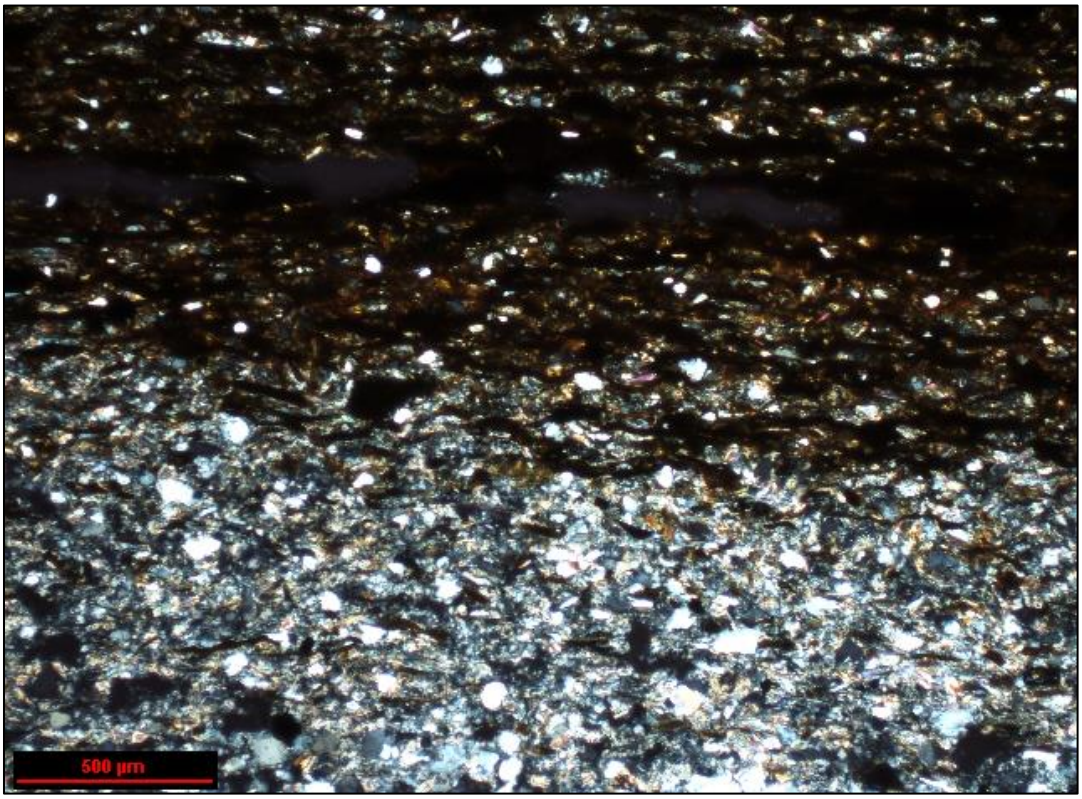

FIGURE 31: PHOTOMICROGRAPHS OF A THIN SECTION SHOWING WELL DEVELOPED BEDDING AND SORTING ON A MICROSCALE

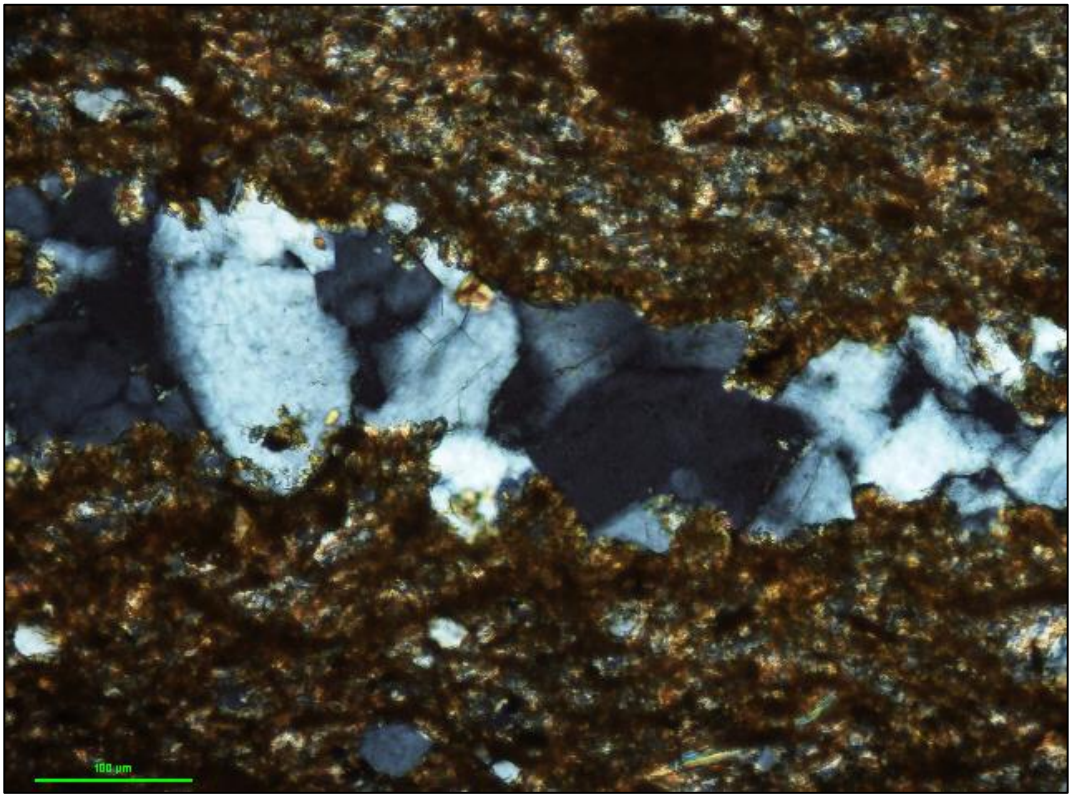

FIGURE 32: PHOTOMICROGRAPHS OF A THIN SECTION SHOWING STRAINING IN A QUARTZ LENSE

CHAPTER 4: ANALYSIS OF DATA AND EVALUATION OF SITE

In this chapter the data is analysed and the parameters deduced for evaluating the site. The six aspects that need evaluation are the bearing capacity, settlement, slope stability, excavatability of material, wind loads on the shed as well as the management of risks. **Table 9** shows what parameters are needed for each investigation and the applicable method of analysis.

TABLE 9: ASPECTS CONSIDERED FOR EVALUATION

Aspect considered	Parameters Required	Method of Analysis
Bearing Capacity	UCS / Point load Index & RQD & Joint information → RMR → c & phi	Terzaghi (1943)
Settlement	E Modulus	Elastic Stress Distribution Steinbrenner (1934)
Slope Stability	GPS data Joint survey PGA	GeoSlope - SLOPE/W Prokon - Geotechnical
Excavatability of Material	DCP Point Load Strength Joint Spacing	Franklin *et al.,* (1971)
Wind Load on Shed	Wind Speed Steel Section Properties	Prokon - Frame Analysis
Risk Management	N/A	Risk Assessment Matrix

In this chapter, seismic design, general soil/rock profile and excavatability of materials will not be discussed, as there is no data that needs to be analysed to investigate that aspect.

4.1. BEARING CAPACITY

It is important to determine the bearing capacity of the rock to ensure that the rock will withstand the forces induced by the S/LLR. To determine the ultimate bearing capacity of the rock, q_{ult} in [Pa], Terzaghi's equations are used:

$$q_{ult} = cN_cS_c + \gamma DN_q + 0.5\gamma BN_\gamma S_\gamma \quad (16)$$

Where: c = cohesion of the rock in [Pa];

γ = unit weight of the rock in [N/m^3];

B = width of foundation in [m];

D = depth of foundation in in [m];

$S_c = 1.3$ for square foundations; and

$S_\gamma = 0.8$ for square foundations.

According to Stagg and Zienkiewicz (1968) the bearing-capacity factors for sound rock are approximated by:

$$N_c = 5\,tan^4\left(45° + \frac{\emptyset}{2}\right) \tag{17}$$

$$N_q = tan^6\left(45° + \frac{\emptyset}{2}\right) \tag{18}$$

$$N_\gamma = N_q - 1 \tag{19}$$

Where: $\emptyset$ = internal friction angle of the rock in [°, degrees].

The cohesion and internal friction angle of the rock can be determined by calculating the rock mass rating (RMR). To calculate the RMR the strength of the rock, rock quality designation (RQD) and information about the joints are required. The rock strength is the results from both the UCS and point load test and the joint information from the core logging sheet. The RQD value can be calculated as follows:

$$RQD = \frac{Length\ of\ core\ pieces > 100\ mm\ in\ length}{Total\ length\ of\ core\ run} \times 100 \tag{20}$$

The obtained RQD % for the three cores is as follows:

$$RQD_1 = \frac{300 + 290}{330 + 300 + 370} \times 100 = 59.0\ \%$$

$$RQD_2 = \frac{200 + 330 + 190}{150 + 600 + 650} \times 100 = 51.4\ \%$$

$$RQD_3 = \frac{200 + 100}{500 + 480} \times 100 = 30.6\ \%$$

The Rock Mass Rating (RMR) was determined by a system proposed by Bieniawski (1989), seen in **Table 10**, and the *c* and $\emptyset$ values can be obtained from it. **Table 11** shows the RMR values of each core run with the corresponding lower bound, and thus conservative, *c* and $\emptyset$ values. More detailed calculations of the RMR for each sample can be found in **Appendix F**.

TABLE 10: ROCK MASS RATING SYSTEM (BIENIAWSKI, 1989)

A. CLASSIFICATION PARAMETERS AND THEIR RATINGS									
Parameter			Range of values						
1	Strength of intact rock material	Point-load strength index	>10 MPs	4-10 MPa	2-4 MPa	1-2 MPa	Fort his low range –uniaxial compressive test is preferred		
		Uniaxial comp. strength	>250 MPa	100-250 MPa	50-100 MPa	25-50 MPa	5-25 MPa	1-5 Mpa	<1 MPa
	Rating		15	12	7	4	2	1	0
2	Drift cone Quality RQD		90% - 100%	75% - 90%	50% - 75%	25% - 50%	<25%		
	Rating		20	17	13	8	3		
3	Spacing of discontinuities		>2m	0.6–2m	200–600mm	60-200mm	<60mm		
	Rating		20	15	10	8	5		
4	Condition of discontinuities (See E)		Very rough surfaces Not continuous No separation Unweathered wall rock	Slightly rough surfaces Separation <1mm Slightly weathered walls	Slightly rough surfaces Separation <1mm Highly weathered walls	Slicksided surfaces or Gouge <5mm thick or Separation 1-5mm, continuous	Soft gouge >5mm thick Or Separation >5mm Continuous		
	Rating		30	25	20	10			
5	Ground water	Inflow per 10m tunnel length (l/m)	None	<10	10-25	25-125	>125		
		(Joint water press)/ (Major principal(??)	0	<0.1	0.1-0.2	0.2-0.5	>0.5		
		General condition	Completely dry	Damp	Wet	Dripping	Flowing		
	Rating		15	10	7	4	0		

B. RATING ADJUSTMENT FOR DISCONTINUITY ORIENTATIONS (See F)						
Strike and dip orientations		Very favourable	Favourable	Fair	Unfavourable	Very Unfavourable
Ratings	Tunnels & mines	0	-2	-5	-10	-12
	Foundations	0	-2	-7	-15	-25
	Slopes	0	-5	-25	-50	

C. ROCK MASS CLASSES DETERMINED FROM TOTAL RATINGS						
Rating		100←81	80←61	60←41	40←21	<21
Class number		I	II	III	IV	V
Description		Very good rock	Good rock	Fair rock	Poor rock	Very poor rock

D. MEANING OF ROCK CLASSES						
Class number		I	II	III	IV	V
Average stand-up time		20 years for 15m span	1 year for 10m span	1 week for 5m span	10 hours for 2.5m span	30 min for 1m span
Cohesion of rock mass (kPa)		>400	300-400	200-300	100-200	<100
Friction angle of rock mass (deg)		>45	35-45	25-35	15-25	<15

E. GUIDELINES FOR CLASSIFICATION OF DISCONTINUITY conditions						
Discontinuity length (persistence)		<1m	1-3m	3-10m	10-20m	>20m
Rating		6	4	2	1	0
Separation (aperture)		None	<0.1mm	0.1-1.0mm	1-5mm	>5mm
Rating		6	5	4	1	0
Roughness		Very rough	Rough	Slightly rough	Smooth	Slickensided
Rating		6	5	3	1	0
Infilling (gouge)		None	Hard filling <5mm	Hard filling >5mm	Soft filling <5mm	Soft filling >5mm
Rating		6	4	2	2	0
Weathering		Unweathered	Slightly weathered	Moderately weathered	Highly weathered	Decomposed
Rating		6	5	3	1	0

F. EFFECT OF DISCONTINUITY STRIKE AND DIP ORIENTATION IN TUNNELING **			
Strike perpendicular to tunnel axis		Strike parallel to tunnel axis	
Drive with dip-Dip 45-90°	Drive with dip-Dip 20-45°	Dip 45-90°	Dip 20-45°
Very favourable	Favourable	Very favourable	Fair
Drive against dip-Dip 45-90°	Drive against dip-Dip 20-45°	Dip 0-20-Irrespective of strike°	
Fair	Unfavourable	Fair	

TABLE 11: RMR DATA

Sample	Rating	Rock Class	Cohesion c	Friction Angle $\emptyset$
1	48	III – Fair Rock	200 kPa	25°
2	48	III – Fair Rock	200 kPa	25°
3	43	III – Fair Rock	200 kPa	25°

To determine the unit weight, the values from **Table 7** are used and calculated as follow:

$$\gamma = \frac{2523.64 + 2561.95 + 2462.46 + 2586.73\ [kg/m^3]}{4} * 9.81 = 24855.6\ N/m^3 = 24.86\ kN/m^3$$

The bearing capacity factors were calculated as follow:

$$N_c = 5\ tan^4\left(45° + \frac{25}{2}\right) = 30.35$$

$$N_q = tan^6\left(45° + \frac{25}{2}\right) = 14.96$$

$$N_\gamma = 14.96 - 1 = 13.96$$

Table 12 shows all the parameters needed to calculate q_{ult}.

TABLE 12: BEARING CAPACITY CALCULATION PARAMETERS

$\boldsymbol{c}$	$200\ kPa$	$\boldsymbol{S_c}$	1.3
$\boldsymbol{\gamma}$	$24.86\ kN/m^3$	$\boldsymbol{S_\gamma}$	0.8
$\emptyset$	20°	$\boldsymbol{N_c}$	30.35
$\boldsymbol{B}$	$4.52\ m$	$\boldsymbol{N_q}$	14.96
$\boldsymbol{D}$	$0.60\ m$	$\boldsymbol{N_\gamma}$	13.96

$$q_{ult} = 200\ 000 * 30.35 * 1.3 + 24\ 860 * 0.60 * 14.96 + 0.5 * 24\ 860 * 4.52 * 13.96 * 0.8$$

$$= 7\ 891\ 000 + 223\ 143.36 + 627\ 458.44$$

$$q_{ult} = 8.74\ MPa$$

To determine if the ground will support the S/LLR, the load it exerts on the ground should be calculated and compared to the ultimate bearing capacity. The total load comprises of the weight of the S/LLR as well as the weight of the foundation. The total load applied, q_{app} in [Pa], can be calculated as follows:

$$q_{app} = \frac{F_{S/LLR} + F_F}{A} \tag{21}$$

Where: $F_{S/LLR}$ = force of the S/LLR in [N];

F_F = force of the base in [N]; and

A = area of the foundation in [m²].

$$F_{S/LLR} = 70\ 000\ N$$

According to SANS 10160-2:2011, density of concrete is 24 kN/m^3. F_F can be calculated as follows:

$$F_F = Volume\ of\ base\ \times density\ of\ concrete$$

$$= (4.52 * 5.97 * 0.60) \times 24\ 000$$

$$= 388\ 575\ N$$

Thus,

$$q_{app} = \frac{70\ 000 + 388\ 575}{4.52 * 5.97} = 16\ 994\ Pa = 17\ kPa$$

Comparing the capacity, q_{ult}, to the applied pressure, q_{app}:

$$q_{ult} > q_{app}$$

$$8740\ kPa > 17\ kPa$$

It is clear from the above results that the bearing capacity of the rock is more than sufficient to withstand the load of the structure.

4.2. SETTLEMENT

Settlement is more often of concern than the bearing capacity. It is important to calculate the settlement to ensure that foundation would not crack, and would stay stable after construction is completed. The total settlement, S_{TF} in [mm], can be calculated by **Equation 22**. This equation is based on elastic stress distribution.

$$S_{TF} = F_R F_D \sum_{i=0}^{z} \frac{\Delta\sigma_z}{E} \Delta z \tag{22}$$

Where: F_R = rigidity correction as 0.8 for a rigid loaded area;

F_D = Fox's depth correction factor according to Day (1987);

σ_z = vertical stress in [kPa];

E = Young's modulus in [MPa]; and

z = vertical depth in [m].

According to Steinbrenner (1934) the vertical stress can be calculated as follows:

$$\sigma_z = k \times q_{app} \tag{23}$$

Where: q_{app} = applied load in [N] and

k = influence factor.

The influence factor, k, can be calculated as follows:

$$k = \frac{1}{2\pi}\left[\frac{m \times n}{\sqrt{1+m^2+n^2}} \times \frac{1+m^2+2n^2}{(1+n^2)(m^2+n^2)} + \sin^{-1}\left(\frac{m}{\sqrt{m^2+n^2}\sqrt{1+n^2}}\right)\right] \tag{24}$$

Where: $m = \frac{L}{B}$;

$n = \frac{z}{0.5B}$;

and: L = length of foundation in [m];

B = width of foundation in [m]; and

z = depth under foundation in [m].

A correlation of rock modulus can be used with the UCS value to determine the Young's modulus, E (Peck (1976) and Deere (1968)). The design line was used and the corresponding modulus obtained was 600 MPa. As the value of n change with depth, Excel was used to ease calculation. **Table 13** shows the parameters used in the calculation of the settlement.

TABLE 13: SETTLEMENT CALCULATION PARAMETERS

$\boldsymbol{B}$	$4.52\ m$	γ	$24.86\ kN/m^3$
$\boldsymbol{L}$	$5.97\ m$	$\boldsymbol{E}$	$600\ MPa$
$\boldsymbol{D}$	$0.60\ m$	$\boldsymbol{F_R}$	0.8
$\boldsymbol{q_{app}}$	$17\ kPa$	$\boldsymbol{F_D}$	0.97

The full calculation of the settlement can be seen in **Appendix G**. The settlement was calculated as 0.1 mm. This value can be considered conservative as conservative values were used in the calculation, and the weight of the soil removed was not subtracted from the applied pressure. These calculations show that settlement would not be a factor affecting the operations of the S/LLR.

4.3. SLOPE STABILITY

The use of software for slope stability analysis ensures rapid results and more complex problems can be solved. Software packages are readily available and it is easy to choose one that best suits the user's needs.

4.3.1. GEOSLOPE – SLOPE/W

GeoSlope is a software programme consisting of 8 subsections. The section that can be used to determine slope stability of earth and rock slopes is the SLOPE/W section. This section has three features, namely define, solve and contour. In the define section the cross-section of the problem is defined, the solve section runs the analysis and the contour section displays the results of the solve section.

SLOPE/W can use the following methods of analysis:

- Ordinary Method of Slices;
- Bishop's Modified Method;
- Janbu Simplified;
- Spencer;
- Morgenstern-Price;
- Army Corps of Engineers; and
- Lowe and Karafiath.

SLOPE/W is a user friendly software programme. According to Chen and Liu (2010), the accuracy is very good and the quality of the report and graphical output is excellent.

In order to use *SLOPE/W* to analyse the probability of a circular failure, the data obtained from the survey had to be processed with *Surfer9*. A contour map was then drawn, from which a 3D model was created. **Figure 33** shows the 3D model with the contour map as an overlay. *Surfer9* was used to create a cross section from the model, and this data was then used in SLOPE/W to analyse the probability of failure.

All of the sections' properties were chosen in such a way that results would be comparable with previous studies done as mentioned in ***Section 2.3.*** The soil properties in **Table 14** were used in the analysis of all sections in SLOPE/W. The bottom layer starts at a depth of 1 m below the lowest point of the section and is 20 m thick. Below this layer, there is bedrock that is impenetrable.

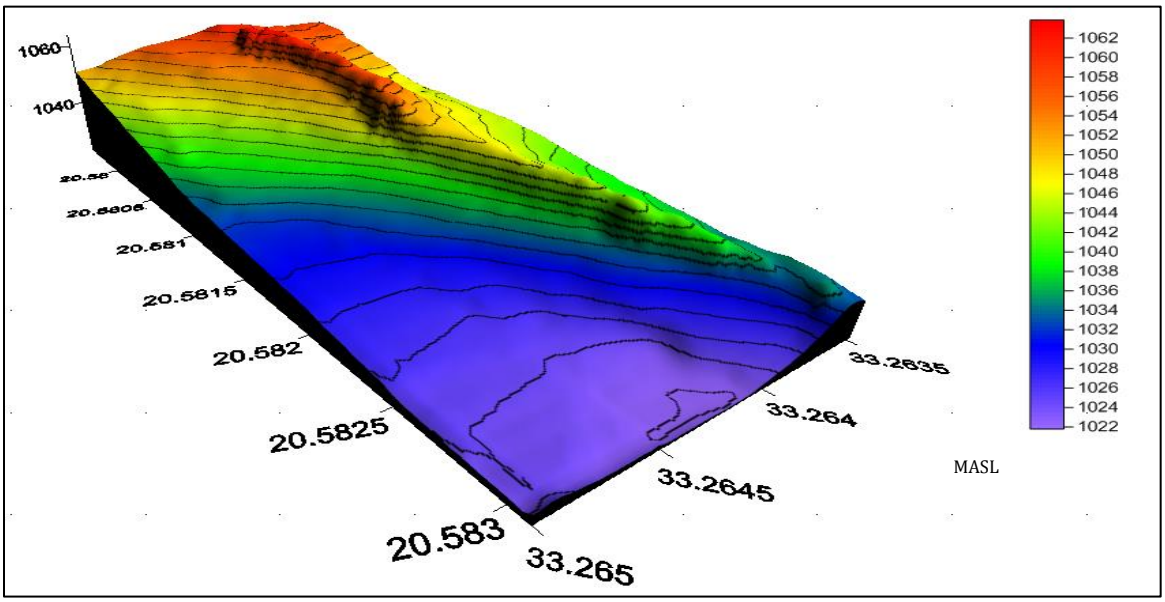

FIGURE 33: 3D MODEL OF AREA ADJACENT TO S/LLR

TABLE 14: SOIL PROPERTIES (VISSER 2012)

Layer	ɣ	c	ø
	[kN/m^3]	[kN/m]	[Degrees]
Top Layer	18	8	36
Bottom Layer	23	42	42

Two cross-sections were chosen and used to analyse the probability of circular failure. The geometry of the hill is uniform, which is why it is assumed that these cross-sections represent the general slope. Both cross-sections are situated on the southern side of the hill. A failure in any of the slopes can cause a movement, which will affect the stability of the S/LLR.

With the use of SLOPE/W and the Bishop's method, a Factor of Safety (FOS) was calculated for each cross-section. The image generated by SLOPE/W for the critical slip surface can be seen in **Figure 34 (a), (b)** and **(c)**. Referring back to **Figure 34 (b),** in this section there is a slight protrusion close to the toe of the slope. The stability for the slope without this protrusion was calculated as well, to ensure safety if this protrusion was to be removed by construction. More details on each analysis can be seen in **Appendix H**. The FOS obtained from the analysis can be seen in **Table 15**. The critical FOS is given along with the next four highest values.

TABLE 15: FACTORS OF SAFETY FOR CIRCULAR SLIP

	Critical FOS	Second Lowest FOS	Third Lowest FOS	Fourth Lowest FOS	Fifth Lowest FOS
Cross-section 1	2.335	2.349	2.352	2.357	2.374
Cross-section 2: With protrusion	1.894	1.960	2.056	2.133	2.201
Cross-section 2: Without protrusion	1.847	1.913	2.009	2.014	2.057

A FOS of 1.5 against circular failure is assumed to be safe for this type of construction. From the results, it can be seen that the lowest FOS is 1.847, and thus the area is safe against circular failure.

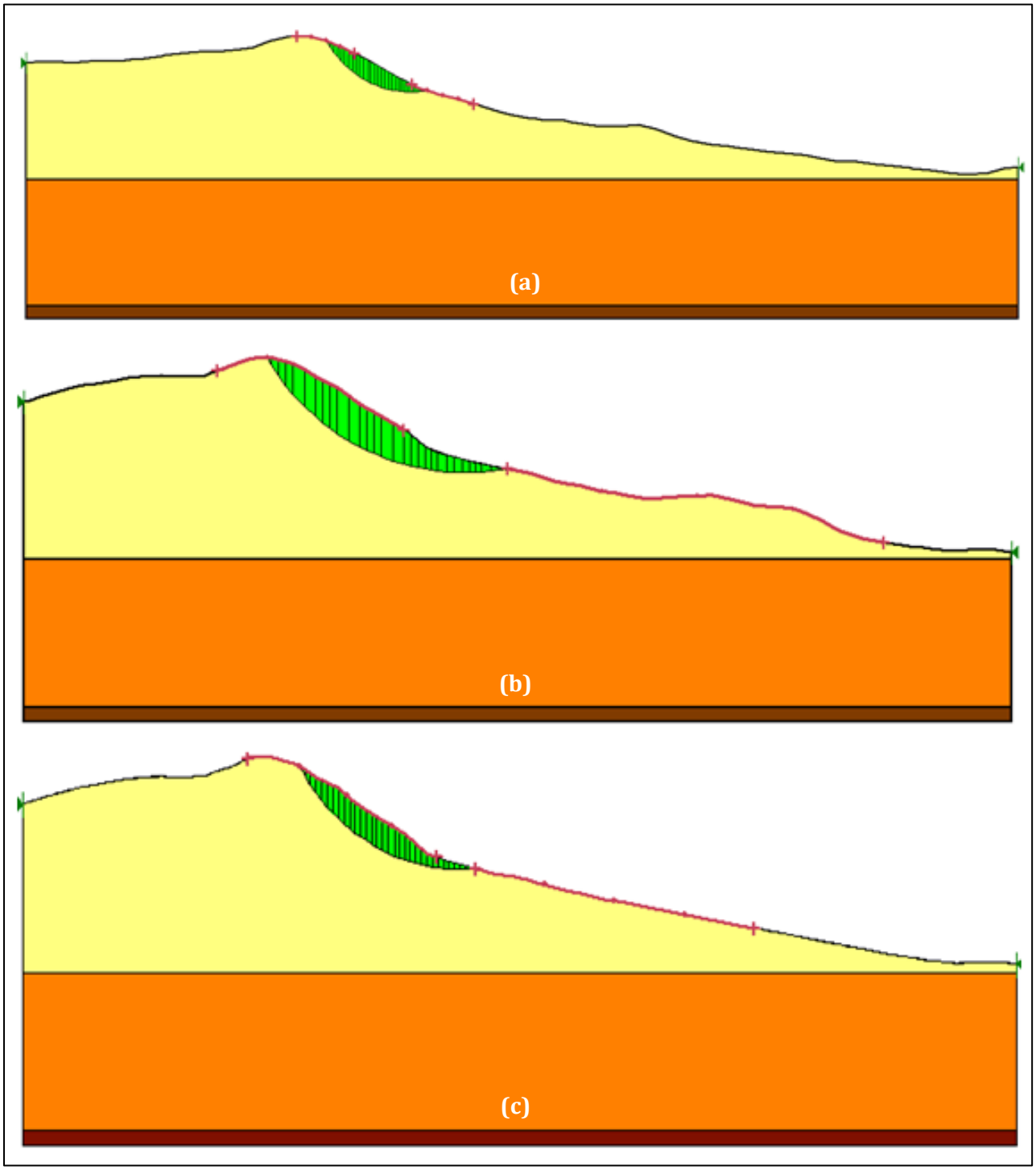

FIGURE 34: IMAGES CREATED BY SLOPE/W WITH (A) CROSS-SECTION 1, (B) CROSS-SECTION 2 AND (C) CROSS-SECTION 2 WITHOUT PROTRUSION.

4.3.2. PROKON - GEOTECHNICAL

With the use of the program ROCKPF for planar failure in rock slopes and WEDGE for tetrahedral wedge analysis, the FOS can be determined for each type of failure. A deterministic analysis can be used when all parameters are known. A probabilistic analysis can be used when not all parameters are specifically known, but a range of values are known. The program then iterates between the given values, and the user can see the effect that these values have on the FOS.

The presence of pore water pressure can be included in the calculations. External loads and anchor forces can also be taken into consideration, if necessary. Specification of the tension crack depth and/or length allows the user to analyse with more detail. The conventions used in Prokon are defined in **Table 16**.

TABLE 16: CONVENTIONS USED IN PROKON

Symbol	Definition	Unit
$\mathbf{H_c}$	Cutting height	m
$\mathbf{H_p}$	Slip plane height	m
$\mathbf{Ø_c}$	Cutting angle	°
$\mathbf{Ø_p}$	Slip plane angle	°
$\mathbf{Ø_u}$	Upper slope angle	°
Z	Tension crack depth	m
$\mathbf{Z_w}$	Water depth in crack	m
T	Anchor force	kN/m
β	Anchor dip from horizontal	°
E	External load	kN/m
$\mathbf{H_1}$	Vertical height of slope	M
T	Cable force	kN

4.3.2.1. Planar Failure Analysis

In order to use Prokon - ROCKPF to analyse the probability of a planar failure due to a cutting made on the Northern side of the hill, the data obtained from the joint survey have been used. The appropriate range of $Ø_p$ was identified, where the highest value was chosen as 63°. In Prokon it is required that $Ø_p > Ø_u$ and as the slope of the hill ($Ø_u$) was determined to be 27°, the range of $Ø_p$ is between 63° and 28°. Values in this range were chosen to determine the FOS. Water on the slip plane was not taken into account. Both cutting depths (1 m and 2 m) at a cutting angle ($Ø_c$) of 75° were tested with all values of $Ø_p$. The FOS obtained from this analysis is shown in **Table 17**. The complete set of results, obtained from the Prokon analysis, can be found in **Appendix I**.

TABLE 17: FACTORS OF SAFETY FOR PLANAR FAILURE

Cutting Depth	$Ø_p$ = 63°	$Ø_p$ = 46°	$Ø_p$ = 37°	$Ø_p$ = 28°
	FOS	FOS	FOS	FOS
1m	2.85	1.39	1.28	1.27
2m	1.41	0.79	0.79	0.85

From the results one can see that it is not safe to make a cutting on the Northern side of the slope. The FOS is smaller than 1.5 for all of the cases, except at a cutting depth of 1 m and Øp = 63°.

4.3.2.2. Wedge Failure Analysis

When the joint survey values were used in *Prokon,* no wedge was kinematically feasible. This indicates that the geometry of the slope is such that no wedge can form. A wedge failure is feasible if the three main dip directions form a wedge (Croukamp, 2013). The main directions were determined from the Rose Diagram, as seen in the middle of **Figure 25.** The main directions are presented in **Table 4**.

4.4. EXCAVATABILITY OF MATERIAL

The first step in excavating materials is to determine the depth of the excavation. The DCP test results divide the soil into different layers. Layers with a high DN value have lower strength and layers with a low DN value have higher strength. From **Figure 35**, a difference in strength can be seen where the top layer thickness varies from 95 to 170 mm and a harder material can be found below. The calculations of the DN-values can be seen in **Appendix J**.

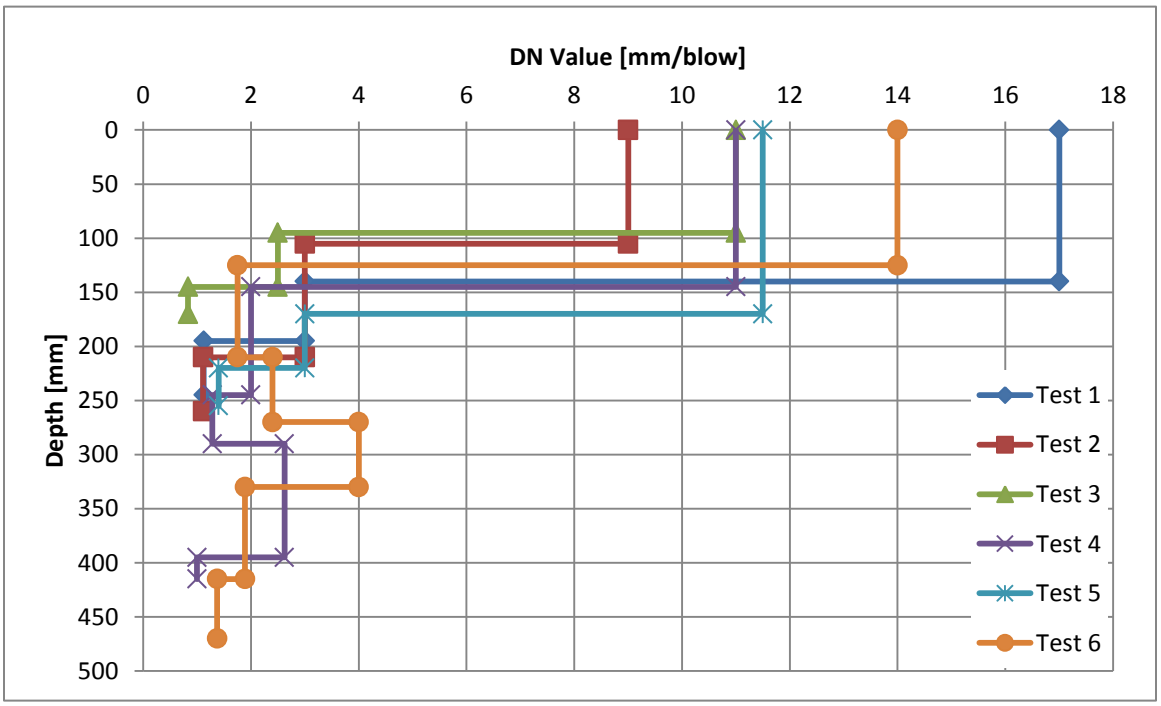

FIGURE 35: DN VALUES VERSUS DEPTH

The point load strength and the fracture spacing, of the intact rock can be used for the assessment of excavatability. The excavation of rock masses can be done with different methods such as digging, ripping and blasting. Digging is the removal of soil by hand, ripping is with the use of a long claw-like device on the back of a bulldozer and blasting is the controlled use of explosives. It is important to select the most effective method for the project. By using the chart proposed by Franklin (1971), a method can be selected as illustrated in **Figure 36**.

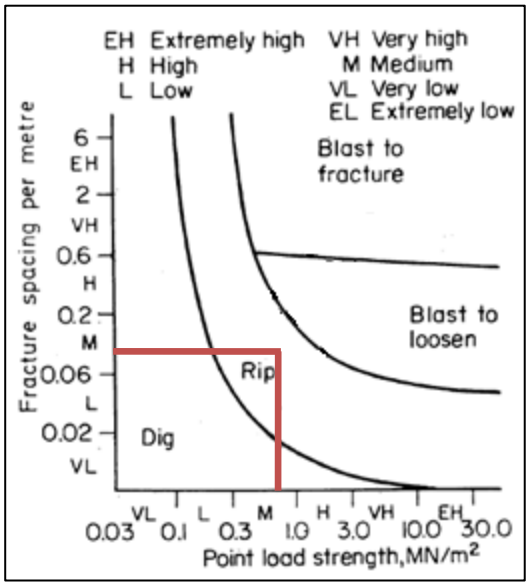

FIGURE 36: METHOD SELECTION (FRANKLIN, 1971)

The chart indicates that the ripping method should be used to excavate material, however, the chart is quite conservative and predicts more difficult excavation conditions than is actually the case with modern machinery (Tsiambaos & Saroglou, 2009).

4.5. WIND LOADS

The effects of the wind on the runoff shed needs to be determined to ensure the safety of the instruments. This will be done with *Prokon – Portal Frame Analysis* which incorporates the SANS 10160-3:2011. Two wind directions were identified: a wind force parallel to the tracks and a force perpendicular to the tracks. In each case the doors of the shed could be open or closed, thus resulting in four possible load cases. Only the worst case would be investigated, as it is a small structure, and would generally not be affected by the wind. The worst case is a wind force parallel to the tracks with the doors of the shed open.

TABLE 18: PARAMETERS USED IN PROKON CALCULATION

<table>
<tr><td>Peak wind speed</td><td>$v_p(z) = 40m/s$</td></tr>
<tr><td>Terrain category</td><td>B</td></tr>
<tr><td>Reference height</td><td>$z_e = 5.454\ m$</td></tr>
<tr><td>Peak wind speed pressure</td><td>$q_p = \frac{1}{2} \times \rho \times {v_p}^2(z)$
$= \frac{1}{2} \times 1.06 \times 40^2$
$= 848\ kg/s^2/m$
$= 8318.88\ N/s^2/m$</td></tr>
<tr><td>Pitch of roof (Duel pitch roof)</td><td>$\sin^{-1}\left(\frac{654}{3114}\right) = 12°$</td></tr>
<tr><td>Parameters used to determine coefficients</td><td><table><tr><th>b</th><th>d</th><th>h</th><th>e</th><th>h/d</th></tr><tr><td>5970</td><td>6360</td><td>5454</td><td>5970</td><td>0.85≈1</td></tr></table></td></tr>
<tr><td>External pressure coefficient</td><td><table><tr><th></th><th>Zone A</th><th>Zone B</th><th>Zone C</th><th>Zone D</th><th>Zone E</th><th>Zone F</th><th>Zone G</th><th>Zone H</th><th>Zone I</th></tr><tr><td>C_{pe}</td><td>-1.2</td><td>-0.8</td><td>-0.5</td><td>+0.8</td><td>-0.5</td><td>-1.39</td><td>-1.3</td><td>-0.63</td><td>-0.53</td></tr></table></td></tr>
<tr><td>Internal pressure coefficient</td><td>$C_{pi} = 0.9 \times C_{pe}$ (*NOTE 1)</td></tr>
<tr><td>External pressure</td><td>$w_i = q_p \times C_{pe}$</td></tr>
<tr><td>Internal pressure</td><td>$w_e = q_p \times C_{pi}$</td></tr>
</table>

NOTE 1: If the openings are located in zones with different values of external pressure, an area weighted average value of C_{pe} shall be used.

With the use of the values in **Table 18** and *Prokon – Portal Frame Analysis,* the wind pressure on the shed was calculated for the worst case. **Figure 37** illustrates these calculated pressures. The analysis includes the self-weight of the structure as the section properties of the columns, rafters, purlins, side rails and eaves beams have been specified. The maximum deflection obtained from the analysis was 2.2 mm. This indicates that the design of the runoff shed is sufficient to withstand wind forces at the MSGO site.

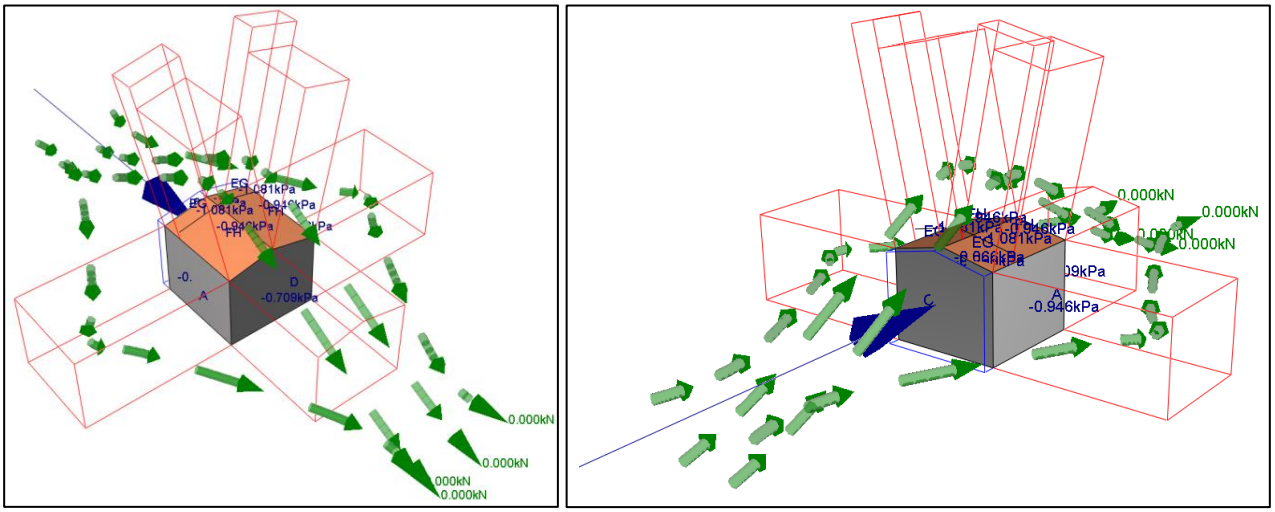

FIGURE 37: WIND PRESSURE ON THE RUNOFF SHED

4.6. RISK MANAGEMENT

A risk is as an event or situation that can occur, which can either have a positive or negative impact on the project, it can have more than one cause and more than one impact. Management of risks is a very important aspect of the process, as it will determine the structural integrity and the life span of the foundation. Risk management is an on-going process, which consists of identifying the risks, minimizing them and monitoring those which cannot be excluded. It is important to consider a wide variety of factors, including business and administrative aspects. Business aspects include procurement, estimating and tendering, budget control and economic assessment; where administrative aspects include organisation and financial management. **Figure 38** shows how risks should be managed.

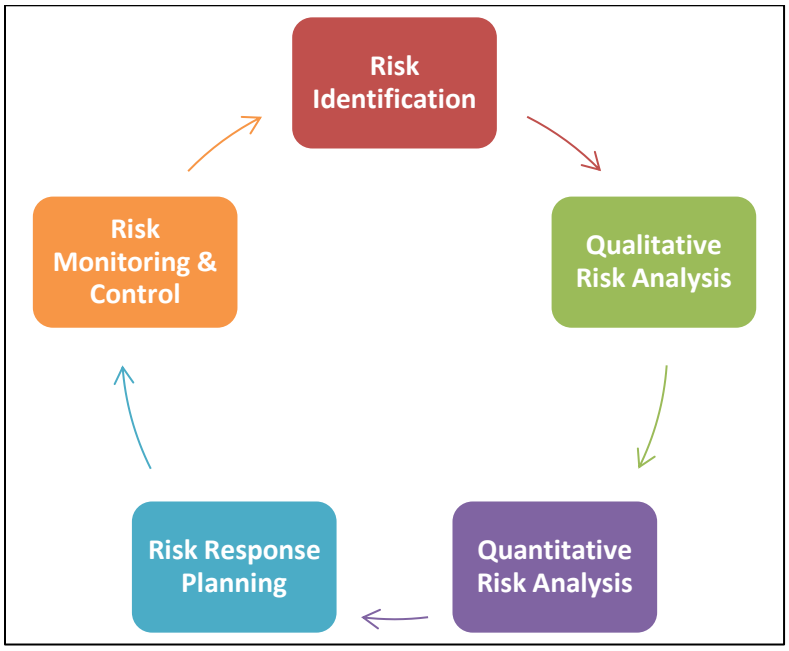

FIGURE 38: RISK MANAGEMENT

Identified risks should be quantified. **Table 19** shows a risk assessment matrix where the probability and the consequences are taken into consideration. Each of the above mentioned factors gets a score and the higher the total score, the more attention the risk needs. This table is used to score the importance of the risks in the risk register as seen in **Table 20**. It is important to define an action to mitigate each risk. Finding an economically viable solution to prevent the occurrence of risks is an important aspect of risk management.

TABLE 19: RISK ASSESSMENT MATRIX

Likelihood	**Consequences**				
	Insignificant (1) (Minor problem easily handled by normal day to day processes)	**Minor (2)** (Some disruption possible, e.g. damage equal to R50 000)	**Moderate (3)** (Significant time/resources required, e.g. damage equal to R100 000)	**Major (4)** (Operations severely damaged, e.g. damage equal to R500 000)	**Catastrophic (5)** (Business survival is at risk, e.g. damage greater or equal to R1 million)
Almost Certain (5) (e.g. >90% chance)	**High (6)**	**High (7)**	**Extreme (8)**	**Extreme (9)**	**Extreme (10)**
Likely (4) (e.g. between 50% and 90% chance)	**Moderate (5)**	**High (6)**	**High (7)**	**Extreme (8)**	**Extreme (9)**
Moderate (3) (e.g. between 10% and 50% chance)	**Low (4)**	**Moderate (5)**	**High (6)**	**Extreme(7)**	**Extreme (8)**
Unlikely (2) (e.g. between 3% and 10% chance)	**Low (3)**	**Low (4)**	**Moderate (5)**	**High (6)**	**Extreme (7)**
Rare (1) (e.g. <3% chance)	**Low (2)**	**Low (3)**	**Moderate (4)**	**High (5)**	**High (6)**

This risk register, in **Table 20**, only focuses on a few risks and there are many more risks that may occur, thus the risks in this register should not be regarded as the only possible risks that may occur. The importance of a competent, reliable and experienced geotechnical engineer is of utmost importance (Wium, 2014), as engineering judgement plays a big role in the decisions made.

TABLE 20: RISK REGISTER

Risk	Mitigating measures	Importance according to Table 18 (Likelihood + Consequence)
Incomplete geotechnical data:		
Varying soil conditions: No information on rock profile below 1,5m depth	Drilling of one geotechnical borehole on centre of base to 10 m depth.	(2+2) **Low**
Performance risks		
Bearing capacity failure	Found on competent rock.	**Negligible**
Settlement	Found on competent rock.	**Negligible** Settlements < 0,5 mm
Swell of shale	Conduct free swell tests.	(2+2) **Low**
Slope stability	Selection of site on stable ground with low relief.	**Negligible**
Damage due to seismicity	Follow code requirements.	**Negligible** Low PGA (Figure 4)
Construction risks		
Increased volume of rock excavation	Make appropriate allowance in contract for rock excavation volumes.	(3+2) **Moderate**
Soft material below designed founding level	Make allowance for excavation of soft material and replacement with mass concrete in contract document.	(3+2) **Moderate**
Construction quality	Registered geotechnical engineer on site.	(3+4) **Extreme**
Availability of resources	Order and deliver materials before construction where possible. Procure from reliable sources.	(2+3) **Moderate**
Equipment failure	Procure from reliable sources, make allowance for delays in project planning.	(2+3) **Moderate**
General risks		
Site access difficulties	Complete construction/ rehabilitation of access road before construction of S/LLR foundation commence.	**Negligible**
Productivity of labour, labour disputes or strikes	State expectations from labourers in contract before work commences. Make allowance for delays in project planning.	(4+2) **High**
Security of site	Procure a reliable security company to ensure safety during project.	(2+2) **Low**
Consequential losses	The contract should define the indemnities for consequential losses.	(1+4) **High**

CHAPTER 5: CONCLUSION AND RECOMMENDATIONS

From the results obtained in Chapter 4 the following conclusions and recommendations can be made.

5.1. BEARING CAPACITY

By using the UCS or point load index, the RQD and information about the joints, the rock can be rated by the RMR system proposed by Bieniawski (1989). From this system a *c* and Ø value can be determined and used in Terzhagi's equation for bearing capacity, **Equation 17**. By using the bearing capacity factors proposed by Stagg and Zienkiewicz (1968), a bearing capacity of 8.74 MPa was calculated for the rock mass. The applied bearing pressure of 17 kPa is much smaller than the bearing capacity of the rock and thus a safe assumption can be made that the rock mass is more than sufficient to withstand the load of the structure.

5.2. SETTLEMENT

Settlement is more often of concern than the bearing capacity. The settlement can be calculated with **Equation 23**, which is based on an elastic stress distribution. Steinbrenner's (1934) method for determining the vertical stress was used. The UCS results and chart proposed by Peck (1976) and Deere (1968), were used to determine the Young's modulus and with the use of Excel, the total settlement was calculated as 0.1 mm. This is a conservative value as the weight of the soil removed was not subtracted from the applied pressure.

From the result of this calculation it is clear that settlement would not be a factor influencing the operation of the S/LLR. As the weight of the foundation itself is 84% of the applied pressure, little to no settlement will occur after the concrete has hardened. It is thus recommended that the level of the foundation should be calibrated after the hardening of the concrete and before the instrument is placed.

5.3. SLOPE STABILITY

The 3D model of the site showed a good representation of the actual terrain. The circular slip analysis, on the southern side of the ridge, was completed with SLOPE/W, and a safety factor greater than 1.5 was obtained. This shows that the slope is stable and the probability for any circular failure is small.

The planar failure analysis, on the northern side of the ridge, was completed with Prokon and indicated that the maximum cutting depth of the access road should be 1 m. The FOS for the cutting depth equal to 2 m, is smaller than 1 and thus the slope is not stable. A solution to this problem could be the use of

anchor cables or a retaining wall, but it is an expensive option. Wedge failure along the road cutting is not kinematically feasible and thus poses no threat to the stability of the slope.

It is recommended that an alternative route for access to the S/LLR should be investigated. However, if it is chosen to be at the foot of the southern side of the hill, the toe can yield due to the reduced stabilising moment caused by road excavation, which in turn will reduce the FOS for circular failure.

5.4. EXCAVATABILITY OF MATERIAL

Excavatability is the term used to describe the ease of excavating material. First the DCP values were used to determine a DN value and give a corresponding strength of the soil layers. From this it can be determined that the top 95 to 170 mm is a softer soil, which can be excavated by hand.

The point load strength and the fracture spacing of the intact rock mass, can be used for the assessment of excavatability. This assessment was done with a chart proposed by Franklin *et al.,* (1971). The chart indicates that the ripping method should be used, thus a bulldozer would be needed. It is recommended to excavate the top soil with the bulldozer as well, as it would save a lot of time and labour costs.

5.5. WIND LOADS

To determine if the shed would withstand the forces of the wind at the MSGO site an analysis was done with *Prokon – Portal Frame Analysis* which incorporates the SANS 10160-3:2011. The maximum deflection obtained from the analysis was 2.2 mm. This indicates that the design of the runoff shed is sufficient to withstand the forces induced by the wind.

5.6. FINAL REMARKS

The conclusion that can be drawn from this study is that the design of the foundations of the S/LLR at MSGO will be the same as at HartRAO. This conclusion can be made as none of the factors that were evaluated have shown a destabilising effect on the S/LLR. This option is beneficial to the project as no consulting services would be required to design a new foundation, resulting in saving costs.

The shale at the MSGO site is impermeable to water, but water can still penetrate along bedding planes causing the lumps to slake. It is recommended that when the excavation is made, a mass concrete layer of at least 10 MPa should be keyed into the exposed founding rock mass. This will level the surface and protect the exposed shale against slaking. Van Wyk (2013) determined that the shale at the MSGO site is prone to slaking after five wet/dry cycles. It is thus important that the rock mass exposed after excavation should immediately be covered to prevent slaking.

The petrographic studies have shown that clay minerals such as kaolinite and chlorite are present in the samples. Since these are non-expansive minerals, it can be concluded that the rock mass is non-expansive. As the effect of a swelling rock mass can have a destabilising effect on the foundation, it is recommended that a free swell test should be done to determine quantitatively if this could be a problem.

The depth of the influence sphere underneath a foundation is twice the width, being roughly 10 m in this case. The final recommendation is to drill at least one core of 10 m deep at the centre of the foundation. This will verify the strength of the founding material and that no discontinuities exist underneath the foundation as there is no information on the rock profile deeper than 1.5 m.

BIBLIOGRAPHY

ALLEY, C.O., 1972. Story of the development of the Apollo 11 laser ranging retro-reflector experiment, in Adventures in Experimental Physics, edited by B. Maglich, pp. 132-149, 1972.

American Society of Testing and Materials (ASTM)., 2002. Standard Test Method for Unconfined Compressive Strength of Intact Rock Core Specimens, D2938-95(R02).

ANONYMOUS, 1993. History of Laser Ranging and MLRS. 1993. [Online]. Available: http://www.csr.utexas.edu/mlrs/history.html [2014, June 6].

ANONYMOUS, 2010. Matjiesfontein info, [Online]. Available: http://www.matjiesfontien.com/ [2013, October 12]

ANONYMOUS, 2013. How does BGS classify landslides? Online] Available: http://www.bgs.ac.uk/science/landUseAndDevelopment/landslides/How_does_BGS_classify_landslides.html [September, 2013].

ANONYMOUS, 2014. Weatherbase, Sutherland, South Africa Travel Weather Averages. 2015. [ONLINE] Available: http://www.weatherbase.com/weather/weather.php3?s=687220&cityname=Sutherland-South-Africa. [2014, October 18].

ANONYMOUS, 2015. Western Cape Tourist Map - Western Cape South Africa • mappery. 2015. [ONLINE] Available at: http://www.mappery.com/Western-Cape-Tourist-Map. [Accessed 18 September 2015].

BIENIAWSKI, Z.T., 1989. Engineering Rock Mass Classifications. New York: Wiley.

BOTHA, R., 2015. Laser Pulse, E-mail to R. Botha [Online], 8 September. Available E-mail: roelf@hartrao.ac.za.

BRINK, A.B.A., 1981. Engineering Geology of South Africa. Volume 2. Pretoria: Building Publications.

BRINK, A.B.A., 1983. Engineering Geology of South Africa. Volume 3. Pretoria: Building Publications.

CHAPRONT, J., FRANCOU, G., 1973. Lunar Laser Ranging stations and reflectors [Online]. Available: http://www.checktheevidence.com/pdf/Laser%20ranging%20-%20Apollo%20Reflectors%20etc%20on%20The%20Moon.pdf [2014, March 16]

CHEN, K. AND LIU, J. 2010., PC Guided Design Method in Analysis for Rock Slope Stability in Geotechnical Engineering. Paper presented at 2010 2nd International Conference on Mechanical and Electronics Engineering, ICMEE 2010, August 1, 2010 - August 3. 2010.

COMBRINCK, L., FOURIE, C.J.S., CROUKAMP, L. and SAUNDERS, I., 2007. Report on preliminary geotechnical and tropospheric site investigation for a proposed space geodetic observatory near Matjiesfontein in the Great Karoo. South African Journal of Geology, 110(2), pp. 225-234.

COMBRINCK, L., 2015. Personal interview. 6 May. Hartebeesthoek Radio Astronomy Observatory.

Core Logging Committee of the South African Section of the Association of Engineering Geologists., 1976. A guide to core logging for rock engineering, in Symposium for Rock Engineering. Johannesburg: 71-86.

CRAIG, R.F., 2004. Craig's soil mechanics. 7 edn. New York: Taylor & Francis.

CROUKAMP, L., 2013. Personal interview. 7 August, Matjiesfontein.

CROUKAMP, L., ROSSOUW, J.J., FOURIE, C.J.S., COMBRINCK, L., 2011. Foundation requirements for a lunar laser ranger facility at matjiesfontein, South Africa. South African Journal of Geology, 114 (3-4): 573–576.

DAY, P.W., 1987. Prediction of Settlement. Lecture Course Programme 1987 Geotechnical Division.

DAY, P.W., 2014. Foundation Types. Unpublished class notes (Foundation Design 811). Stellenbosch: University of Stellenbosch.

DAS, B.M., 2002. Principles of Geotechnical Engineering. Bill Stenquist

DEERE, D.U., 1968, Geological Considerations, K.G. Stagg and O.C. Zienkiewicz, Rock Mechanics in Engineering Practice, Wiley, New York.

DE WET, M., 2013. Personal interview. 1 October, Stellenbosch.

DICKEY, J.O., BENDER, P.L., FALLER, J.E., 1994. "Lunar Laser Ranging: A Continuing Legacy of the Apollo Program", Science, Jul 22, pp.482-490.

DUNCAN, C., 1980. Toppling Rock Slope Failures Examples of Analysis and Stabilization. Unpublished paper delivered at The 21st U.S. Symposium on Rock Mechanics May 27 - 30, 1980, Rolla.

ECOSENSE, 2010. Proposed Matjiesfontein geodesy station. Environmental screening report edn. Stellenbosch: Ecosense Consulting Environmentalists.

ECOSENSE, 2015. Proposed Matjiesfontein geodesy station. Environmental screening report edn. Stellenbosch: Ecosense Consulting Environmentalists.

FRANKLIN, JA., BROCH, E., WALTON, G., 1971 Logging the mechanical character of rock. Trans Inst Min Metall 80:A1–A9

HOEK, E. and BRAY, J.W., 1981, Rock Slope Engineering: The Institute of Mining and Metallurgy, London, England.

HUNT, R.E., 2005, Geotechnical Engineering Investigation Handbook 2nd edn. CRC Press

JOHNSON, M.R., Anhaeusser, C.R., Thomas, R.J., 2006. The Geology of South Africa: Geological Society of South Africa, Johannesburg and the Council for Geoscience, Pretoria.

JONES, E.M., GLOVER, K., 2013. [Online]. Available: http://www.hq.nasa.gov/alsj/ [2015, March 30].

KIJKO, A., GRAHAM, G., BEJAICHUND, M., ROBLIN, D.L., BRANDT, M.B.C., 2003. Probabilistic Peak Ground Acceleration and Spectral Seismic Hazard Maps for South Africa.

LORY, J., [S.a.]. Structures of clays [Online] Available: http://soils.missouri.edu/about.asp [2015, Augustus 2].

MATHEWSON, C.C., 1981. Engineering geology. Merrill

MURPHY, T.W., 2013. Lunar laser ranging: the millimeter challenge. Reports on progress in physics. Physical Society (Great Britain), 76(7), p.076901. Available at: http://www.ncbi.nlm.nih.gov/pubmed/23764926.NASA. 1971. [Online]. Available: http://spaceflight.nasa.gov/gallery/images/apollo/apollo14/html/as14-67-09386.html [2015, Augustus 21].

NORMAN, N. & WHITFIELD, G., 2006. Geological Journeys. 1st ed. Cape Town: Struik Nature.

PECK, R.B., 1976, Rock Foundations for Structures, Rock Engineering for Foundations and Slopes. Proc. ASCE, Vol. 2: 1-21.

PETTERSEN, C., 2014. Study on the Swelling Potential of some Selected Rocks Catrine Pettersen., Norwegian University of Science and Technology

SHORT, N.M., 2005. Remote Sensing Tutorial [Online] Available: http://fas.org/irp/imint/docs/rst/Intro/Part2_1c.html [2014, July 15]

SILVERBERG, E.C., 1974, Operation and performance of a lunar laser ranging station, Appl. Opt., 13, 565-574, 1974.

STAGG, K.G., ZIENKIEWICZ, O.C., 1968, Rock Mechanics in Engineering Practice, John Wiley & Sons, New York.

STEINBRENNER, W., 1934. Tafeln zur setzungsberschnung. Die Strasse, 1: 121-124.

TARBUCK, E.J., LUTGENS, F.K., TASA, D., 1996. Earth. Prentice Hall

TERZAGHI, K., 1943, Theoretical Soil Mechanics, John Wiley & sons, New York, 5100pp.

TSIAMBAOS, G., SAROGLOU, H., 2009. Excavatability assessment of rock masses using the Geological Strength Index (GSI), in Bulletin of Engineering Geology and the Environment (2010) 69:13–27

ULUSAY, R., HUDSON, J.A., 2006, The Complete ISRM Suggested Methods for Rock Characterization, Testing and Monitoring: 1974-2006. Turkey: pp 53-60

VAN WYK, P., 2013. Rock Mechanics for Construction of the Gravimeter Vault at the Matjiesfontein Space Geodesy and Earth Observation Observatory. Unpublished Master's Thesis. Stellenbosch: University of Stellenbosch.

VEILLET, C., MANGIN, J.F., CHABAUBIE, J.E., DUMOLIN, C., FERAUDY, D. AND TORRE, J.M., 1993, Lunar Laser Ranging at CERGA for the Ruby Period (1981-1986), in Contributions of Space Geodesy to Geodynamics: Technology (eds D. E. Smith and D. L. Turcotte), American Geophysical Union, Washington, D. C.. doi: 10.1029/GD025p0189

VISSER, D., 2012. GPS survey and slope analysis at the Matjiesfontein Space Geodesy site for the emplacement of a Lunar Laser Ranger Unpublished BEng mini thesis. Stellenbosch: Stellenbosch University.

VISSER, J.N., VAN NIEKERK, B.N. & VAN DER MERWE, S.W., 2004. Sediment transport of the late Palaeozoic glacial Dwyka Group in the southwestern Karoo Basin. South African Journal of Geology, 100(3), pp. 223-236.

WATERS, J., 2011. Geotechnical Investigation of Palaeo-landslides at the Matjiesfontein Geodesy Observatory. Unpublished BEng mini thesis. Stellenbosch: Stellenbosch University.

WIUM, J., 2014. Personal interview. 31 July 2014, Stellenbosch.

ZHANG, C.L., WIECZOREK, K. AND XIE, M.L., 2010. Swelling experiments on mudstones., Journal of Rock Mechanics and Geotechnical Engineering, 2 (1): 44–51.

APPENDIX A: AS-BUILT DRAWINGS

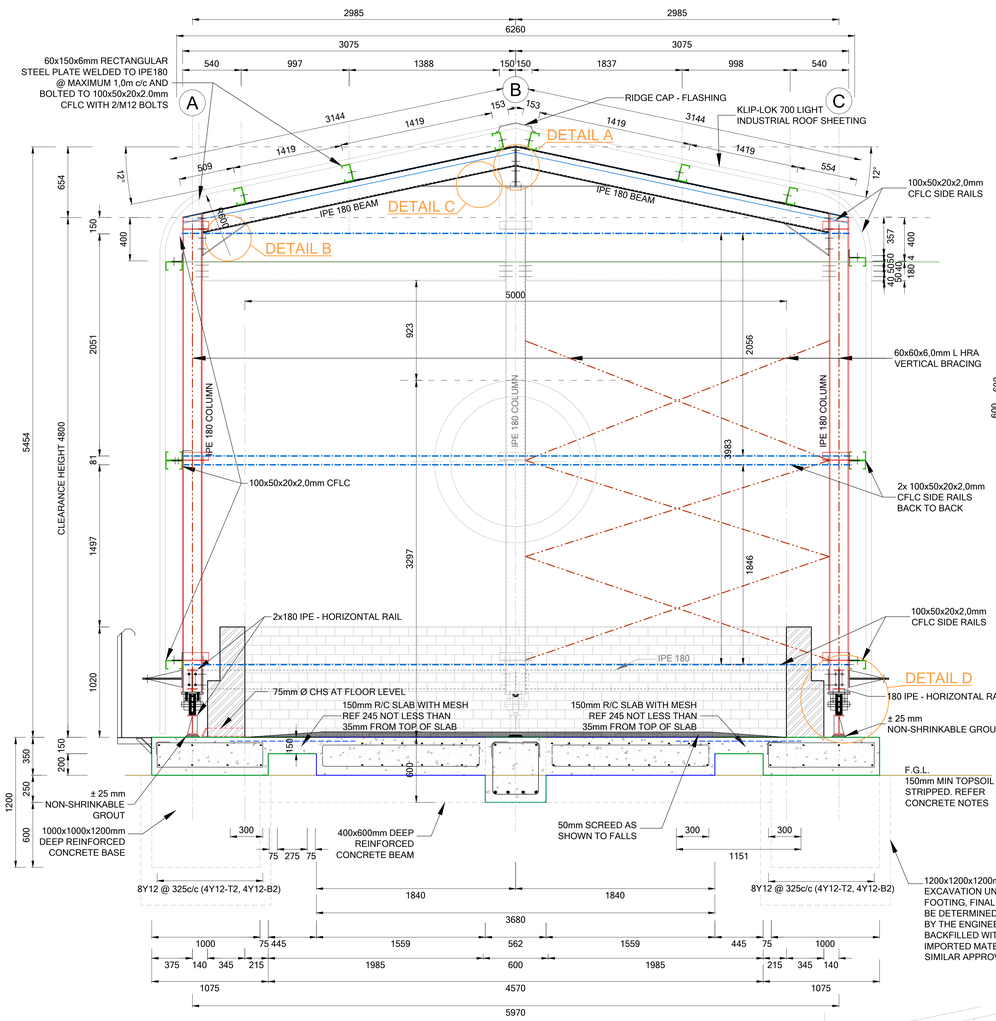

SECTION A-A
SCALE 1:20

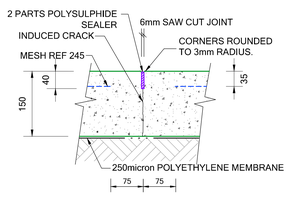

SECTION TYPICAL SAW JOINT
SCALE 1:5

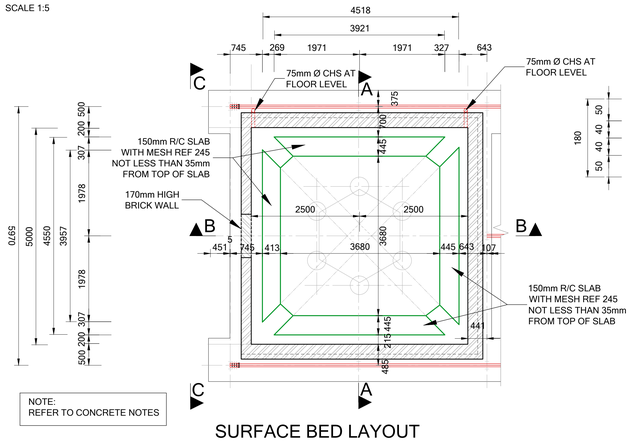

NOTE:
REFER TO CONCRETE NOTES

SURFACE BED LAYOUT
SCALE 1:50

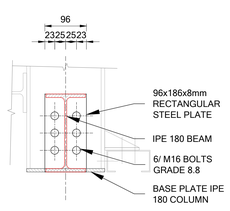

DETAIL K
SCALE 1:5

LEGEND:
SJ - SAW CUT JOINT
IJ - ISOLATION JOINT
MJ - MOVEMENT JOINT
CJ - CONSTRUCTION JOINT

NOTE:
- PROVIDE CONSTRUCTION JOINTS WHERE CASTING OF CONCRETE IS INTERUPTED AND CONTINUED AT A LATER STAGE.
- SAWCUT JOINTS TO BE CUT WITHIN 24 HOURS OF CASTING.

NOTE:
REFER TO DRAWING L2325/S2 FOR MORE DETAILS AND SECTIONS

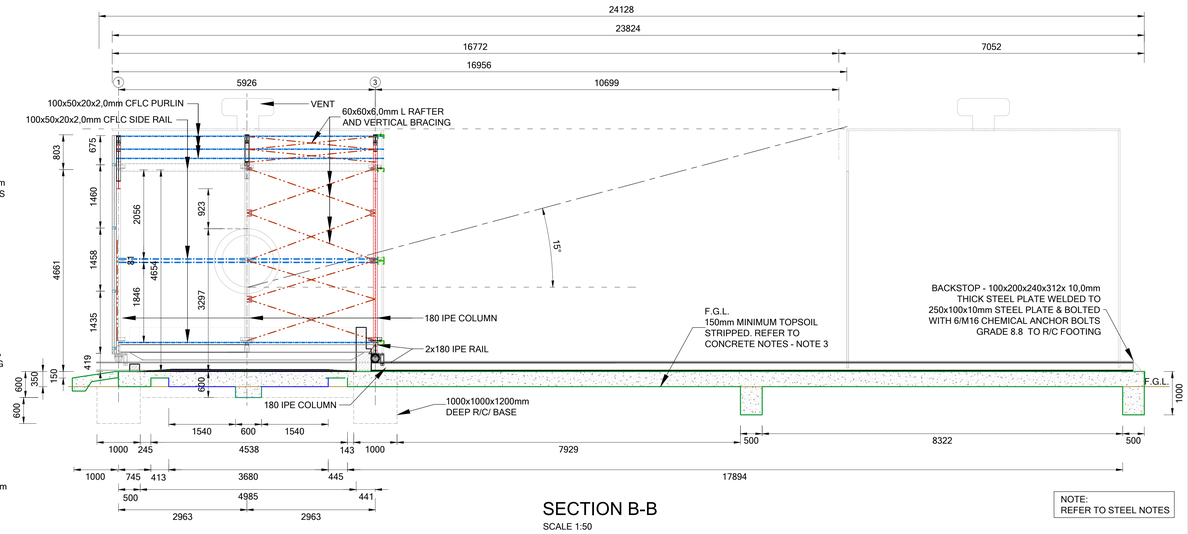

SECTION B-B
SCALE 1:50

NOTE:
REFER TO STEEL NOTES

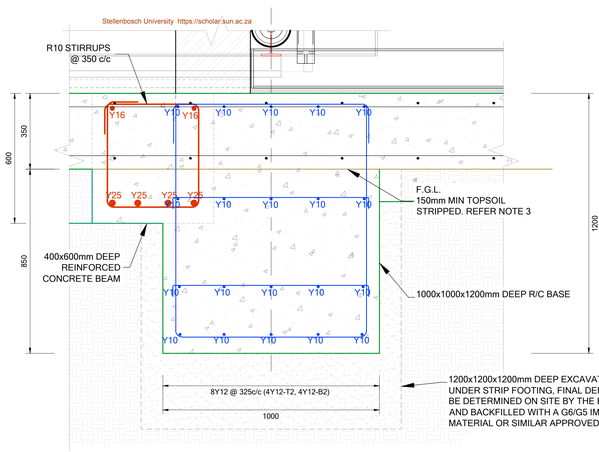

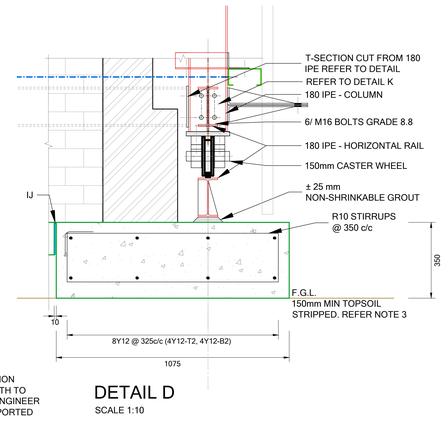

DETAIL D
SCALE 1:10

DETAIL M: BASE & BEAM
SCALE 1:10

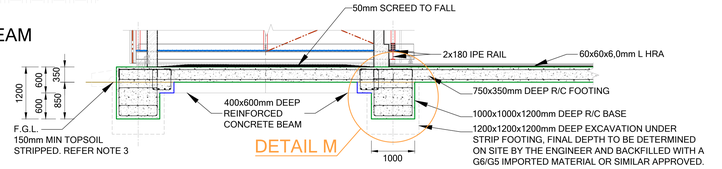

SECTION D-D
SCALE 1:50

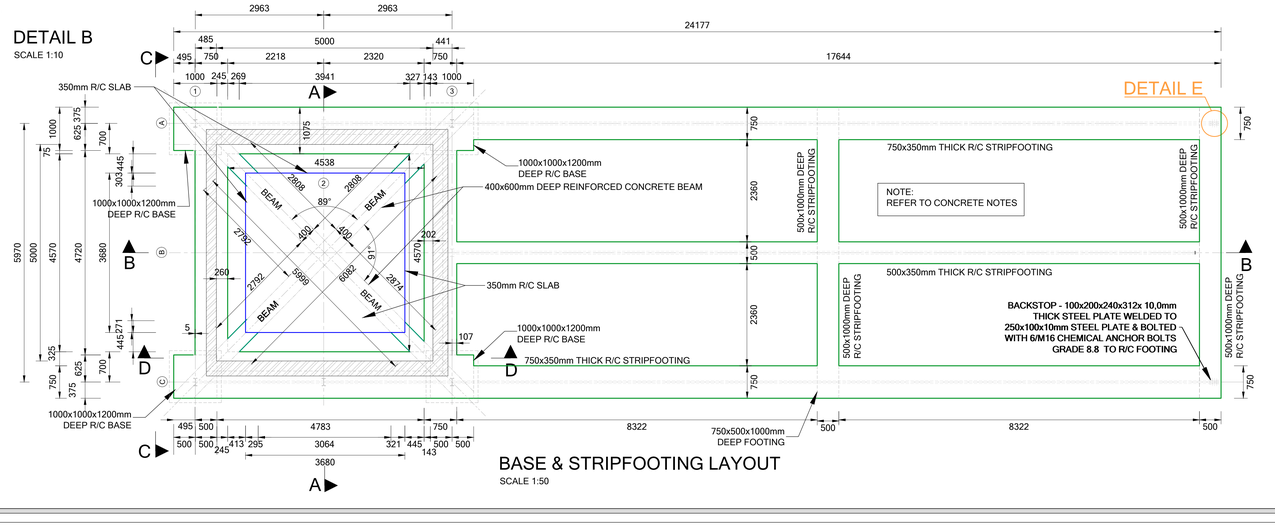

BASE & STRIPFOOTING LAYOUT
SCALE 1:50

DRAWINGS MUST NOT BE SCALED. FIGURED DIMENSIONS ONLY MAY BE USED. DIMENSIONS SHOULD BE VERIFIED IN FIELD AND ANY DISCREPANCIES REPORTED TO THE ENGINEER IMMEDIATLY. THIS DRAWING IS COPYRIGHT AND THE PROPERTY OF ENDECON AND MUST NOT BE RETAINED, COPIED OR USED WITHOUT AUTHORITY.

CONCRETE NOTES:

1. ALL CONCRETE WORK TO BE DONE IN ACCORDANCE WITH S.A.B.S. 1200, 28 DAY STRENGTH :-
   1.1. REINFORCED CONCRETE = 25Mpa/19mm.
   1.2. REINFORCED CONCRETE GROUND FLOOR = 30Mpa/19mm.
   1.3. CONCRETE SURFACE BED = 20Mpa/19mm.
   1.4. BLINDING/STRIP FOOTINGS = 20Mpa/19mm.
   1.5. REINFORCED CONCRETE COLUMNS = 30Mpa/19mm.
2. MIN. CONCRETE COVER TO MAIN REINFORCEMENT:-
   2.1. BASES = 50mm TOP & 75mm BOTTOM.
3. NO CONCRETE MAY BE POURED BEFORE THE ENGINEER HAS APPROVED FOUNDATION CONDITIONS AND ALL REINFORCEMENT.
4. NO DIMENSIONS MUST BE SCALED ON THE DRAWING, CONTACT THE ENGINEER. ALL DIMENSIONS AND LEVELS TO BE CHECKED ON SITE BEFORE STARTING WORK.
5. CONCRETE WORK SHOULD BE TO DEGREE OF ACCURACY 2 AS PER SABS 1200 G CLAUSE 6.

STEEL NOTES:

1) ALL WELDS TO BE FULL STRENGTH FILLET WELDS ALL ROUND WITH THICKNESS OF SMALLER CONNECTED ELEMENT
2) ALL STEEL TO BE GRADE 350W
3) ALL BOLTS TO BE GRADE 8.8
4) PAINT SPECIFICATION -
   I. CORROSION PROTECTION TO SABS 1200 HC AND MUST BE READ IN CONJUNCTION WITH SABS 0120 SECTION HC PART 3
   II. PAINT SYSTEM ALKYD-013-016 IS USED 1st COAT: ZINC PHOSPHATE 30 MICRON (DFT) TO SABS 678 2nd COAT: GENERAL TYPE UNDERCOAT 30 MICRON (DFT)
   TO SABS 681. 3rd COAT: ALKYD ENAMEL 30 MICRON TO SABS 630, COLOUR ACC. TO ARCHITECT.
5) CLEANING OF STEEL TO SABS 064 AND SIS 05 59 00 ST2.

Rev. Her.	Description Beskrywing	Date Datum	By Deur
07	UPDATED AS BUILT CHANGES	01/08/2011	PDP
06	ADDED DIMENSION, UPDATED SECT B-B	20/05/2011	PDP
05	BEAMS ADDED, SURFACE BED CHANGED	6/04/2011	PDP
04	ADJUSTED STRIPFOOTINGS (1mx1mx1m)	30/03/2011	PDP
03	ADDED DETAILS, CFLC, ETC	04/02/2011	PDP
02	ADDED 180 IPE'S FRONT & BACK, CHANGED DOORS	03/02/2011	PDP
01	GENERAL UPDATE	27/01/2011	PDP

AMENDMENTS/WYSIGING

SERVICE: STRUCTURE — DIENS

DESIGNED/ONTWERP	DJ ERASMUS
DRAWN/GETEKEN	P DU PREEZ
CAD FILE NAME/CAD LÊER NAAM	
CHECKED/NAGESIEN	DJ ERASMUS
APPROVED/GOEDGEKEUR	

ENDECON
UBUNTU (PTY) LTD
ENGINEERING CONSULTANTS
P.O. BOX 477
FAUNA PARK
0787
Tel: +27 (15) 291-3363
Fax: +27 (15) 291-3403
E-mail : limpopo@endecon.co.za

CLIENT / KLIENT: SPACE GEODESY HartRAO

PROJECT / PROJEK: OBSERVATORY TELESCOPE HOUSING

TITLE / TITEL: BASES, STRIPFOOTING, STEEL STRUCTURE, DETAILS & SECTIONS - AS BUILT PLAN

DATE/DATUM	OCTOBER 2010
SCALE/SKAAL	AS SHOWN

SCALE REF. / SKAAL VERWYS.: 4.0 2.0 0 2.0 4.0 / 3.0 1.0 1.0 3.0 meter

CONSULTANT DWG. NO. / KONSULTANT TEK. NR.: P2325/S1 — 07

CLIENT DWG. NO. / KLIËNT TEK. NO.:

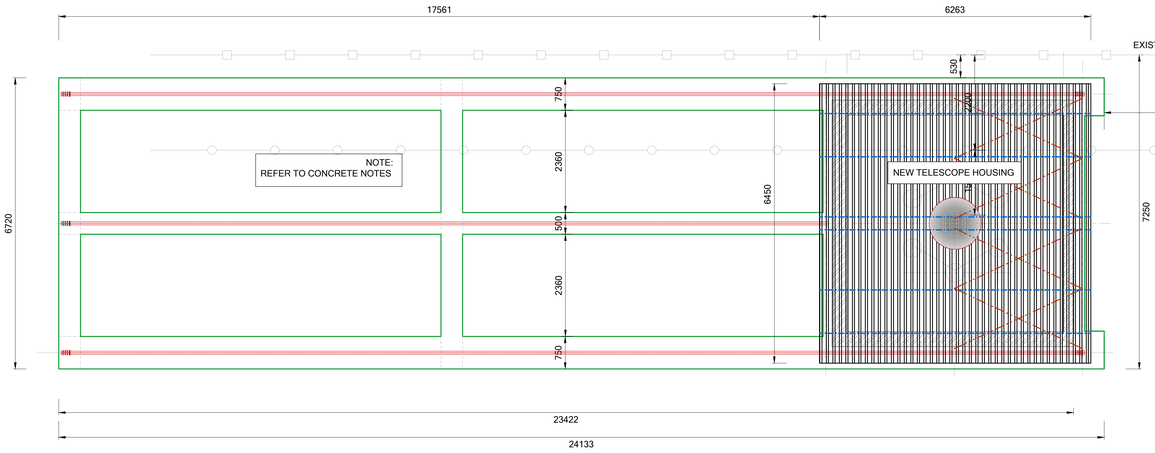

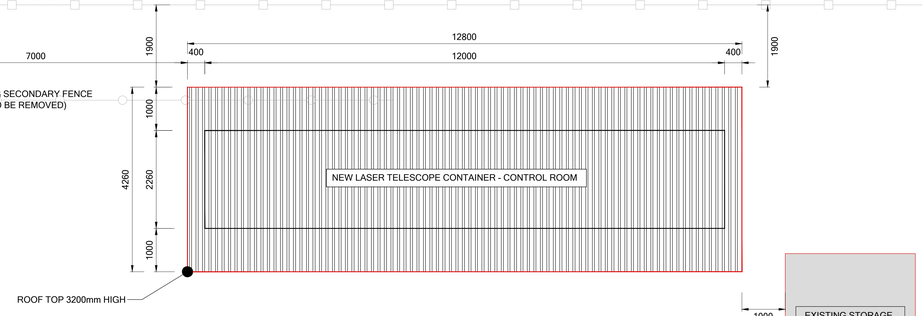

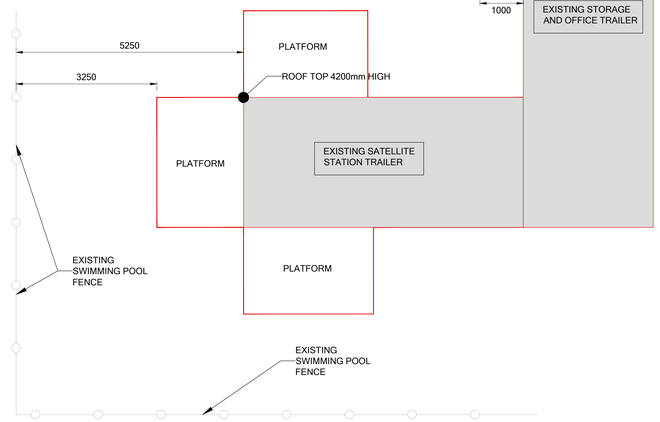

PROPOSED SITE LAYOUT
SCALE 1:50

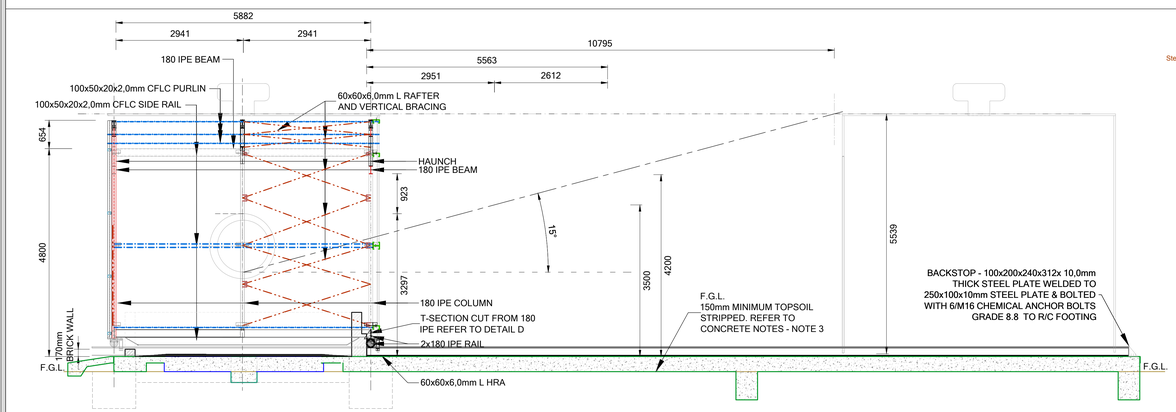

PLAN SHOWING VISUAL CLEARANCE
SCALE 1:50

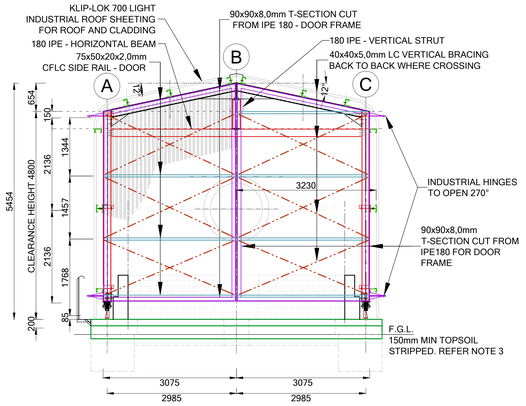

ELEVATION C-C
SCALE 1:50

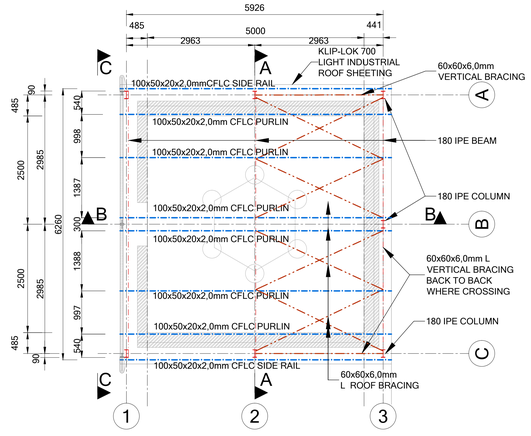

ROOF LAYOUT
SCALE 1:50

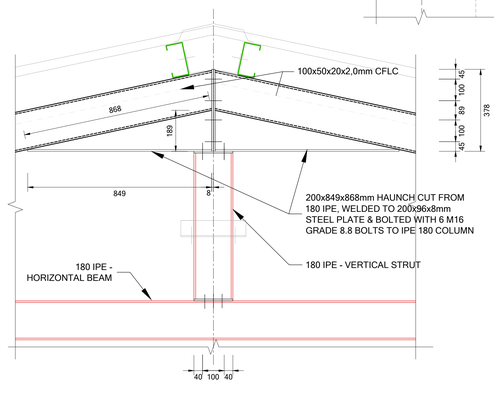

DETAIL C
SCALE 1:10

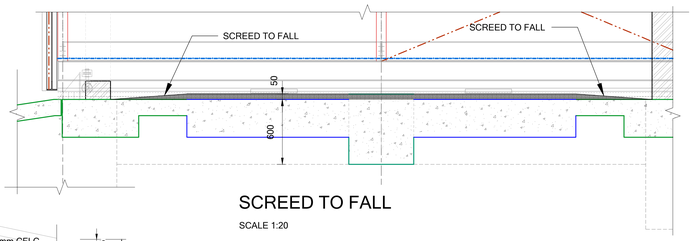

SCREED TO FALL
SCALE 1:20

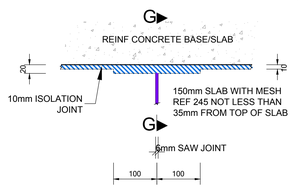

PLAN DETAIL SHOWING INTERSECTION OF SAW- AND ISOLATION JOINT
SCALE 1:5

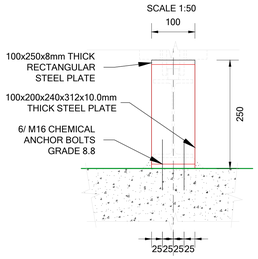

SECTION F-F
SCALE 1:5

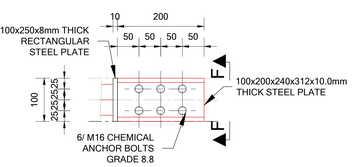

DETAIL E
SCALE 1:5

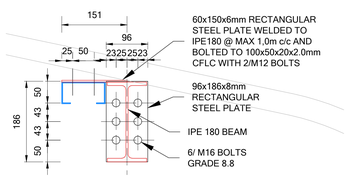

SECTION E-E
SCALE 1:5

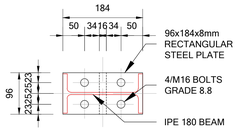

SECTION K-K
SCALE 1:5

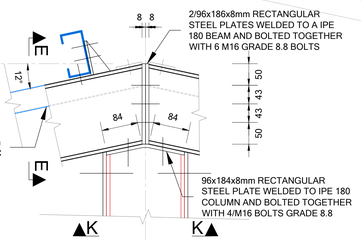

DETAIL A
SCALE 1:5

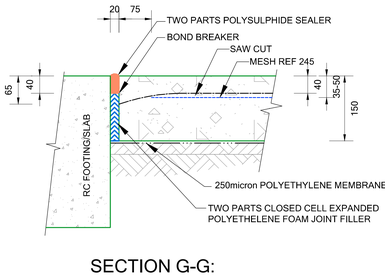

SECTION G-G:
TYPICAL ISOLATION JOINT
SCALE 1:5

DRAWINGS MUST NOT BE SCALED. FIGURED DIMENSIONS ONLY MAY BE USED. DIMENSIONS SHOULD BE VERIFIED IN FIELD AND ANY DISCREPANCIES REPORTED TO THE ENGINEER IMMEDIATLY. THIS DRAWING IS COPYRIGHT AND THE PROPERTY OF ENDECON AND MUST NOT BE RETAINED, COPIED OR USED WITHOUT AUTHORITY.

CONCRETE NOTES:

1. ALL CONCRETE WORK TO BE DONE IN ACCORDANCE WITH S.A.B.S. 1200, 28 DAY STRENGTH :-
   1.1. REINFORCED CONCRETE = 25Mpa/19mm.
   1.2. REINFORCED CONCRETE GROUND FLOOR = 30Mpa/19mm.
   1.3. CONCRETE SURFACE BED = 20Mpa/19mm.
   1.4. BLINDING/STRIP FOOTINGS = 20Mpa/19mm.
   1.5. REINFORCED CONCRETE COLUMNS = 30Mpa/19mm.
2. MIN. CONCRETE COVER TO MAIN REINFORCEMENT:-
   2.1. BASES = 50mm TOP & 75mm BOTTOM.
3. NO CONCRETE MAY BE POURED BEFORE THE ENGINEER HAS APPROVED FOUNDATION CONDITIONS AND ALL REINFORCEMENT.
4. NO DIMENSIONS MUST BE SCALED ON THE DRAWING, CONTACT THE ENGINEER. ALL DIMENSIONS AND LEVELS TO BE CHECKED ON SITE BEFORE STARTING WORK.
5. CONCRETE WORK SHOULD BE TO DEGREE OF ACCURACY 2 AS PER SABS 1200 G CLAUSE 6.

STEEL NOTES:

1) ALL WELDS TO BE FULL STRENGTH FILLET WELDS ALL ROUND WITH THICKNESS OF SMALLER CONNECTED ELEMENT
2) ALL STEEL TO BE GRADE 350W
3) ALL BOLTS TO BE GRADE 8.8
4) PAINT SPECIFICATION -
   I. CORROSION PROTECTION TO SABS 1200 HC AND MUST BE READ IN CONJUNCTION WITH SABS 0120 SECTION HC PART 3
   II. PAINT SYSTEM ALKYD-013-016 IS USED 1st COAT: ZINC PHOSPHATE 30 MICRON (DFT) TO SABS 678 2nd COAT: GENERAL TYPE UNDERCOAT 30 MICRON (DFT)
   TO SABS 681. 3rd COAT: ALKYD ENAMEL 30 MICRON TO SABS 630, COLOUR ACC. TO ARCHITECT.
5) CLEANING OF STEEL TO SABS 064 AND SIS 05 59 00 ST2.

NOTE:
REFER TO DWG L2325/S1 FOR MORE DETAILS AND SECTIONS

Rev. Her.	Description Beskrywing	Date Datum	By Deur
03	UPDATED SHEET, DETAILS FROM S1	06/04/2011	PDP
02	CHANGED BUILDING POSITIONS	15/02/2011	PDP
01	ADDED DETAIL H & MOVED DETAILS FROM L2325/S1 TO -/S2	04/02/2011	PDP

AMENDMENTS/WYSIGING

SERVICE / DIENS

STRUCTURE

DESIGNED/ONTWERP	DJ ERASMUS
DRAWN/GETEKEN	P DU PREEZ
CAD FILE NAME/CAD LÊER NAAM	
CHECKED/NAGESIEN	DJ ERASMUS
APPROVED/GOEDGEKEUR	

ENDECON
UBUNTU (PTY) LTD
ENGINEERING CONSULTANTS
P.O. BOX 477
FAUNA PARK
0787
Tel: +27 (15) 291-3363
Fax: +27 (15) 291-3403
E-mail : limpopo@endecon.co.za

CLIENT / KLIENT

SPACE GEODESY
HartRAO

PROJECT / PROJEK

OBSERVATORY
TELESCOPE HOUSING

TITLE / TITEL

PROPOSED SITE
LAYOUT & ROOF
AS-BUILT PLAN

DATE/DATUM	FEBRUARY 2011
SCALE/SKAAL	AS SHOWN

SCALE REF. / SKAAL VERWYS.
4.0 2.0 0 2.0 4.0
3.0 1.0 1.0 3.0
meter

CONSULTANT DWG. NO. / KONSULTANT TEK. NR.
P2325/S2
03

CLIENT DWG. NO. / KLIËNT TEK. NO.

APPENDIX B: CONSTRUCTION SITE PHOTOS

FIGURE 39: CONSTRUCTION OF THE S/LLR FOUNDATION AT HARTRAO: TRACKS

FIGURE 40: CONSTRUCTION OF THE S/LLR FOUNDATION AT HARTRAO: BASE

FIGURE 41: CONSTRUCTION OF THE S/LLR FOUNDATION AT HARTRAO: COMPLETED

FIGURE 42: PLACING OF THE S/LLR ON THE BASE OF THE FOUNDATION

FIGURE 43: THE S/LLR AT HARTRAO, WITH RUN-OFF SHED IN BACKGROUND

APPENDIX C: UCS TEST SAMPLES

FIGURE 44: SAMPLES AFTER UCS TESTING. (A) SAMPLE 1C, (B) SAMPLE 2C, (C) SAMPLE 2D AND (D) SAMPLE 2E.

APPENDIX D: POINT LOAD TEST SAMPLES

FIGURE 45: SAMPLES AFTER POINT LOAD TESTING. (A) SAMPLE 1D, (B) SAMPLE 1E, (C) SAMPLE 2G AND (D) SAMPLE 2F.

FIGURE 46: SAMPLES AFTER POINT LOAD TESTING. (A) SAMPLE 3C, (B) SAMPLE 3D, (C) SAMPLE 3E AND (D) SAMPLE 3F.

APPENDIX E: PETROGRAPHIC ANALYSES

SAMPLE NO.: 1A - SANDY MUDSTONE

MACROSCOPIC ROCK DESCRIPTION

Fine to very fine-grained, light brown to cream-coloured rock with alternating light and dark layers (<1cm) and irregular parches of orange to dark brown colour occurring locally.

MICROSCOPIC ROCK DESCRIPTION

Composition: Quartz (70%), Clay minerals (15%), Mica (5%), Iron oxide (5%), Feldspar (5%)
Rock fragments (<1%), Carbon (<1%)

Grain size: Fine-grained (47µm to 130µm)

Sorting: Poorly

Rounding: Poorly rounded

Clast/matrix supported: Clast supported layers alternating with matrix supported layers

Other textures: Horisontal layers and discolourations

Description: The rock is a rhythmically layered sedimentary rock consisting of lighter and darker interlayers and irregular patches of darker colour. Lighter coloured layers are composed of quartz and feldspar (80%) set in a clay and mica-rich matrix (20%) (**Figure 39**). Quartz and feldspar in these layers is poorly rounded and is poorly sorted. Some straining was observed with some quartz grains showing overgrowths. Feldspar shows some alteration in the centres of some grains. Mica and clay minerals are mainly randomly orientated with some elongated grains observed locally. Iron oxide occurs in the matrix and enhances the horizontal layering. Darker coloured layers are finer-grained and dominated by a matrix (90%) consisting of iron oxide, clay minerals and mica orientated parallel to bedding with minor quartz (10%) (**Figure 40**).

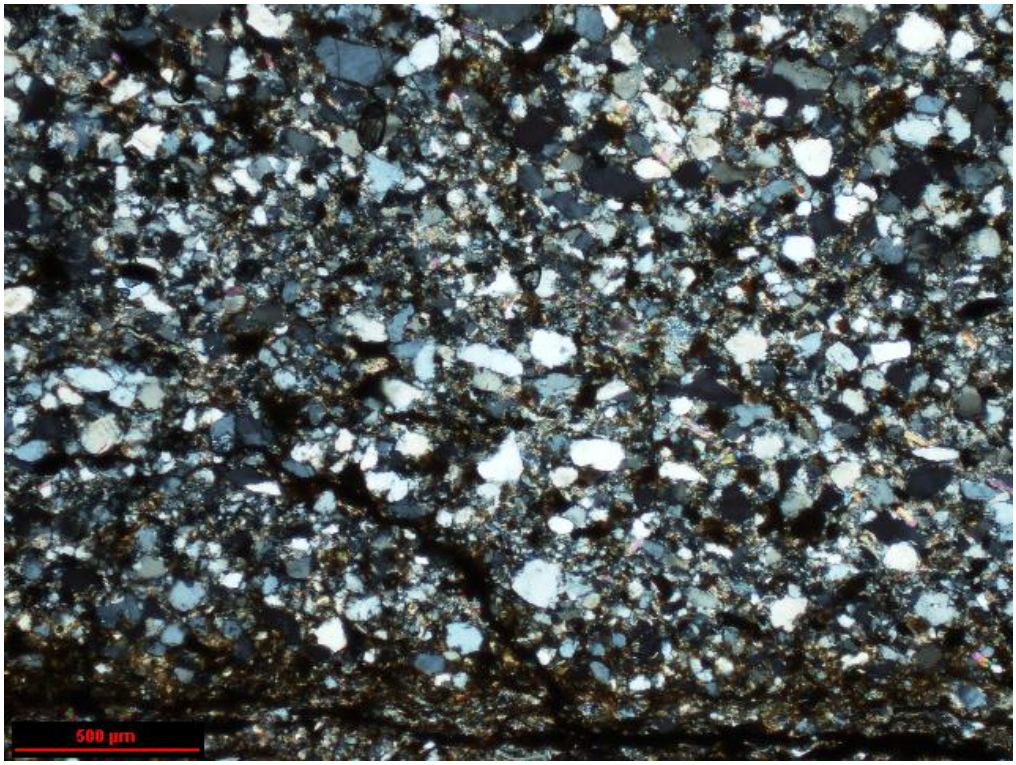

FIGURE 47: PHOTOMICROGRAPHS OF A THIN SECTION SHOWING ANGULAR TO SUB-ANGULAR QUARTZ IN A CLAY-MICA MATRIX

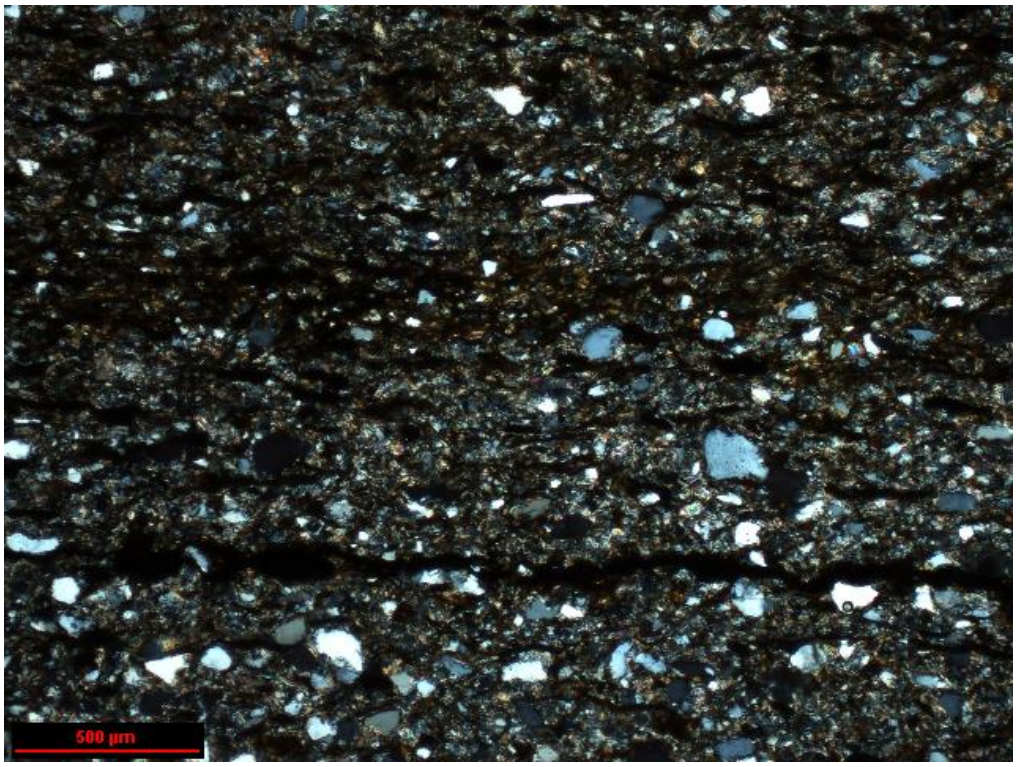

FIGURE 48: PHOTOMICROGRAPHS OF A THIN SECTION SHOWING ANGULAR TO SUB-ANGULAR QUARTZ IN A CLAY-MICA MATRIX OF MATRIX SUPPORTED LAYERS

SAMPLE NO.: 1B_1 - SANDY MUDSTONE

MACROSCOPIC ROCK DESCRIPTION

Very fine-grained, light brown to cream-coloured rock with alternating light and dark layers.

MICROSCOPIC ROCK DESCRIPTION

Composition: Quartz (40%), Clay minerals (10%), Mica (10%), Iron oxide (40%), Feldspar (<1%) Rock fragments (<1%)

Grain size: Fine-grained (40µm to 100µm)

Sorting: Moderately

Rounding: Angular to sub-angular (0.2 to 0.3)

Clast/matrix supported: Clast supported layers alternating with matrix supported layers

Other textures: Horisontal layers, Rhythmite

Description: The rock is a rhythmically layered sedimentary rock consisting of interlayers of lighter and darker colour. Lighter coloured layers are composed of quartz (90%) set in a clay and mica-rich matrix (<10%) (**Figure 41**). Quartz in these layers is angular to sub-angular and is moderately sorted. Some straining was observed with some quartz grains showing overgrowths.

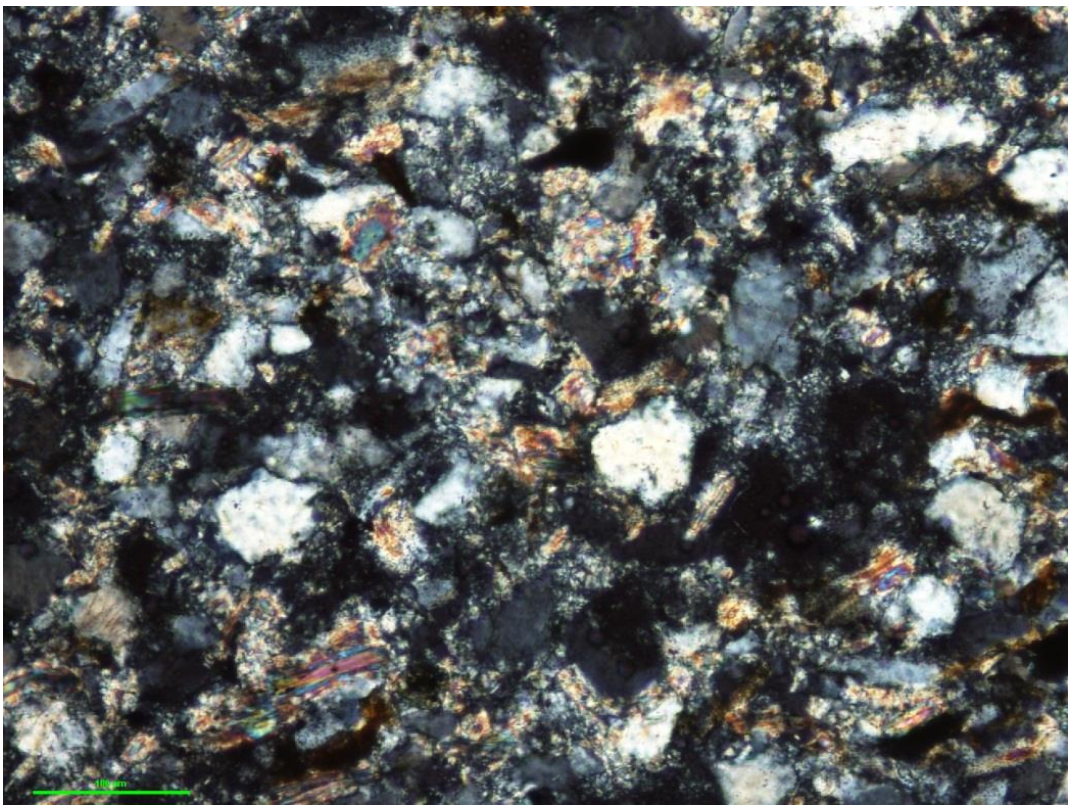

FIGURE 49: PHOTOMICROGRAPHS OF A THIN SECTION SHOWING ANGULAR TO SUB-ANGULAR QUARTZ IN A CLAY-MICA MATRIX. NOTE SOME STRAINING IN QUARTZ

SAMPLE NO.: 1B_2 - SANDY MUDSTONE

MACROSCOPIC ROCK DESCRIPTION

Very fine-grained, light brown to cream-coloured rock with alternating light and dark layers.

MICROSCOPIC ROCK DESCRIPTION

Composition: Quartz (30%), Clay minerals (40%), Mica (10%), Iron oxide (20%), Feldspar (<1%)
Rock fragments (<1%)

Grain size: Fine-grained (<66µm)

Sorting: Moderately to poorly

Rounding: Angular to unrounded

Clast/matrix supported: Clast supported layers alternating with matrix supported layers

Other textures: Horisontal layers, Rhythmite

Description: The rock is a rhythmically layered sedimentary rock consisting of interlayers of lighter and darker colour. Lighter coloured layers are composed of quartz (75%) (± feldspar) set in a clay and mica-rich matrix (15%). Quartz in these layers is angular to sub-angular and is moderately sorted. Some quartz grains show overgrowths and straining was observed with some signs of recrystalisation. The matrix consists of mica and clay (including smectite) mainly unoriented. Some elongated mica grains were observed.

SAMPLE NO.: 2A - MUDSTONE

MACROSCOPIC ROCK DESCRIPTION

Very fine-grained, brown coloured rock with alternating light and dark layers.

MICROSCOPIC ROCK DESCRIPTION

Composition: Quartz (%), Clay minerals (%), Mica (%), Iron oxide (%), Feldspar (%)
Rock fragments (<1%), Carbon (%) (extremely fine grained makes description extremely difficult)

Grain size: Very fine-grained (<40µmm)

Sorting: Moderately

Rounding: Angular to sub-angular

Clast/matrix supported: Clast supported layers alternating with matrix supported layers

Other textures: Horizontal layers, Rhythmite

Description: The rock is a rhythmically layered sedimentary rock consisting of lighter and darker brown interlayers (**Figure 42** and **Figure 43**). The rock is extremely fine grained which makes description extremely difficult.

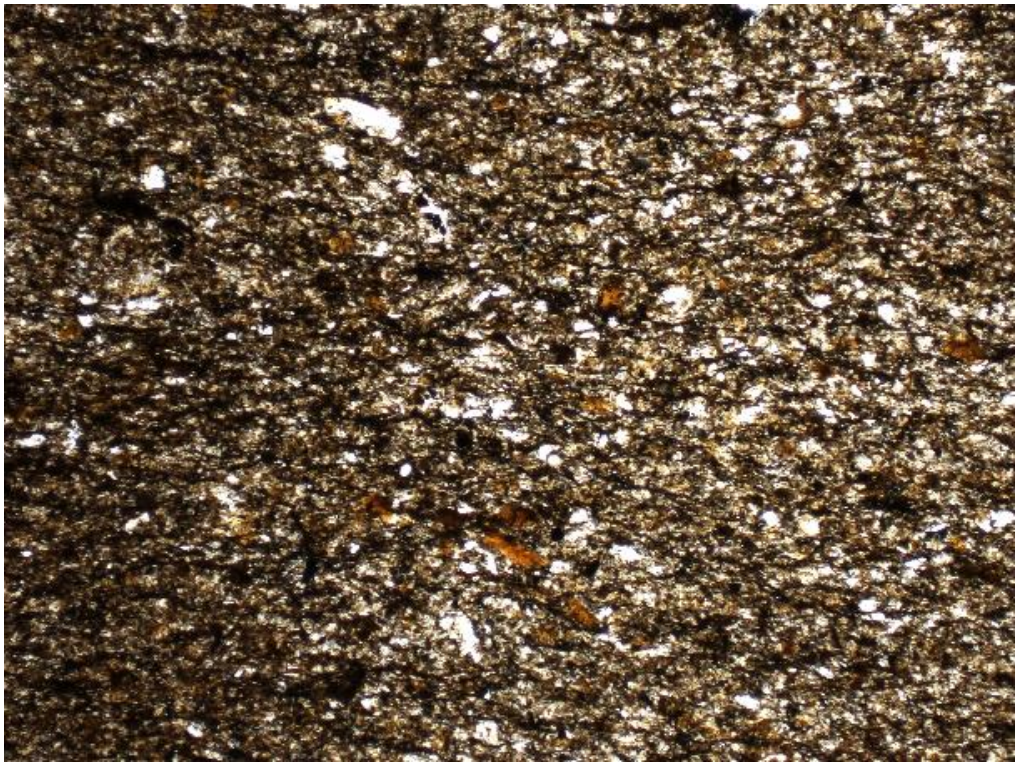

FIGURE 50: PHOTOMICROGRAPHS OF A THIN SECTION SHOWING ANGULAR TO SUB-ANGULAR QUARTZ IN A CLAY-MICA MATRIX

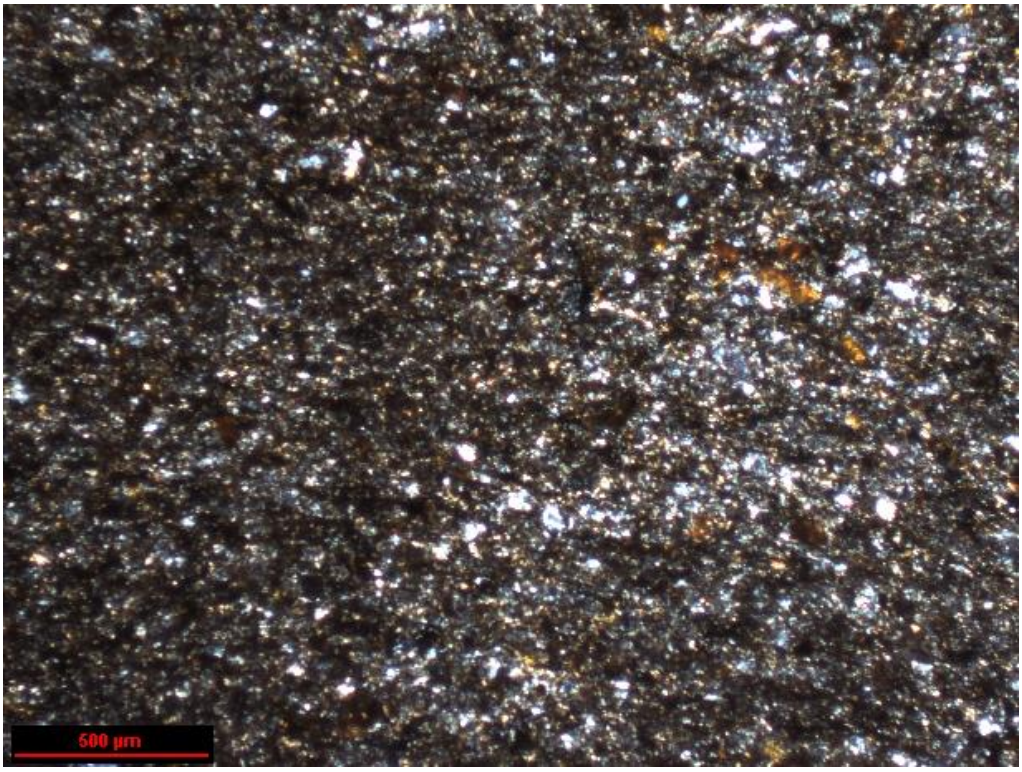

FIGURE 51: PHOTOMICROGRAPHS OF A THIN SECTION SHOWING ANGULAR TO SUB-ANGULAR QUARTZ IN A CLAY-MICA MATRIX

SAMPLE NO.: 2B - SANDY MUDSTONE

MACROSCOPIC ROCK DESCRIPTION

Fine to very fine-grained, browncoloured rock with alternating light and dark brown layers (<1cm).

MICROSCOPIC ROCK DESCRIPTION

Composition: Quartz (30%), Clay minerals (10%), Mica (5%), Iron oxide (55%), Feldspar (<1%), Rock fragments (<1%), Carbon (<1%)

Grain size: Fine-grained (18µm to 65µm)

Sorting: Poorly

Rounding: Angular to sub-angular

Clast/matrix supported: Matrix supported layers

Other textures: Horisontal layers, Rhythmite

Description: The rock is a rhythmically layered sedimentary rock consisting of lighter and darker brown coloured interlayers (Figure 4a). Lighter coloured layers are composed of quartz (80%) set in a clay and mica-rich matrix (20%) (**Figure 44**). Quartz in these layers is angular to sub-angular and is poorly sorted. Some straining in the quartz grains occurs but no signs of recrystallisation were observed. Some quartz grains show overgrowths. Mica and clay minerals are mainly randomly orientated with some elongated grains observed locally. Iron oxide occurs in the matrix and enhances the horizontal layering (**Figure 45**). Darker coloured layers are dominated by iron oxide, clay minerals and mica orientated parallel to bedding with minor quartz (<10%).

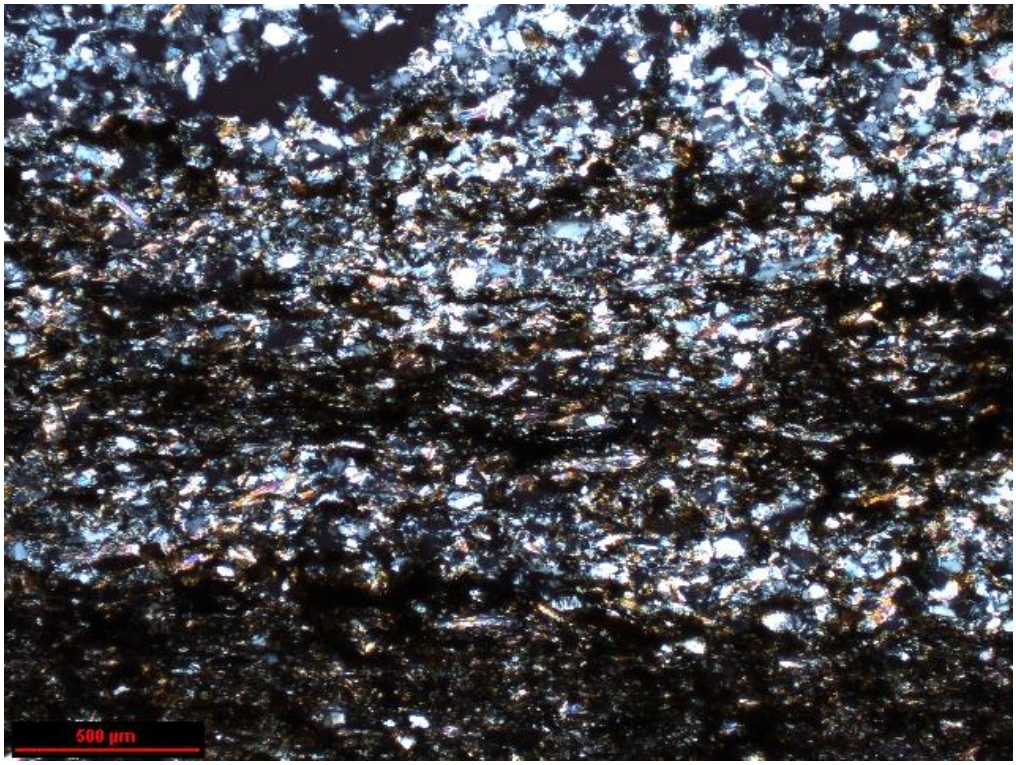

FIGURE 52: PHOTOMICROGRAPHS OF A THIN SECTION SHOWING ANGULAR TO SUB-ANGULAR QUARTZ IN A CLAY-MICA MATRIX. NOTE DARK AND LIGHT RITHMIC LAYERING

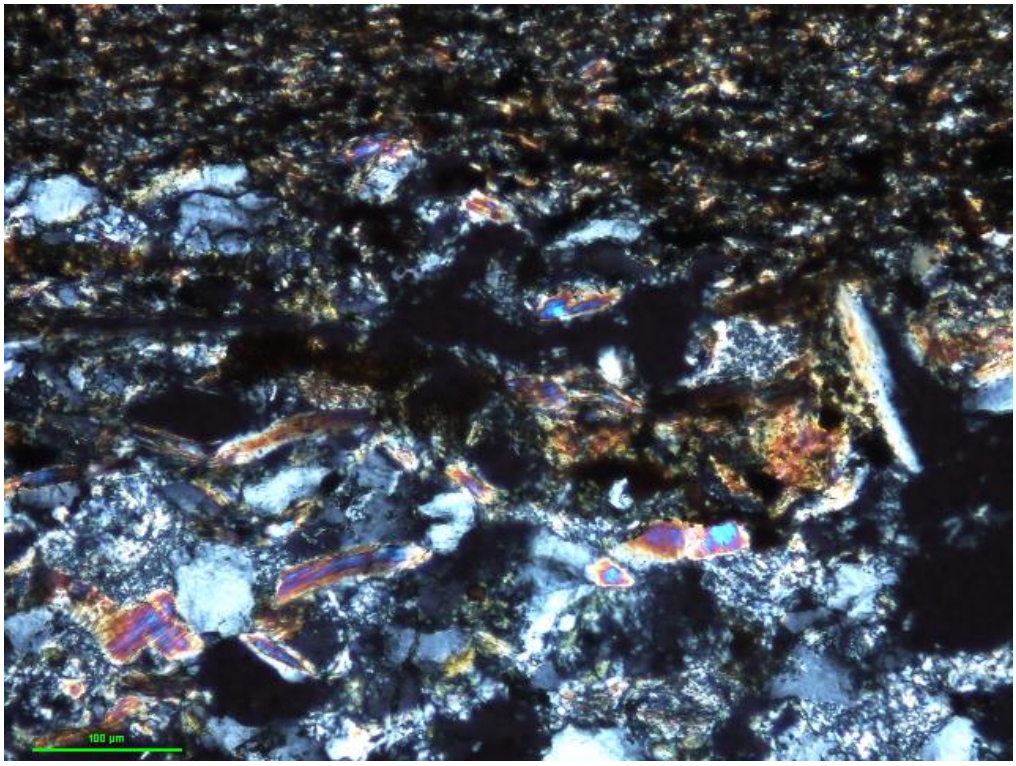

FIGURE 53: PHOTOMICROGRAPHS OF A THIN SECTION SHOWING ANGULAR TO SUB-ANGULAR QUARTZ IN A CLAY-MICA MATRIX. CLOSE-UP VIEW OF STRAINING IN QUARTZ AND CLAY-MINERALS IN THE MATRIX

SAMPLE NO.: 3A - SANDY MUDSTONE

MACROSCOPIC ROCK DESCRIPTION

Fine to very fine-grained, light brown to cream-coloured rock with alternating light and dark layers (<1cm) and irregular parches of orange to dark brown colour occurring locally.

MICROSCOPIC ROCK DESCRIPTION

Composition: Quartz (70%), Clay minerals (15%), Mica (5%), Iron oxide (5%), Feldspar (5%) Rock fragments (<1%), Carbon (<1%)

Grain size: Fine-grained (40µm to 100µm)

Sorting: Poorly

Rounding: Unrounded to angular

Clast/matrix supported: Matrix supported layers

Other textures: Horizontal layers and discolorations

Description: The rock is a rhythmically layered sedimentary rock consisting of lighter and darker interlayers (<2cm). Lighter coloured layers are composed of quartz and feldspar (80%) set in a clay and mica-rich matrix (20%). Quartz in these layers is unrounded to angular (**Figure 46**) and is poorly sorted. Some straining was observed with some quartz grains showing overgrowths. Mica and clay minerals are mainly randomly orientated with some elongated grains observed locally. Iron oxide occurs in the matrix and enhances the horizontal layering. Darker coloured layers are finer-grained and dominated by a matrix (90%) consisting of iron oxide, clay minerals and mica orientated parallel to bedding with minor quartz (10%).

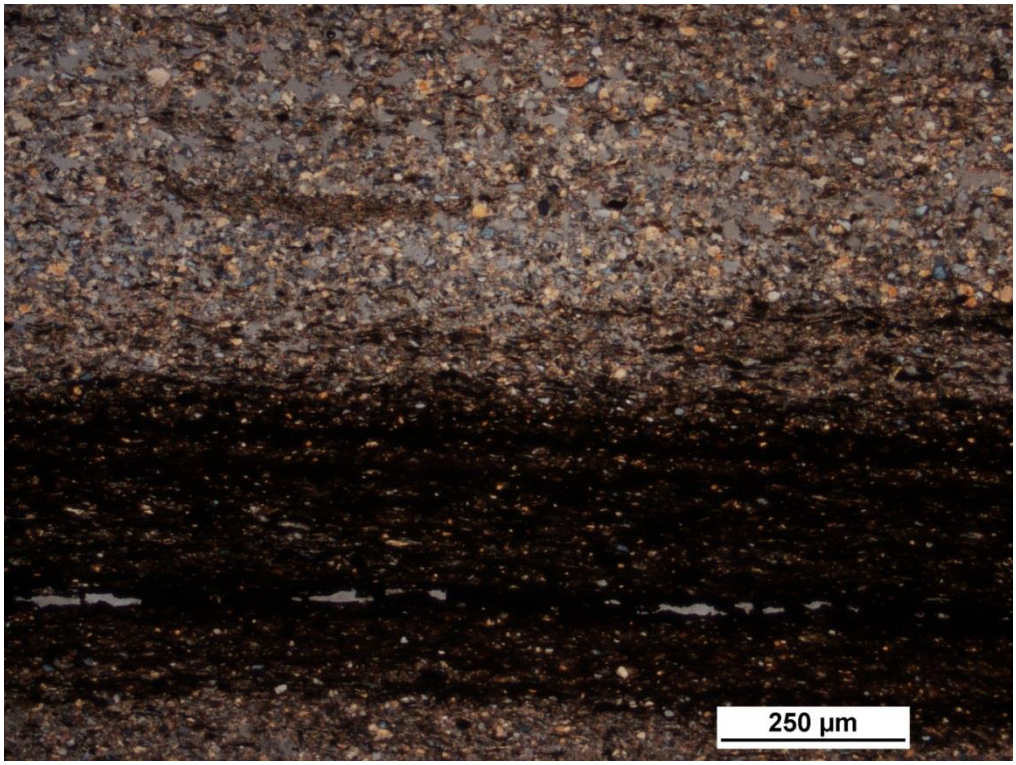

FIGURE 54: PHOTOMICROGRAPHS OF A THIN SECTION SHOWING UNROUNDED TO ANGULAR QUARTZ IN A CLAY-MICA MATRIX

SAMPLE NO.: 3B - SANDY MUDSTONE

MACROSCOPIC ROCK DESCRIPTION

Fine to very fine-grained, light brown to cream-coloured rock with alternating light and dark layers (<1cm).

MICROSCOPIC ROCK DESCRIPTION

Composition: Quartz (20%), Clay minerals (30%), Mica (5%), Iron oxide (45%), Feldspar (<1%)
Rock fragments (<1%), Carbon (<1%)

Grain size: Fine-grained (30µm to 60µm)

Sorting: Moderately

Rounding: Sub-angular

Clast/matrix supported: Clast supported layers alternating with matrix supported layers

Other textures: Horizontal layers, Rhythmite

Description: The rock is a rhythmically layered sedimentary rock consisting of lighter and darker interlayers (**Figure 47**). Lighter coloured layers are composed of quartz (80%) set in a clay and mica-rich matrix (20%). Quartz in these layers is sub-angular and is moderately sorted (**Figure 48**). Some straining was observed with some quartz grains showing recrystallisation (**Figure 47** to **Figure 50**). Mica and clay minerals are mainly randomly orientated with some elongated grains observed locally. Iron oxide occurs in the matrix and enhances the horizontal layering (**Figure 48** to **Figure 50**). Darker coloured layers are dominated by a matrix (90%) consisting of iron oxide, clay minerals and mica orientated parallel to bedding with minor quartz (10%).

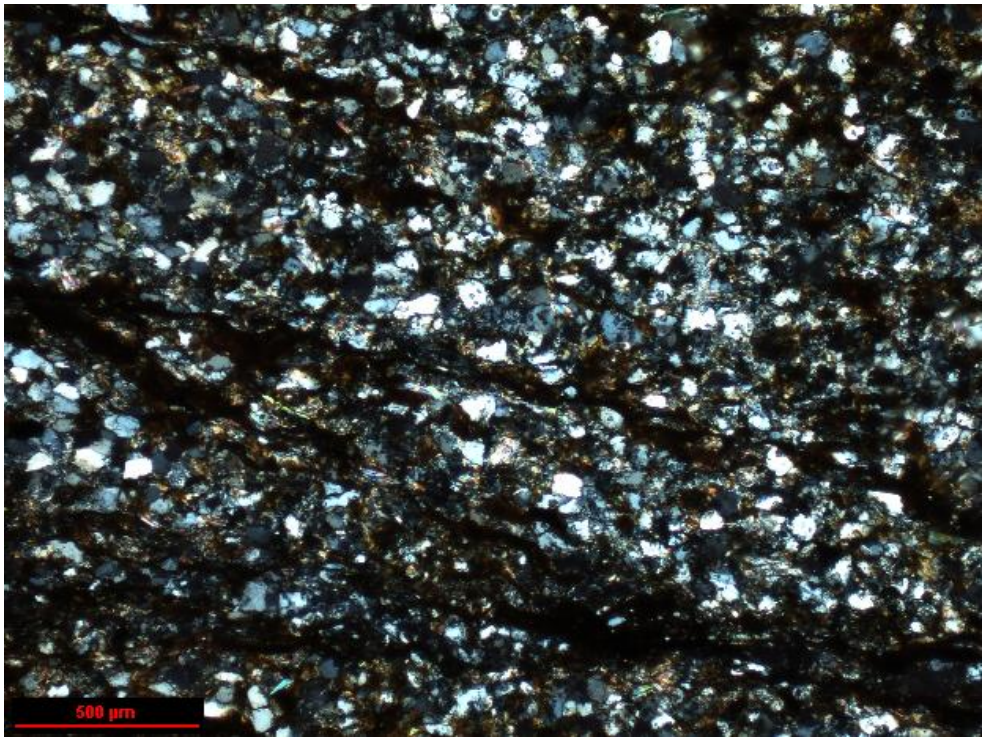

FIGURE 55: PHOTOMICROGRAPHS OF A THIN SECTION SHOWING ANGULAR TO SUB-ANGULAR QUARTZ IN A CLAY-MICA MATRIX

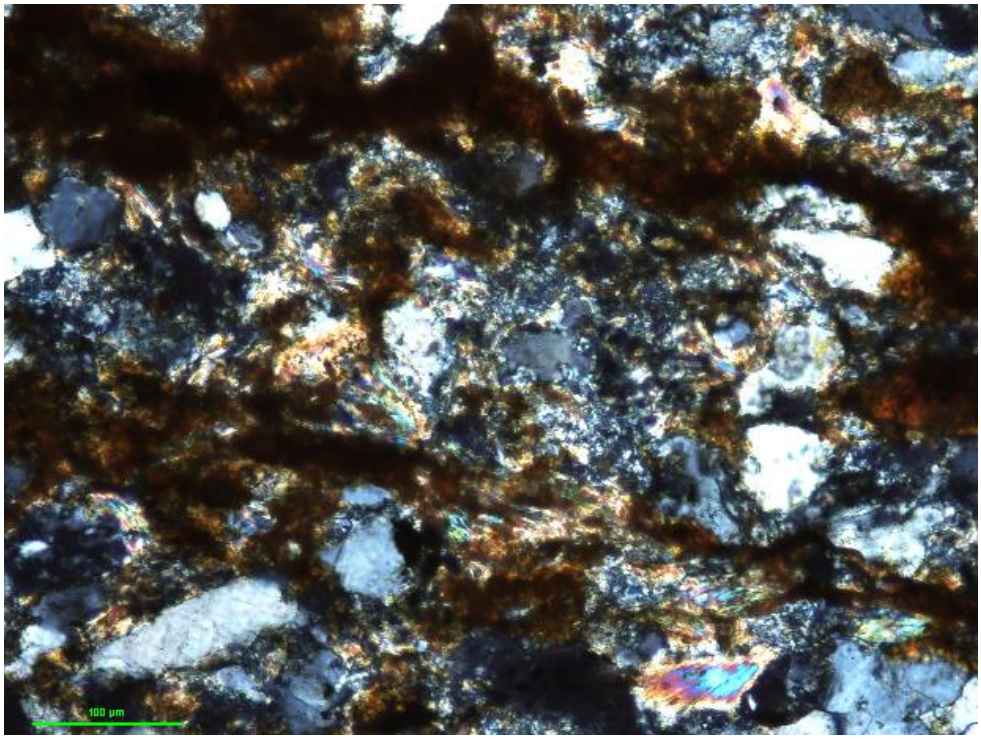

FIGURE 56: PHOTOMICROGRAPHS OF A THIN SECTION SHOWING ANGULAR TO SUB-ANGULAR QUARTZ IN A CLAY-MICA MATRIX. CLOSE-UP VIEW OF QUARTZ-DOMINATED LAYER SHOWING STRAINING AND RECRYSTALLISATIONIN QUARTZ, OVERGROWTHS AND CLAY-MICA MATRIX AS WELL AS IRON OXIDE STAINING

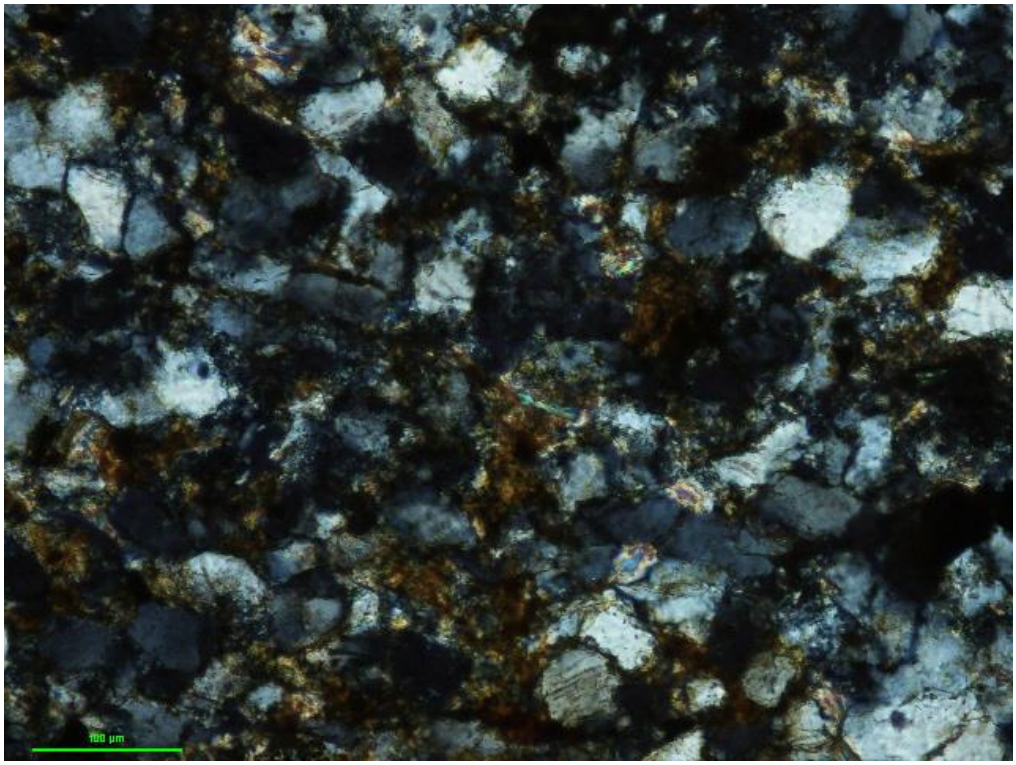

FIGURE 57: PHOTOMICROGRAPHS OF A THIN SECTION SHOWING ANGULAR TO SUB-ANGULAR QUARTZ IN A CLAY-MICA MATRIX. SHOWING STRAINING AND RECRYSTALLISATIONIN QUARTZ, OVERGROWTHS AND CLAY-MICA MATRIX AS WELL AS IRON OXIDE STAINING

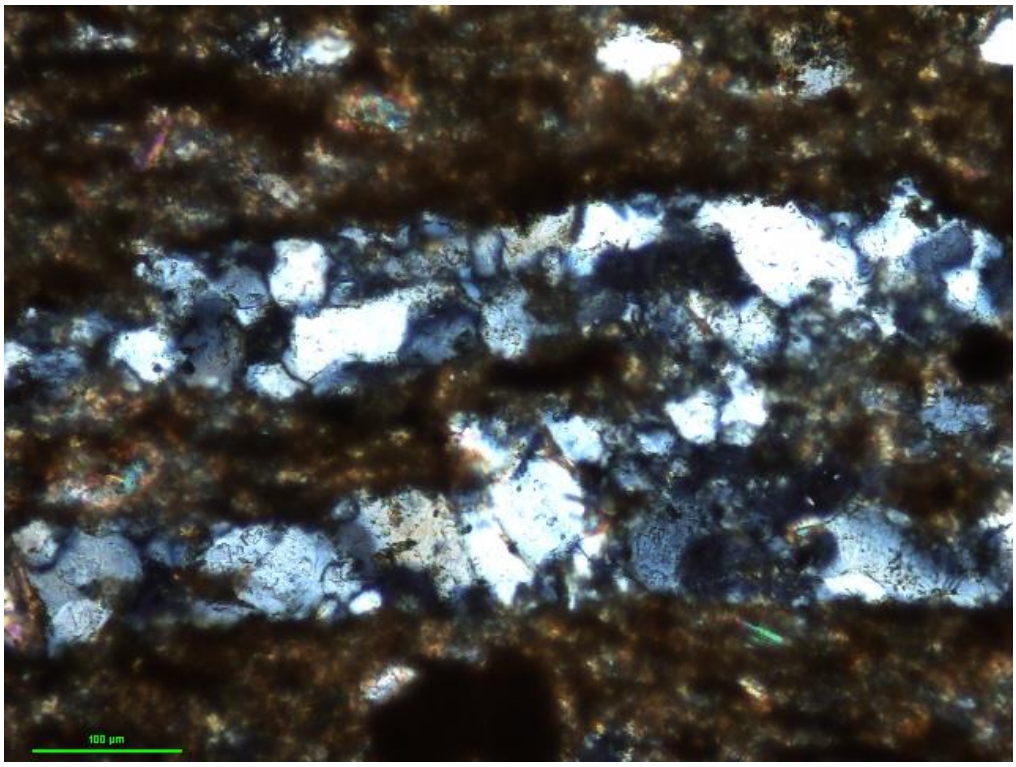

FIGURE 58: PHOTOMICROGRAPHS OF A THIN SECTION SHOWING ANGULAR TO SUB-ANGULAR QUARTZ IN A CLAY-MICA MATRIX. NOTE SOME STRAINING IN QUARTZ

APPENDIX F: RMR CALCULATIONS

BOREHOLE 1

A. CLASSIFICATION PARAMETERS AND THEIR RATINGS									
Parameter			Range of values						
1	Strength of intact rock material	Point-load strength index	>10 MPs	4-10 MPa	2-4 MPa	1-2 MPa	Fort his low range –uniaxial compressive test is preferred		
		Uniaxial comp. strength	>250 MPa	100-250 MPa	50-100 MPa	25-50 MPa	5-25 MPa	1-5 Mpa	<1 MPa
	Rating		15	12	7	4	2	1	0
2	Drift cone Quality RQD		90% - 100%	75% - 90%	50% - 75%	25% - 50%	<25%		
	Rating		20	17	13	8	3		
3	Spacing of discontinuities		>2m	0.6–2m	200–600mm	60-200mm	<60mm		
	Rating		20	15	10	8	5		
4	Condition of discontinuities (See E)		Very rough surfaces Not continuous No separation Unweathered wall rock	Slightly rough surfaces Separation <1mm Slightly weathered walls	Slightly rough surfaces Separation <1mm Highly weathered walls	Slicksided surfaces or Gouge <5mm thick or Separation 1-5mm, continuous	Soft gouge >5mm thick Or Separation >5mm Continuous		
	Rating		30	25	20	10			
5	Ground water	Inflow per 10m tunnel length (l/m)	None	<10	10-25	25-125	>125		
		(Joint water press)/ (Major principal(??)	0	<0.1	0.1-0.2	0.2-0.5	>0.5		
		General condition	Completely dry	Damp	Wet	Dripping	Flowing		
	Rating		15	10	7	4	0		
B. RATING ADJUSTMENT FOR DISCONTINUITY ORIENTATIONS (See F)									
Strike and dip orientations			Very favourable	Favourable	Fair	Unfavourable	Very Unfavourable		
Ratings	Tunnels & mines		0	-2	-5	-10	-12		
	Foundations		0	-2	-7	-15	-25		
	Slopes		0	-5	-25	-50			
C. ROCK MASS CLASSES DETERMINED FROM TOTAL RATINGS									
Rating			100←81	80←61	60←41	40←21	<21		
Class number			I	II	III	IV	V		
Description			Very good rock	Good rock	Fair rock	Poor rock	Very poor rock		
D. MEANING OF ROCK CLASSES									
Class number			I	II	III	IV	V		
Average stand-up time			20 years for 15m span	1 year for 10m span	1 week for 5m span	10 hours for 2.5m span	30 min for 1m span		
Cohesion of rock mass (kPa)			>400	300-400	200-300	100-200	<100		
Friction angle of rock mass (deg)			>45	35-45	25-35	15-25	<15		

$$Rating = 2 + 13 + 5 + 20 + 15 - 7 = 48$$

BOREHOLE 2

A. CLASSIFICATION PARAMETERS AND THEIR RATINGS									
Parameter			Range of values						
1	Strength of intact rock material	Point-load strength index	>10 MPs	4-10 MPa	2-4 MPa	1-2 MPa	Fort his low range –uniaxial compressive test is preferred		
		Uniaxial comp. strength	>250 MPa	100-250 MPa	50-100 MPa	25-50 MPa	5-25 MPa	1-5 Mpa	<1 MPa
	Rating		15	12	7	4	2	1	0
2	Drift cone Quality RQD		90% - 100%	75% - 90%	50% - 75%	25% - 50%	<25%		
	Rating		20	17	13	8	3		
3	Spacing of discontinuities		>2m	0.6–2m	200–600mm	60-200mm	<60mm		
	Rating		20	15	10	8	5		
4	Condition of discontinuities (See E)		Very rough surfaces Not continuous No separation Unweathered wall rock	Slightly rough surfaces Separation <1mm Slightly weathered walls	Slightly rough surfaces Separation <1mm Highly weathered walls	Slicksided surfaces or Gouge <5mm thick or Separation 1-5mm, continuous	Soft gouge >5mm thick Or Separation >5mm Continuous		
	Rating		30	25	20	10			
5	Ground water	Inflow per 10m tunnel length (l/m)	None	<10	10-25	25-125	>125		
		(Joint water press)/ (Major principal(??)	0	<0.1	0.1-0.2	0.2-0.5	>0.5		
		General condition	Completely dry	Damp	Wet	Dripping	Flowing		
	Rating		15	10	7	4	0		
B. RATING ADJUSTMENT FOR DISCONTINUITY ORIENTATIONS (See F)									
Strike and dip orientations			Very favourable	Favourable	Fair	Unfavourable	Very Unfavourable		
Ratings	Tunnels & mines		0	-2	-5	-10	-12		
	Foundations		0	-2	-7	-15	-25		
	Slopes		0	-5	-25	-50			
C. ROCK MASS CLASSES DETERMINED FROM TOTAL RATINGS									
Rating			100←81	80←61	60←41	40←21	<21		
Class number			I	II	III	IV	V		
Description			Very good rock	Good rock	Fair rock	Poor rock	Very poor rock		
D. MEANING OF ROCK CLASSES									
Class number			I	II	III	IV	V		
Average stand-up time			20 years for 15m span	1 year for 10m span	1 week for 5m span	10 hours for 2.5m span	30 min for 1m span		
Cohesion of rock mass (kPa)			>400	300-400	200-300	100-200	<100		
Friction angle of rock mass (deg)			>45	35-45	25-35	15-25	<15		

$$Rating = 2 + 13 + 5 + 20 + 15 - 7 = 48$$

BOREHOLE 3

A. CLASSIFICATION PARAMETERS AND THEIR RATINGS									
Parameter			Range of values						
1	Strength of intact rock material	Point-load strength index	>10 MPs	4-10 MPa	2-4 MPa	1-2 MPa	Fort his low range –uniaxial compressive test is preferred		
		Uniaxial comp. strength	>250 MPa	100-250 MPa	50-100 MPa	25-50 MPa	5-25 MPa	1-5 Mpa	<1 MPa
	Rating		15	12	7	4	2	1	0
2	Drift cone Quality RQD		90% - 100%	75% - 90%	50% - 75%	25% - 50%	<25%		
	Rating		20	17	13	8	3		
3	Spacing of discontinuities		>2m	0.6–2m	200–600mm	60-200mm	<60mm		
	Rating		20	15	10	8	5		
4	Condition of discontinuities (See E)		Very rough surfaces Not continuous No separation Unweathered wall rock	Slightly rough surfaces Separation <1mm Slightly weathered walls	Slightly rough surfaces Separation <1mm Highly weathered walls	Slicksided surfaces or Gouge <5mm thick or Separation 1-5mm, continuous	Soft gouge >5mm thick Or Separation >5mm Continuous		
	Rating		30	25	20	10			
5	Ground water	Inflow per 10m tunnel length (l/m)	None	<10	10-25	25-125	>125		
		(Joint water press)/ (Major principal(??)	0	<0.1	0.1-0.2	0.2-0.5	>0.5		
		General condition	Completely dry	Damp	Wet	Dripping	Flowing		
	Rating		15	10	7	4	0		
B. RATING ADJUSTMENT FOR DISCONTINUITY ORIENTATIONS (See F)									
Strike and dip orientations			Very favourable	Favourable	Fair	Unfavourable	Very Unfavourable		
Ratings	Tunnels & mines		0	-2	-5	-10	-12		
	Foundations		0	-2	-7	-15	-25		
	Slopes		0	-5	-25	-50			
C. ROCK MASS CLASSES DETERMINED FROM TOTAL RATINGS									
Rating			100←81	80←61	60←41	40←21	<21		
Class number			I	II	III	IV	V		
Description			Very good rock	Good rock	Fair rock	Poor rock	Very poor rock		
D. MEANING OF ROCK CLASSES									
Class number			I	II	III	IV	V		
Average stand-up time			20 years for 15m span	1 year for 10m span	1 week for 5m span	10 hours for 2.5m span	30 min for 1m span		
Cohesion of rock mass (kPa)			>400	300-400	200-300	100-200	<100		
Friction angle of rock mass (deg)			>45	35-45	25-35	15-25	<15		

$$Rating = 2 + 8 + 5 + 20 + 15 - 7 = 43$$

APPENDIX G: SETTLEMENT CALCULATIONS

Foundation Data		
Width (B)	4.52	m
Length (L)	5.97	m
Depth	0.6	m
Applied Pressure	17	kPa
m (L/B)	1.321	
Soil Data		
Bulk Density	24.86	kN/m^3
Young's Modulus E	600	MPa
Correction Factors		
Rigidity (F_r)	0.8	
Depth (Fox) (F_d)	0.971	
dZ (depth increment)	0.25	m
Settlement	**0.1**	**mm**

z (mid layer)	n (z/0.5B)	k	Δσ	dS	S
[m]			[kPa]	[mm]	[mm]
0.725	0.0553	0.250	17.0	0.006	0.1
0.975	0.1659	0.249	17.0	0.005	0.09
1.225	0.2765	0.247	16.8	0.01	0.09
1.475	0.3872	0.243	16.5	0.01	0.08
1.725	0.4978	0.237	16.1	0.01	0.08
1.975	0.6084	0.229	15.5	0.01	0.07
2.225	0.719	0.219	14.9	0	0.07
2.475	0.8296	0.207	14.1	0	0.06
2.725	0.9403	0.196	13.3	0	0.06
2.975	1.0509	0.184	12.5	0	0.05
3.225	1.1615	0.172	11.7	0	0.05
3.475	1.2721	0.160	10.9	0	0.05
3.725	1.3827	0.149	10.2	0	0.04
3.975	1.4934	0.139	9.5	0	0.04
4.225	1.604	0.129	8.8	0	0.04
4.475	1.7146	0.120	8.2	0	0.03
4.725	1.8252	0.112	7.6	0	0.03
4.975	1.9358	0.104	7.1	0	0.03
5.225	2.0465	0.097	6.6	0	0.03
5.475	2.1571	0.091	6.2	0	0.02
5.725	2.2677	0.085	5.8	0	0.02
5.975	2.3783	0.079	5.4	0	0.02
6.225	2.4889	0.074	5.1	0	0.02
6.475	2.5996	0.070	4.8	0	0.02
6.725	2.7102	0.065	4.5	0	0.01
6.975	2.8208	0.062	4.2	0	0.01
7.225	2.9314	0.058	3.9	0	0.01
7.475	3.042	0.055	3.7	0	0.01
7.725	3.1527	0.052	3.5	0	0.01
7.975	3.2633	0.049	3.3	0	0.01
8.225	3.3739	0.046	3.1	0	0.01
8.475	3.4845	0.044	3.0	0	0.01
8.725	3.5951	0.041	2.8	0	0
8.975	3.7058	0.039	2.7	0	0
9.225	3.8164	0.037	2.5	0	0
9.475	3.927	0.036	2.4	0	0
9.725	4.0376	0.034	2.3	0	0
9.975	4.1482	0.032	2.2	0	0
10.225	4.2588	0.031	2.1	0	0

APPENDIX H: CIRCULAR FAILURE

SECTION 1 ANALYSIS

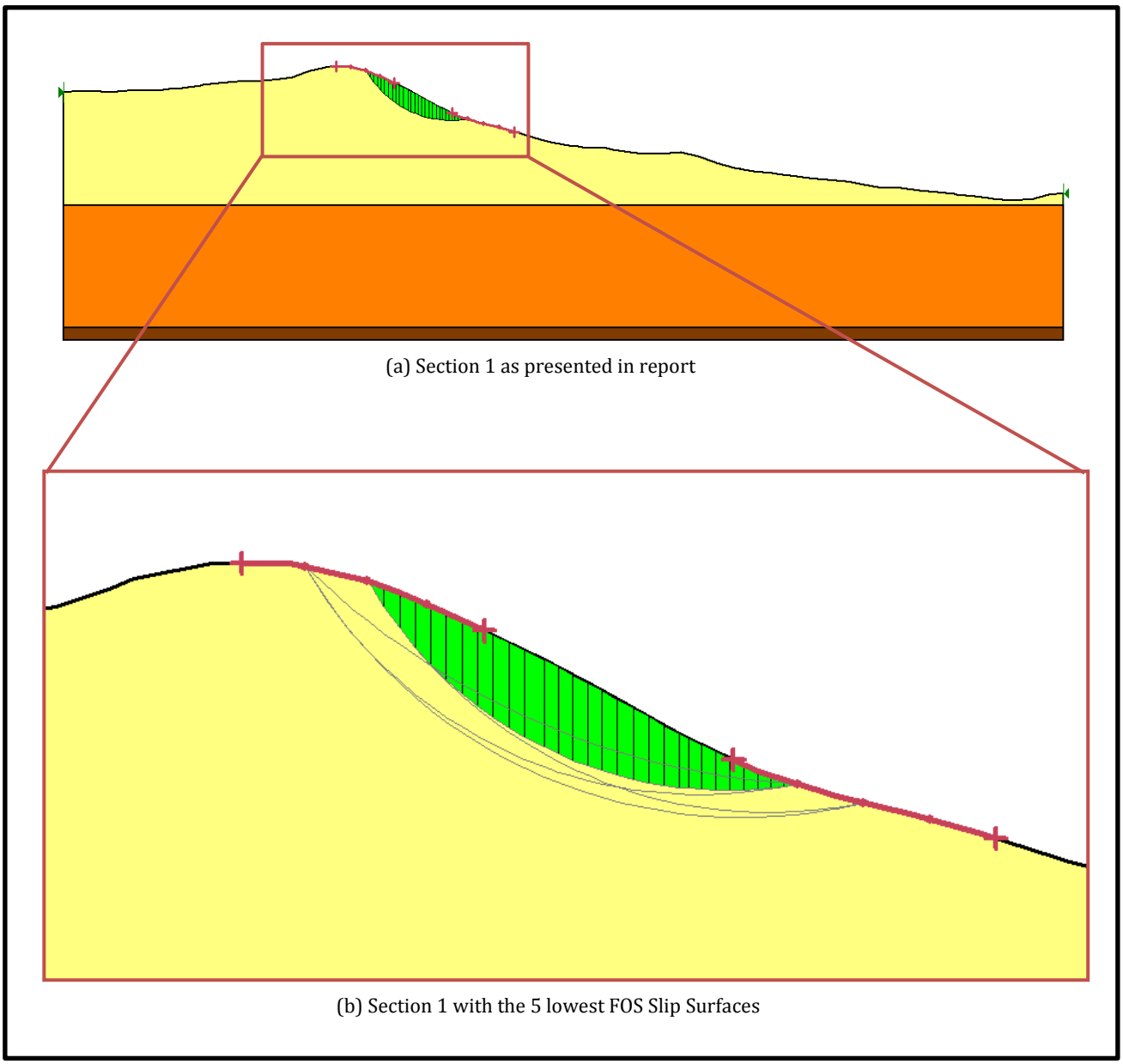

(a) Section 1 as presented in report

(b) Section 1 with the 5 lowest FOS Slip Surfaces

FIGURE 59: SECTION 1 FOR CIRCULAR FAILURE ANALYSIS

SLOPE/W Analysis Report

Project Settings

Length (L) Units: Meters
Time (t) Units: Seconds
Force (F) Units: kN
Pressure (p) Units: kPa
Strength Units: kPa
Unit Weight of Water: 9.807 kN/m³
View: 2D
Element Thickness: 1

Analysis Settings

SLOPE/W Analysis

Kind: SLOPE/W
Method: Bishop
Settings
PWP Conditions Source: (none)
Slip Surface
Direction of movement: Left to Right
Use Passive Mode: No
Slip Surface Option: Entry and Exit
Critical slip surfaces saved: 1
Optimize Critical Slip Surface Location: No
Tension Crack
Tension Crack Option: (none)
F of S Distribution
F of S Calculation Option: Constant
Advanced
Number of Slices: 30
F of S Tolerance: 0.001
Minimum Slip Surface Depth: 0.1 m
Optimization Maximum Iterations: 2,000
Optimization Convergence Tolerance: 1e-007
Starting Optimization Points: 8
Ending Optimization Points: 16
Complete Passes per Insertion: 1
Driving Side Maximum Convex Angle: 5 °
Resisting Side Maximum Convex Angle: 1 °

Materials

Top Layer

Model: Mohr-Coulomb
Unit Weight: 18 kN/m³
Cohesion': 8 kPa
Phi': 36 °
Phi-B: 0 °

Bottom Layer

Model: Mohr-Coulomb
Unit Weight: 23 kN/m³
Cohesion': 42 kPa
Phi': 42 °
Phi-B: 0 °

Bedrock

Model: Bedrock (Impenetrable)

Slip Surface Entry and Exit

Left Projection: Range
Left-Zone Left Coordinate: (44.71883, 1,046.4464) m
Left-Zone Right Coordinate: (59.61153, 1,041) m
Left-Zone Increment: 4
Right Projection: Range
Right-Zone Left Coordinate: (61.16998, 1,040.1339) m
Right-Zone Right Coordinate: (73.99993, 1,035.7691) m
Right-Zone Increment: 4
Radius Increments: 4

Slip Surface Limits

Left Coordinate: (0, 1,042.3095) m
Right Coordinate: (164.12266, 1,025.7356) m

CURRENT SLIP SURFACE

Slip Surface: 58

F of S: 2.335

Volume: 36.76358 m³

Weight: 661.74444 kN

Resisting Moment: 9,870.1319 kN-m

Activating Moment: 4,227.3294 kN-m

F of S Rank: 1

Exit: (66.281839, 1,037.8761) m

Entry: (49.6028, 1,045.7605) m

Radius: 16.024204 m

Centre: (63.542124, 1,053.6643) m

SECTION 2 ANALYSIS

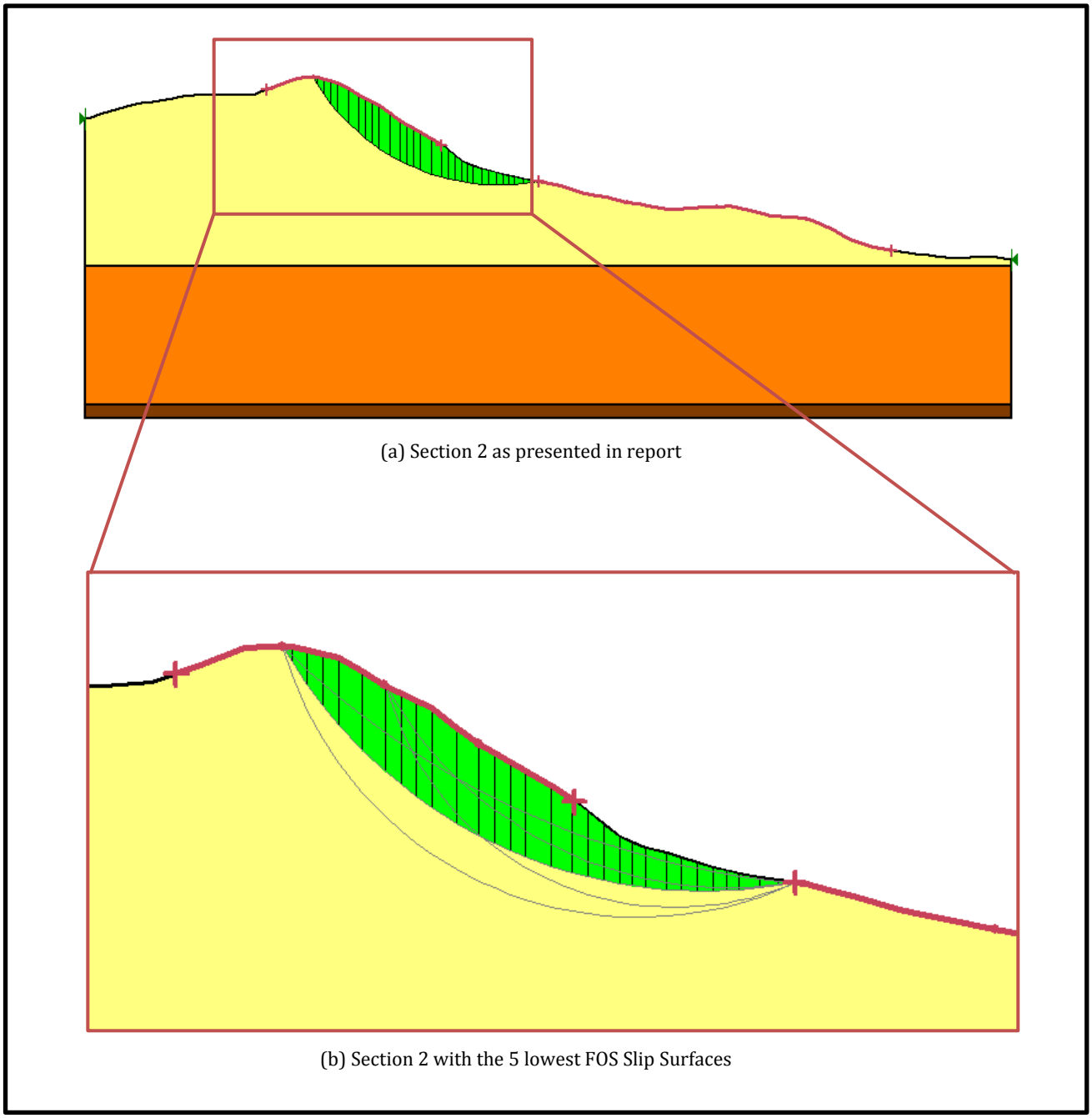

(a) Section 2 as presented in report

(b) Section 2 with the 5 lowest FOS Slip Surfaces

FIGURE 60: SLOPE 2 WITH PROTRUSION FOR CIRCULAR FAILURE ANALYSIS

SLOPE/W Analysis Report

Project Settings

Length (L) Units: meters
Time (t) Units: Seconds
Force (F) Units: kN
Pressure (p) Units: kPa
Strength Units: kPa
Unit Weight of Water: 9.807 kN/m³
View: 2D
Element Thickness: 1

Analysis Settings

SLOPE/W Analysis

Kind: SLOPE/W
Method: Bishop
Settings
PWP Conditions Source: (none)
Slip Surface
Direction of movement: Left to Right
Use Passive Mode: No
Slip Surface Option: Entry and Exit
Critical slip surfaces saved: 1
Optimize Critical Slip Surface Location: No
Tension Crack
Tension Crack Option: (none)
F of S Distribution
F of S Calculation Option: Constant
Advanced
Number of Slices: 30
F of S Tolerance: 0.001
Minimum Slip Surface Depth: 0.1 m
Optimization Maximum Iterations: 2,000
Optimization Convergence Tolerance: 1e-007
Starting Optimization Points: 8
Ending Optimization Points: 16
Complete Passes per Insertion: 1
Driving Side Maximum Convex Angle: 5 °
Resisting Side Maximum Convex Angle: 1 °

Materials

Top Layer

Model: Mohr-Coulomb
Unit Weight: 18 kN/m³
Cohesion': 8 kPa
Phi': 36 °
Phi-B: 0 °

Bottom Layer

Model: Mohr-Coulomb
Unit Weight: 23 kN/m³
Cohesion': 42 kPa
Phi': 42 °
Phi-B: 0 °

Bedrock

Model: Bedrock (Impenetrable)

Slip Surface Entry and Exit

Left Projection: Range
Left-Zone Left Coordinate: (26.17951, 1,053.9402) m
Left-Zone Right Coordinate: (51.5143, 1,045.8807) m
Left-Zone Increment: 4
Right Projection: Range
Right-Zone Left Coordinate: (65.5138, 1,040.7223) m
Right-Zone Right Coordinate: (116.36028, 1,030.7152) m
Right-Zone Increment: 4
Radius Increments: 4

Slip Surface Limits

Left Coordinate: (0, 1,049.7643) m
Right Coordinate: (133.7446, 1,029.4197) m

CURRENT SLIP SURFACE

Slip Surface: 58

F of S: 2.335

Volume: 36.76358 m³

Weight: 661.74444 kN

Resisting Moment: 9,870.1319 kN-m

Activating Moment: 4,227.3294 kN-m

F of S Rank: 1

Exit: (66.281839, 1,037.8761) m

Entry: (49.6028, 1,045.7605) m

Radius: 16.024204 m

Centre: (63.542124, 1,053.6643) m

SECTION 2 EXTRA ANALYSIS

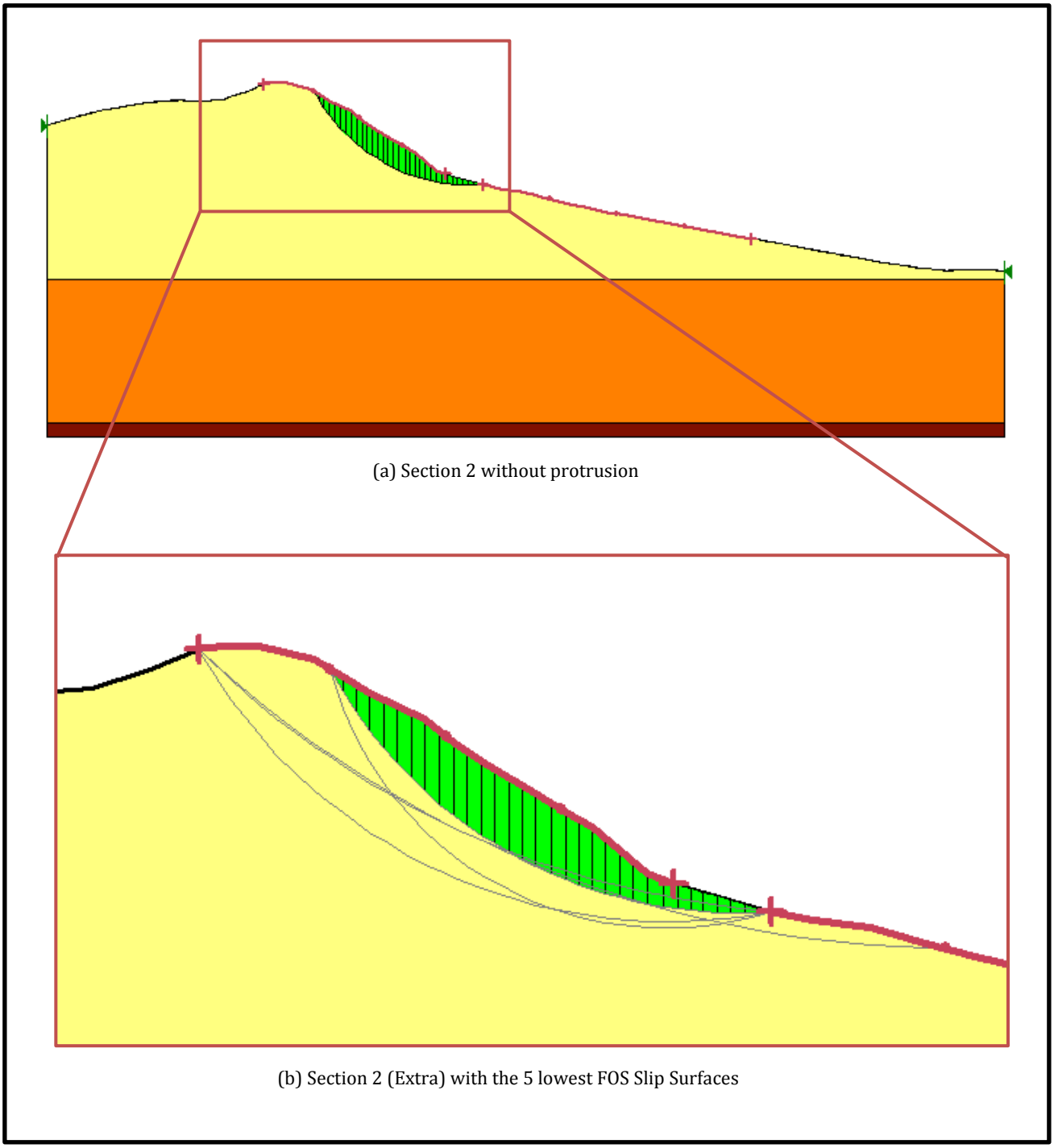

(a) Section 2 without protrusion

(b) Section 2 (Extra) with the 5 lowest FOS Slip Surfaces

FIGURE 61: SECTION 2 WITHOUT PROTRUSION FOR CIRCULAR FAILURE ANALYSIS

SLOPE/W Analysis Report

Project Settings

Length (L) Units: meters
Time (t) Units: Seconds
Force (F) Units: kN
Pressure (p) Units: kPa
Strength Units: kPa
Unit Weight of Water: 9.807 kN/m³
View: 2D
Element Thickness: 1

Analysis Settings

SLOPE/W Analysis

Kind: SLOPE/W
Method: Bishop
Settings
PWP Conditions Source: (none)
Slip Surface
Direction of movement: Left to Right
Use Passive Mode: No
Slip Surface Option: Entry and Exit
Critical slip surfaces saved: 1
Optimize Critical Slip Surface Location: No
Tension Crack
Tension Crack Option: (none)
F of S Distribution
F of S Calculation Option: Constant
Advanced
Number of Slices: 30
F of S Tolerance: 0.001
Minimum Slip Surface Depth: 0.1 m
Optimization Maximum Iterations: 2,000
Optimization Convergence Tolerance: 1e-007
Starting Optimization Points: 8
Ending Optimization Points: 16
Complete Passes per Insertion: 1
Driving Side Maximum Convex Angle: 5 °
Resisting Side Maximum Convex Angle: 1 °

Materials

Top Layer

Model: Mohr-Coulomb
Unit Weight: 18 kN/m³
Cohesion': 8 kPa
Phi': 36 °
Phi-B: 0 °

Bottom Layer

Model: Mohr-Coulomb
Unit Weight: 23 kN/m³
Cohesion': 42 kPa
Phi': 42 °
Phi-B: 0 °

Bedrock

Model: Bedrock (Impenetrable)

Slip Surface Entry and Exit

Left Projection: Range
Left-Zone Left Coordinate: (30.3022, 1,055.5143) m
Left-Zone Right Coordinate: (55.73553, 1,043) m
Left-Zone Increment: 4
Right Projection: Range
Right-Zone Left Coordinate: (60.99996, 1,041.5137) m
Right-Zone Right Coordinate: (98.4508, 1,034.0453) m
Right-Zone Increment: 4
Radius Increments: 4

Slip Surface Limits

Left Coordinate: (0, 1,049.7643) m
Right Coordinate: (133.7446, 1,029.4197) m

CURRENT SLIP SURFACE

Slip Surface: 28

F of S: 1.847

Volume: 58.907404 m³

Weight: 1,060.3333 kN

Resisting Moment: 23,128.746 kN-m

Activating Moment: 12,523.865 kN-m

F of S Rank: 1

Exit: (60.999955, 1,041.5137) m

Entry: (37.327862, 1,054.4922) m

Radius: 24.792767 m

Centre: (59.161617, 1,066.2382) m

APPENDIX I: PLANAR FAILURE

PROKON
Software Consultants (Pty) Ltd
Internet: http://www.prokon.com
E-Mail : mail@prokon.com

Job Number		Sheet
Job Title		
Client		
Calcs by	Checked by	Date

Planar failure in rock slopes : DEMO MODE

ED4

Input Data

General Parameters			Probability Dist.	Std. Dev	Minimum	Maximum
Cutting height Hc	(m)	1	Deterministic			
Slip plane height Hp	(m)	0.1	Deterministic			
Cutting angle Øc	(°)	75	Deterministic			
Slip Plane angle Øp	(°)	28	Deterministic			
Upper slope angle Øu	(°)	27	Deterministic			
Tension crack depth Z	(m)	0.7	Deterministic			
Water depth in crack Zw	(m)	0	Deterministic			
Water density γw	(kN/m3)	9.81	Deterministic			
Horiz. Seismic acc	g	0.16	Deterministic			
Vert. Seismic acc	g	0.01	Deterministic			
Anchor force T	(kN/m)		Deterministic			
Anchor dip from horiz. ß	(°)	0	Deterministic			
External load	(kN/m)		Deterministic			
Dip: External load θ	(°)	0	Deterministic			

Rock Parameters			Probability Dist.	Std. Dev	Minimum	Maximum
Rock friction angle Ø	(°)	10	Deterministic		9	11
Rock shear strength C	(kN/m)	50	Deterministic		45	55
Rock density γr	(kN/m3)	25	Deterministic		23	27
Dilation angle i	(°)	10	Deterministic		9	11
% Intact length		15	Deterministic		14	16

Factor of Safety: 1.27

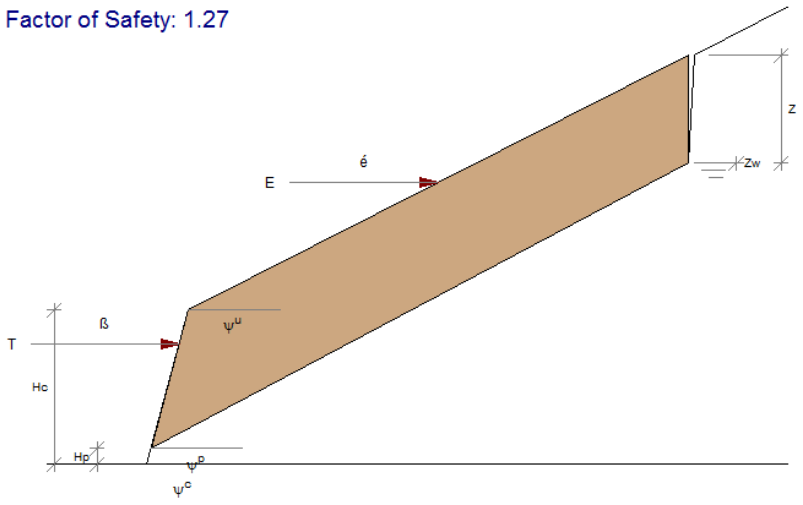

Overall Safety Factor: 1.27

Planar failure in rock slopes : DEMO MODE

E04

Input Data

General Parameters			Probability Dist.	Std. Dev	Minimum	Maximum
Cutting height Hc	(m)	1	Deterministic			
Slip plane height Hp	(m)	0.1	Deterministic			
Cutting angle Øc	(°)	75	Deterministic			
Slip Plane angle Øp	(°)	37	Deterministic			
Upper slope angle Øu	(°)	27	Deterministic			
Tension crack depth Z	(m)	0.6	Deterministic			
Water depth in crack Zw	(m)	0	Deterministic			
Water density γw	(kN/m3)	9.81	Deterministic			
Horiz. Seismic acc	g	0.16	Deterministic			
Vert. Seismic acc	g	0.01	Deterministic			
Anchor force T	(kN/m)		Deterministic			
Anchor dip from horiz. ß	(°)	0	Deterministic			
External load	(kN/m)		Deterministic			
Dip: External load θ	(°)	0	Deterministic			

Rock Parameters			Probability Dist.	Std. Dev	Minimum	Maximum
Rock friction angle Ø	(°)	10	Deterministic		9	11
Rock shear strength C	(kN/m)	50	Deterministic		45	55
Rock density γr	(kN/m3)	25	Deterministic		23	27
Dilation angle i	(°)	10	Deterministic		9	11
% Intact length		15	Deterministic		14	16

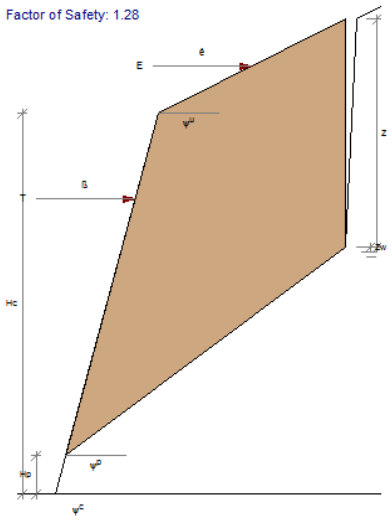

Overall Safety Factor: 1.28

PROKON
Software Consultants (Pty) Ltd
Internet: http://www.prokon.com
E-Mail : mail@prokon.com

Job Number		Sheet
Job Title		
Client		
Calcs by	Checked by	Date

Planar failure in rock slopes : DEMO MODE

E04

Input Data

General Parameters			Probability Dist.	Std. Dev	Minimum	Maximum
Cutting height Hc	(m)	1	Deterministic			
Slip plane height Hp	(m)	0.1	Deterministic			
Cutting angle Øc	(°)	75	Deterministic			
Slip Plane angle Øp	(°)	46	Deterministic			
Upper slope angle Øu	(°)	27	Deterministic			
Tension crack depth Z	(m)	0.5	Deterministic			
Water depth in crack Zw	(m)	0	Deterministic			
Water density γw	(kN/m3)	9.81	Deterministic			
Horiz. Seismic acc	g	0.16	Deterministic			
Vert. Seismic acc	g	0.01	Deterministic			
Anchor force T	(kN/m)		Deterministic			
Anchor dip from horiz. ß	(°)	0	Deterministic			
External load	(kN/m)		Deterministic			
Dip: External load θ	(°)	0	Deterministic			

Rock Parameters			Probability Dist.	Std. Dev	Minimum	Maximum
Rock friction angle Ø	(°)	10	Deterministic		9	11
Rock shear strength C	(kN/m)	50	Deterministic		45	55
Rock density γr	(kN/m3)	25	Deterministic		23	27
Dilation angle i	(°)	10	Deterministic		9	11
% Intact length		15	Deterministic		14	16

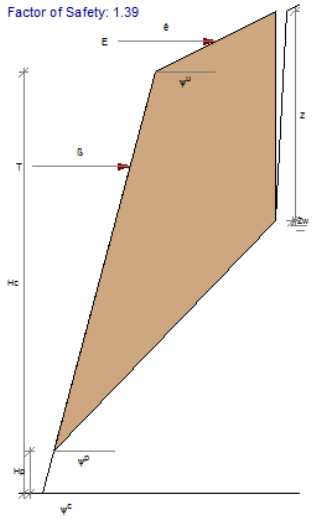

Overall Safety Factor: 1.39

Planar failure in rock slopes : DEMO MODE

E04

Input Data

General Parameters			Probability Dist.	Std. Dev	Minimum	Maximum
Cutting height Hc	(m)	1	Deterministic			
Slip plane height Hp	(m)	0.1	Deterministic			
Cutting angle Øc	(°)	75	Deterministic			
Slip Plane angle Øp	(°)	63	Deterministic			
Upper slope angle Øu	(°)	27	Deterministic			
Tension crack depth Z	(m)	0.3	Deterministic			
Water depth in crack Zw	(m)	0	Deterministic			
Water density γw	(kN/m3)	9.81	Deterministic			
Horiz. Seismic acc	g	0.16	Deterministic			
Vert. Seismic acc	g	0.01	Deterministic			
Anchor force T	(kN/m)		Deterministic			
Anchor dip from horiz. ß	(°)	0	Deterministic			
External load	(kN/m)		Deterministic			
Dip: External load θ	(°)	0	Deterministic			

Rock Parameters			Probability Dist.	Std. Dev	Minimum	Maximum
Rock friction angle Ø	(°)	10	Deterministic		9	11
Rock shear strength C	(kN/m)	50	Deterministic		45	55
Rock density γr	(kN/m3)	25	Deterministic		23	27
Dilation angle i	(°)	10	Deterministic		9	11
% Intact length		15	Deterministic		14	16

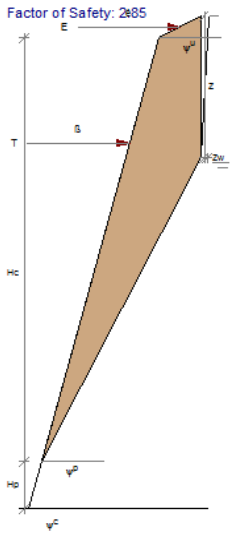

Overall Safety Factor: 2.85

PROKON Software Consultants (Pty) Ltd Internet: http://www.prokon.com E-Mail : mail@prokon.com	Job Number		Sheet
	Job Title		
	Client		
	Calcs by	Checked by	Date

Planar failure in rock slopes : DEMO MODE

E04

Input Data

General Parameters			Probability Dist.	Std. Dev	Minimum	Maximum
Cutting height Hc	(m)	2	Deterministic			
Slip plane height Hp	(m)	0.1	Deterministic			
Cutting angle Øc	(°)	75	Deterministic			
Slip Plane angle Øp	(°)	28	Deterministic			
Upper slope angle Øu	(°)	27	Deterministic			
Tension crack depth Z	(m)	1.5	Deterministic			
Water depth in crack Zw	(m)	0	Deterministic			
Water density γw	(kN/m3)	9.81	Deterministic			
Horiz. Seismic acc	g	0.16	Deterministic			
Vert. Seismic acc	g	0.01	Deterministic			
Anchor force T	(kN/m)		Deterministic			
Anchor dip from horiz. ß	(°)	0	Deterministic			
External load	(kN/m)		Deterministic			
Dip: External load θ	(°)	0	Deterministic			

Rock Parameters			Probability Dist.	Std. Dev	Minimum	Maximum
Rock friction angle Ø	(°)	10	Deterministic		9	11
Rock shear strength C	(kN/m)	50	Deterministic		45	55
Rock density γr	(kN/m3)	25	Deterministic		23	27
Dilation angle i	(°)	10	Deterministic		9	11
% Intact length		15	Deterministic		14	16

Factor of Safety: 0.85

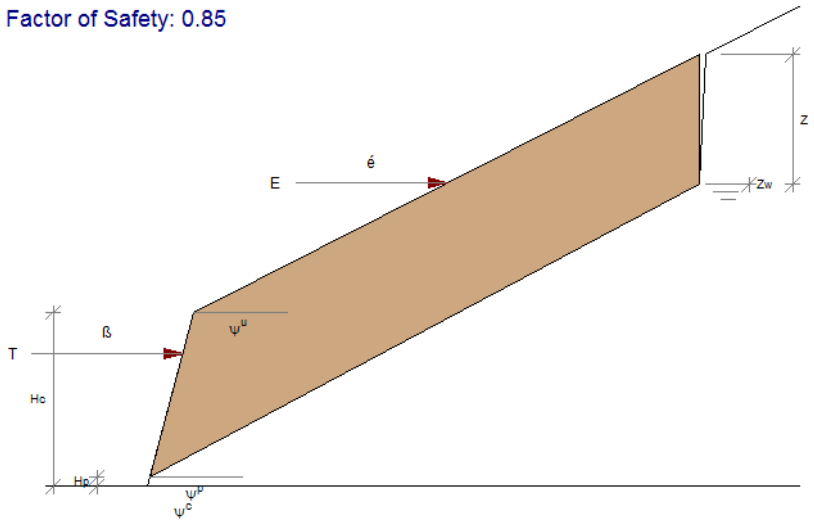

Overall Safety Factor: 0.85

PROKON Software Consultants (Pty) Ltd Internet: http://www.prokon.com E-Mail : mail@prokon.com	Job Number		Sheet
	Job Title		
	Client		
	Calcs by	Checked by	Date

Planar failure in rock slopes : DEMO MODE

E04

Input Data

General Parameters			Probability Dist.	Std. Dev	Minimum	Maximum
Cutting height Hc	(m)	2	Deterministic			
Slip plane height Hp	(m)	0.1	Deterministic			
Cutting angle Øc	(°)	75	Deterministic			
Slip Plane angle Øp	(°)	37	Deterministic			
Upper slope angle Øu	(°)	27	Deterministic			
Tension crack depth Z	(m)	1.2	Deterministic			
Water depth in crack Zw	(m)	0	Deterministic			
Water density γw	(kN/m3)	9.81	Deterministic			
Horiz. Seismic acc	g	0.16	Deterministic			
Vert. Seismic acc	g	0.01	Deterministic			
Anchor force T	(kN/m)		Deterministic			
Anchor dip from horiz. ß	(°)	0	Deterministic			
External load	(kN/m)		Deterministic			
Dip: External load θ	(°)	0	Deterministic			

Rock Parameters			Probability Dist.	Std. Dev	Minimum	Maximum
Rock friction angle Ø	(°)	10	Deterministic		9	11
Rock shear strength C	(kN/m)	50	Deterministic		45	55
Rock density γr	(kN/m3)	25	Deterministic		23	27
Dilation angle i	(°)	10	Deterministic		9	11
% Intact length		15	Deterministic		14	16

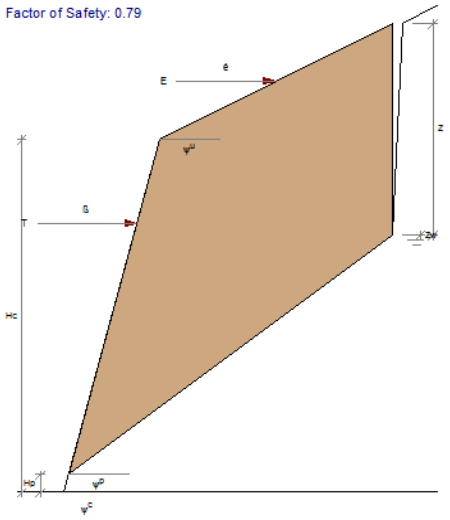

Overall Safety Factor: 0.79

PROKON Software Consultants (Pty) Ltd Internet: http://www.prokon.com E-Mail : mail@prokon.com	Job Number		Sheet
	Job Title		
	Client		
	Calcs by	Checked by	Date

Planar failure in rock slopes : DEMO MODE

E04

Input Data

General Parameters			Probability Dist.	Std. Dev	Minimum	Maximum
Cutting height Hc	(m)	2	Deterministic			
Slip plane height Hp	(m)	0.1	Deterministic			
Cutting angle Øc	(°)	75	Deterministic			
Slip Plane angle Øp	(°)	46	Deterministic			
Upper slope angle Øu	(°)	27	Deterministic			
Tension crack depth Z	(m)	1	Deterministic			
Water depth in crack Zw	(m)	0	Deterministic			
Water density γw	(kN/m3)	9.81	Deterministic			
Horiz. Seismic acc	g	0.16	Deterministic			
Vert. Seismic acc	g	0.01	Deterministic			
Anchor force T	(kN/m)		Deterministic			
Anchor dip from horiz. ß	(°)	0	Deterministic			
External load	(kN/m)		Deterministic			
Dip: External load θ	(°)	0	Deterministic			

Rock Parameters			Probability Dist.	Std. Dev	Minimum	Maximum
Rock friction angle Ø	(°)	10	Deterministic		9	11
Rock shear strength C	(kN/m)	50	Deterministic		45	55
Rock density γr	(kN/m3)	25	Deterministic		23	27
Dilation angle i	(°)	10	Deterministic		9	11
% Intact length		15	Deterministic		14	16

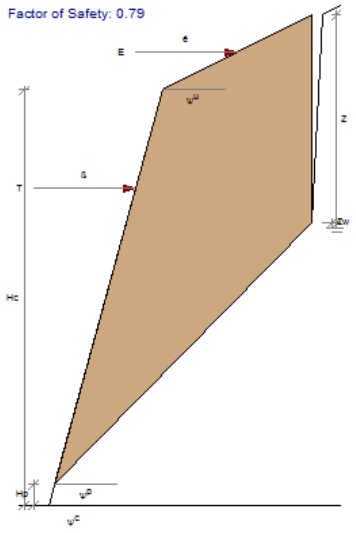

Overall Safety Factor: 0.79

Planar failure in rock slopes : DEMO MODE

E04

Input Data

General Parameters			Probability Dist.	Std. Dev	Minimum	Maximum
Cutting height Hc	(m)	2	Deterministic			
Slip plane height Hp	(m)	0.1	Deterministic			
Cutting angle Øc	(°)	75	Deterministic			
Slip Plane angle Øp	(°)	63	Deterministic			
Upper slope angle Øu	(°)	27	Deterministic			
Tension crack depth Z	(m)	0.6	Deterministic			
Water depth in crack Zw	(m)	0	Deterministic			
Water density γw	(kN/m3)	9.81	Deterministic			
Horiz. Seismic acc	g	0.16	Deterministic			
Vert. Seismic acc	g	0.01	Deterministic			
Anchor force T	(kN/m)		Deterministic			
Anchor dip from horiz. ß	(°)	0	Deterministic			
External load	(kN/m)		Deterministic			
Dip: External load θ	(°)	0	Deterministic			

Rock Parameters			Probability Dist.	Std. Dev	Minimum	Maximum
Rock friction angle Ø	(°)	10	Deterministic		9	11
Rock shear strength C	(kN/m)	50	Deterministic		45	55
Rock density γr	(kN/m3)	25	Deterministic		23	27
Dilation angle i	(°)	10	Deterministic		9	11
% Intact length		15	Deterministic		14	16

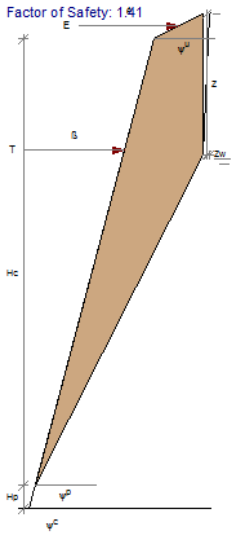

Overall Safety Factor: 1.41

APPENDIX J: DN - VALUES

Blows	Test 1		Test 2		Test 3		Test 4		Test 5		Test 6	
	Depth (mm)	DN-Value	Depth (mm)	DN-Value	Depth (mm)	DN-Value	Depth (mm)	DN-Value	Depth (mm)	DN-Value	Depth (mm)	DN-Value
0	55		60		40		35		55		55	
5	140	**17**	105	**9**	95	**11**	110		135		125	**14**
10	165		130		115		145	**11**	170	**11.5**	140	
15	180		145		125		160		205		145	
20	195	**3**	160		135		175		220	**3**	155	
25	200		175		145	**2.5**	185		235		160	
30	205		185		155		195		240		170	
35	215		200		160		200		245		180	
40	220		210	**3**	165		210		250		190	
45	225		220		170		215		255	**1.4**	205	
50	230		230		170		230		255		210	**1.75**
55	240		230		170	**0.83**	240		255	**0**	225	
60	240		240				245	**2**			240	
65	245	**1.13**	245				250				250	
70			245				255				260	
75			250				260				270	**2.4**
80			260				265				295	
85			260	**1.11**			275				315	
90							280				330	**4**
95							290	**1.29**			340	
100							305				350	
105							315				360	
110							330				365	
115							345				375	
120							360				385	
125							375				390	
130							385				400	
135							395	**2.625**			415	**1.89**
140							400				430	
145							405				430	
150							410				440	
155							415	**1**			450	
160											455	
165											460	
170											465	
175											470	**1.38**